Mixing and mass transfer by rotating jets: Fundamentals and applications

Nordkvist, Mikkel; Villadsen, John

Publication date:
2006

Document Version
Publisher's PDF, also known as Version of record

Mixing and mass transfer by rotating jets: fundamentals and applications

Mikkel Nordkvist
PhD Thesis

Center for Microbial Biotechnology
BioCentrum-DTU
Technical University of Denmark
DK-2800 Kgs. Lyngby
Denmark

This thesis is typeset in LaTeX, and is available in two versions: an electronic format with colored hyperlinks and a printed format.

E-mail: mnq@biocentrum.dtu.dk or min@iso-mix.com

Preface

The submission of this thesis marks the end of my ph.d. study. The ph.d. project was carried out from March 2001 to April 2005 at the Center for Microbial Biotechnology, BioCentrum-DTU at the Technical University of Denmark. The project was financed by a stipend from the Technical University of Denmark, while running costs were financed by the Center for Microbial Technology.

During my study I have been involved in different exciting research projects in the broad field of biotechnology. The research on the use of rotary jet heads for mixing and mass transfer which is presented in this thesis was initially only planned to be a minor part of the study. However, the topic contained a wealth of exciting problems - both of academic and industrial importance.

My involvement in the research project concerning the use of rotary jet heads for mixing and mass transfer started in late 2001. For the remainder of 2001 and during the spring semester of 2002 the first 'batch' of experiments was conducted at the company Toftejorg A/S in Ishøj (Now part of Alfa Laval), and I moved on to other research topics. However, in the fall of 2003 the project on rotary jet heads was revived with the establishment of a pilot-scale reactor at DTU, and yeast cultivations were performed in the system. In the spring of 2004 we decided that the remainder of my study should focus on rotary jet heads, and a major overhaul of the set-ups at the company in Ishøj was initiated to be able to perform experiments in different scales and to improve the set-up in general. Unfortunately problems in the data logging system led to falsified results - which unfortunately was detected after several months of work and close to the submission date of this thesis. This prevents me from presenting any of these results here. In the summer of 2004 Novozymes A/S expressed an interest in the system for enzymatic oxidation of lactose, and this topic - investigated in different scales - became the last topic of my thesis.

I would like to express my gratitude to my supervisor Professor John Villadsen, whose valuable advice and continuing interest in the project cannot be

underestimated. I have always enjoyed the conversations we have had concerning enzyme kinetics, electrode responses, and microbial systems amongst other topics.

Jan Stumpe Hummer and John Åge Lazar from ISO-MIX A/S are thanked for allowing me to use the tanks in Ishøj for characterization of the rotary jet heads. I would also like to thank the rest of the people at the company.

Per Munk Nielsen from Novozymes A/S and Peter Budtz from Chr. Hansen A/S, the persons responsible for the lactose oxidation project at their respective companies, are thanked for advice concerning this part of the project.

I would like to thank Ph.D. Thomas Grotkjær together with whom I did the first experiments in the rotary jet head system. I have also had the pleasure of being supervisor for several M.Sc. students. Michael Jensen and Jonas Vestergaard carried out a project concerning yeast cultivations in the system. Furthermore, Ling Hua did some of the experiments on oxidation of lactose presented in this report as part of his final M.Sc. project.

This thesis is dedicated to my wife Stine and my daughter Anne Kristine whose love and patience has been extraordinary in all phases of this project, especially in the last phase of extensive writing.

Mikkel Nordkvist, December 2005

Contents

Nomenclature

Roman Letters

A_d	Total cross sectional area of nozzles
a	Gas-liquid interfacial area per unit liquid volume
a_d	Gas-liquid interfacial area per unit dispersion volume
c	Concentration
c_A	Concentration of component A
c_A^*	Saturation concentration of component A
c_l	Concentration of oxygen in liquid
c_l^*	Saturation concentration of oxygen
c_{lac}	Concentration of lactobionic acid
D	Impeller diameter
DOT	Dissolved oxygen tension
d	Nozzle diameter
d_Z	Jet diameter at the end of the jet free path
E	Normalized output
E	Oxidase enzyme
E_{ox}	Oxidized form of oxidase
$E_{ox}S$	Complex between oxidized form of oxidase and lactose
E_{red}	Reduced form of oxidase
G	Mass flux
g	Gravitational acceleration
H	Liquid height
He_A	Henry's constant for component A
J_A	Flux of component A
$J_{A,g}$	Flux of component A through gas film
$J_{A,l}$	Flux of component A through liquid film
K_d	Constant in Eq.(3.15)
K_l	Overall mass transfer coefficient
K_m	Michaelis constant

K_{mO}	Michaelis constant for oxygen
K_{mS}	Michaelis constant for lactose
K_p	Constant in Eq.(3.22)
k_1	First order approximation rate constant
k_{cat}	Catalytic rate constant
k_d	Deactivation rate constant
k_g	Mass transfer coefficient for gas film
k_l	Mass transfer coefficient for liquid film
$k_l a$	Volumetric mass transfer coefficient based on liquid volume
$k_l a_d$	Volumetric mass transfer coefficient based on dispersion volume
k_{mix}	Mixing constant
L	Integral scale of turbulence
M	Number of probes
M	Torque
$\dot{m}_b$	Mass flow rate of base
m	Degree of mixing
N	Impeller speed
N	Number of rotary jet heads
n	Ratio of v_g to v_l
n_0	Ratio of v_g to v_l at the pressure of the loop p_0
n_t	Ratio of v_g to v_l at the pressure of the tank p_t
OTR	Volumetric oxygen transfer rate
P	Power input delivered by agitator or pump
P	Product
Po	Power number
p	Pressure
p_0	Pressure in loop (at transmitter)
p_A	Partial pressure of component A
p_O	Partial pressure of oxygen
p_t	Pressure in tank
R	Gas constant
R	Ratio of turbulent kinetic energy dissipation rate at wall to the mean energy dissipation rate per unit mass
Re	Reynolds number
r	Volumetric rate of reaction
$r(\mathrm{SO}_3^{2-})$	Volumetric rate of sulphite oxidation
S	Lactose
T	Absolute temperature

T	Tank diameter
t	Time
t_{mix}	Mixing time
$t_{mix,m}$	Mixing time for a degree of mixing of m
u	Linear velocity
u_d	Jet linear velocity at nozzle outlet
u_t	Linear velocity at nozzle outlet of bubbly flow
u_g	Superficial gas velocity
u_Z	Jet linear velocity at the end of the jet free path
V	Liquid volume
V_g	Volume of gas in dispersion volume
v	Volumetric flow rate
v_g	Gas flow rate
v_l	Liquid flow rate
W_{iso}	Power used for isothermal gas compression
Z	Jet free path length
z	Coordinate in the direction of motion

Greek Letters

Δp	Pressure difference
Δt	Sampling interval
ϵ	Gas holdup
ε	Local turbulent kinetic energy dissipation rate
μ	Dynamic viscosity
ρ_b	Density of base solution
ρ_l	Liquid density

Subscripts

0	Initial value
final	Terminal value
i	At interface
i	i'th time interval
in	In inlet
out	In outlet
T	At tank wall
Z	At the end of the jet free path

Abbreviations

AA	Aminoantipyrine
ABTS	2,2'-azino-bis(3-ethylbenzthiazoline-6-sulfonic acid)
CIP	Cleaning in place
LOX	Lactose oxidase
PFR	Plug flow reactor
RJH	Rotary jet head
RMS	Root mean square
RPM	Rounds per minute
TOPS	N-ethyl-N-sulfopropyl-m-toluidine
vvm	Volume gas per liquid volume per minute

Chapter 1

General introduction

Process intensification is the key to improvement of the economy of existing chemical or biochemical productions, and new plants, especially when designed for large volume/low added-value products must satisfy strict demands for high product yield at low utility costs. With the emergence of new fermentation routes for production of a number of chemical intermediates (e.g. ethanol or lactic acid) and for end-products of rapidly decreasing unit price (e.g. industrial enzymes, single cell protein, and even penicillin) the cost of mixing, mass transfer and heat transfer must be kept at a minimum since the utility costs often account for more than 20% of the total variable production costs. For this reason it becomes imperative to stimulate research and development related to the engineering aspects of bioprocesses. Progress in molecular biology frequently initiates the work towards a new, biochemically based synthesis route for a bulk chemical, but without a parallel development of customized engineering solutions to industrial design problems many high volume bioprocesses will not become economically competitive with existing chemical routes (Leib et al., 2001).

The primary topic of this thesis is liquid mixing and mass transfer. This topic is indeed of importance since some of the biggest challenges encountered during scale-up of laboratory bioprocesses are associated with mixing, mass transfer and heat transfer as exemplified in the following.

Mixing: From various textbooks in chemical reaction engineering (e.g. Levenspiel (1999)) we know that in multiple-reaction systems with at least one non-first order reaction the product yield is a function of the system segregation, which is governed by mixing. Segregation can result in gradients in e.g. substrate concentration, dissolved oxygen, temperature, and pH. Therefore segregation often leads to a decrease in productivity during scale-up due to the non-ideal behavior encountered in large-scale (for a good and short review see Lidén (2002)).

In continuous or fed-batch operation in large-scale there will almost certainly be gradients in the substrate concentration. The impact of such gradients has primarily been investigated for the two microbial systems Baker's yeast (*Saccharomyces cerevisiae*) and *Escherichia coli*.

In 1966 Hansford and Humphrey (1966) reported that the biomass yield in aerobic Baker's yeast cultivation was dependent on substrate mixing. The study was performed in continuous culture at low dilution rate, e.g. 0.02 h^{-1}, in a 5 L bioreactor. The authors used different feed distribution systems and observed that the yield of biomass increased with decreasing mixing time. Fowler and Dunlop (1989) used a scale-down model to investigate the influence of substrate gradients on the physiology of *S. cerevisiae* in aerobic culture. In scale-down systems a stirred laboratory reactor is typically connected to a plug flow reactor (PFR), and fermentation broth is circulated from the stirred reactor through the PFR and back to the stirred reactor. By adding feed in the PFR and controlling the residence time in the PFR inhomogeneities can be mimicked in a small-scale system. George et al. (1998) investigated the production of Baker's yeast in production scale (bubble column with a liquid volume of 120 m^3) and in laboratory scale (stirred reactor with a liquid volume of 10 L) using identical strain, medium and process control. The authors found that the biomass yield on molasses was 6.8% lower in production scale than in the laboratory reactor. Furthermore, the concentrations of fructose and glucose differed with sample location in the production scale reactor with up to 35 mg L^{-1} (the highest fructose concentration measured was 150 mg L^{-1}). A scale-down system was constructed to mimic the large-scale reactor (15 L stirred tank reactor connected to a PFR section with a total volume of 0.85 L). Feed was added in the PFR and the residence time in the PFR was 60 s. The biomass yield in this system was similar to the yield obtained in the production scale system. The oxygen tension in the stirred part of the scale-down system was above 20% of the saturation value, and there was no depletion of oxygen in the PFR-section. Hence the authors concluded that the low biomass yield in the industrial reactor was probably caused by gradients in the sugar concentration and not due to zones of low oxygen content. The Danish Baker's yeast manufacturer Danish Distillers A/S has also observed a lower biomass yield in their large-scale bubble columns than in laboratory-scale reactors (private communication).

Bylund et al. (1998) investigated aerobic fed-batch cultivation of a recombinant protein producing *E. coli* strain in a 12 m^3 reactor with a working volume of 8-9 m^3. Samples of glucose taken from three positions in the reactor showed gradients in the glucose concentration, and concentrations of up to 400 times the mean concentration were found when feed was added to the top of the tank. The biomass yield was up to 20% lower than in lab-scale experiments and more acetate was formed. Later Bylund et al. (1999) inves-

tigated the process further by the use of a scale-down model (15 L stirred tank reactor connected to a PFR section with a total volume of 0.85 L). The dissolved oxygen was always above 30% of the saturation value in both the stirred tank reactor and the PFR. The acetate yield was, however, lower in the scale-down system than in the 12 m^3 reactor. The authors suggested that the large decrease in biomass yield and the increased formation of acetate in large-scale was not directly caused by high local concentrations of glucose but rather by oxygen limitation caused by an increased metabolic rate in zones of high local glucose concentration. Schweder et al. (1999) investigated the effect of glucose gradients on mRNA levels of four stress related genes and three genes responding to oxygen limitation or glucose excess in *E. coli*. The investigation was performed in an aerated 30 m^3 fed-batch reactor with an initial liquid volume of 20 m^3 and by using a scale-down reactor (the same as Bylund et al. (1999)). It was found that the highest level of stress was found in zones with high substrate concentration, and that transcriptional activation occurred when cells were exposed to high substrate concentration for about 10 s. In 2001 Enfors et al. (2001) published the findings of a joint European project concerning physiological responses of *E. coli* to mixing in large-scale bioreactors. It was suggested that the reduced biomass yield in the large-scale is partly due to repeated production/reassimilation of acetate from overflow metabolism and mixed acid fermentation due to local zones with oxygen limitation.

A scale-down model has also been used to investigate the effect of substrate gradients in fed-batch production of lysine by *Corynebacterium glutamicum* (Schilling et al., 1999). In the design used by these authors inhomogeneities were not mimicked by the use of a stirred tank reactor connected to a PFR. Instead a number of circular discs with a hole in the center were inserted into a stirred tank reactor. 5 of these discs were inserted into a 42 L reactor stirred by 6 Rushton turbines. As reference the same reactor was used but with 2 Rushton turbines and no discs inserted. At a stirrer revolution rate of 400 RPM the time for 90% mixing was 10 s in the reference system while the mixing time was 130 s in the system containing the discs. In parallel exponential fed-batch cultivations the limiting substrate leucine was fed onto the liquid surface. Schilling et al. (1999) found that both the biomass yield and the lysine yield were lowered in the system with high mixing time compared to the reference.

Gradients in dissolved oxygen can result if the time constant for oxygen transfer is higher or comparable to the time constant for mixing. Sweere et al. (1988b,a) investigated the effect of fluctuations in dissolved oxygen tension on *S. cerevisiae*. Sweere et al. (1988b) investigated the effect of changing between oxygen unlimited and oxygen limited conditions by shifting between sparging with air and nitrogen in a continuous culture of *S. cerevisiae*. Sweere et al. (1988a) connected two reactors and circulated broth between them.

One reactor was sparged with air while the other was sparged with nitrogen and the system was operated as continuous culture. It was found that the biomass yield decreased and formation of ethanol, acetic acid, and glycerol increased when the circulation time (and thereby the mixing time) increased.

Gradients in pH can also influence bioprocesses. Thus Amanullah et al. (2001) investigated the influence of gradients in pH on the metabolism of a pH-sensitive strain of *Bacillus subtilis* by using a scale-down model consisting of a stirred tank reactor with a working volume of 1 L connected to a 50 mL PFR. 5 M NaOH was introduced in the PFR to keep pH constant at 6.5 in the stirred tank reactor. Different residence times in the loop were used, and it was found that product formation was shifted towards acetate instead of acetoin and 2,3-butanediol when the residence time in the PFR was 60 s or longer. Another example of a biological process which is sensitive to gradients in pH is the production of the bacteriocin, nisin, produced by fermentation by *Lactococcus lactis*. The pH window with optimal production of nisin is quite narrow and found around pH 5.5 (Parente and Ricciardi, 1999). Due to the production of lactic acid (and to some extent acetic acid and formic acid) base must be added to keep pH around the set-point value. According to Danisco A/S - a major producer of nisin - the yield of nisin is dependent on the mixing capabilities of the fermentor. Poor mixing results in local pH values far from the optimal value of 5.5.

Mass transfer: The overall rate of production is determined by the slowest reaction step. Since the volumetric rate of biomass production is proportional to the biomass concentration it is within wide limits possible to increase the rate of the bioreaction by manipulation of the liquid-feed substrate concentrations. If, however, one or more substrates have to be extracted from a gas phase the rate of mass transfer can easily become rate limiting, and the volumetric production rate cannot exceed the limit set by mass transfer. In aerobic fed-batch cultivation of Baker's yeast the maximum productivity - without production of the byproduct ethanol - is in principle achieved if the feed profile is exponential with the exponent being equal to the critical specific growth rate of the yeast, i.e. the maximum specific growth rate without overflow metabolism. This feed profile will, if retained up to high biomass concentrations often result in mass transfer limitations, which will result in production of the unwanted byproduct. Thus the feed profile giving the highest productivity is a profile which is still exponential but with a smaller exponent that depends on the volumetric mass transfer coefficient (Nielsen et al., 2003). However, in practise feeding is often performed at a constant rate to avoid mass transfer limitations.

Often scale-up is performed at constant specific gas flow rate (i.e. at constant vvm) (Nienow, 1998). Actually scale-up at constant vvm will give rise to an increase in the mass transfer coefficient in mechanically stirred bioreactors

if the specific power input is kept constant (Pedersen, 1997) and thus mass transfer becomes better upon scale-up, that is if the impeller is not flooded upon scale-up.

In industrial scale bioreactors it becomes excessively expensive to operate beyond a specific power input of 4-5 kW m^{-3}, a number which can be reached without problems in most laboratory-scale reactors. At constant specific power input the specific gas flow in vvm which can be used without flooding a Rushton turbine also decreases with increasing scale when geometric similarity is maintained upon scale-up. Since it is possible both to operate at a higher specific power input on the small scale, and a higher specific gas flow rate can be used without flooding the impeller, it is possible to reach higher volumetric mass transfer coefficients in lab-scale reactors than in industrial bioreactors. The use of antifoam will result in a decrease in the volumetric mass coefficient and in the large scale it may not be possible to counter this by increasing stirrer speed or gas flow rate. Recently, various mechanical systems have been proposed for foam knockdown, e.g. the inverted hollow spinning cone, a device fitted on the impeller shaft (Cooke et al., 2004). The inverted hollow spinning cone has proved to be efficient in pilot scale culture of *B. subtilis*, a challenging cultivation in terms of foaming (Stocks et al., 2005).

Heat transfer: A high rate of mass transfer can be obtained if a high power input and a high gas flow rate is allowed. If oxygen is a substrate then enriched air or even pure oxygen can be used to enhance the rate of mass transfer. Still, the productivity of the bioreactor can be limited by its capacity for removal of the metabolic heat generated by the bioreaction. In jacketed bioreactors the specific heat transfer area (i.e. the heat transfer area per reactor volume) decreases with $V^{-1/3}$ upon scale-up, where V is the liquid volume. Consequently in large scale, jacketed bioreactors cannot be used in highly heat-evolving processes. Even in bioreactors of the stirred-tank type with heat exchanger surface placed as tubes on the inside of the reactor vessel it may become impossible in large scale to achieve the high volumetric production rate that corresponds to a high mass-transfer/bioreaction rate. Heat must be transferred at a modest temperature driving force from a medium of temperature around 30°C. This leads to high cooling costs, and the required heat transfer area may be difficult to fit into the reactor. Furthermore, the presence of cooling coils inside the tank may lead to relatively stagnant areas behind the coils and a decrease in the volumetric mass transfer coefficient. According to NNE A/S external loops with a plate-type heat exchanger installed have been used in some cases in highly heat-evolving bioproceses. Plate-type heat exchangers have the advantage that the overall heat transfer coefficient is around 10 times higher than with cooling coils when media with physical properties like water are used.

The remainder of this chapter will give a review of mixing and mass transfer. The literature on this subject is vast. It is outside the scope of this thesis to present all this knowledge to the reader. Hence only the most important topics for this thesis work will be presented.

1.1 Mixing

1.1.1 Mixing time measurements

Mixing time, i.e. the time to reach a certain degree of uniformity in miscible liquids, is usually obtained by quantitative stimulus/response techniques where a tracer pulse with properties different from the bulk liquid is injected and the response measured. The location of the measurement sensor(s) is often decided on the basis of qualitative mixing visualization experiments.

Mixing visualization with colorimetric methods

A very simple technique to visualize the flow pattern and the rate of mixing in a transparent system is to inject a concentrated dye pulse and observe the dye movement. However, when a colored tracer is added it is not possible to observe the last region where mixing takes place because this poorly mixed region cannot be seen due to the presence of dye in front of or behind it (Brown et al., 2004). Decolorization techniques where the last point to be mixed remains colored while the rest of the tank content has cleared are therefore to be preferred.

With decolorization techniques the entire content of the transparent vessel is colored using one chemical, and then a pulse of another chemical is added which will react and remove the color. Poorly mixed regions are the last ones to become transparent. Two different decolorization techniques are commonly used: Acid-base reactions in the presence of a suitable pH-indicator such as bromo-phenol blue (blue to yellow) or phenolphthalein (pink to colorless) or the reaction between iodine and thiosulphate in the presence of starch (see Brown et al. (2004) for specific guidelines)

In a number of studies decolorization methods like the iodine/thiosulphate method have been used to estimate mixing time, which is then determined as the period until disappearance of the last traces of color (e.g. Cronin et al. (1994)). One obvious problem with this kind of method is that it is difficult to relate the disappearance of the last wisps of color with a degree of mixing.

Recently, a more quantitative colorimetric method for obtaining mixing time was developed which employs two acid-base indicators, methyl red (red to yellow) and thymol blue (yellow to blue) (Melton et al., 2002). Through

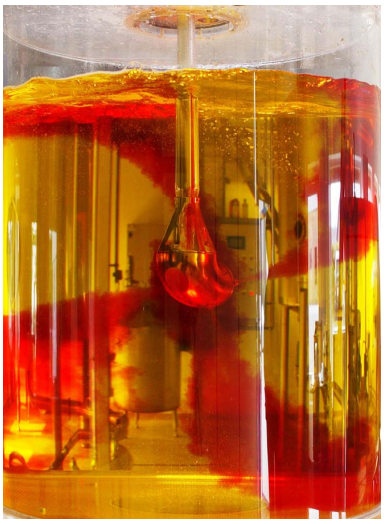

Figure 1.1. Principle of colorization/decolorization method. In this example the water in the tank contains an acid/base indicator and a base pulse is injected through a rotary jet head whereby the color changes from yellow to red. This is an example of a colorization experiment.

appropriate choice of the initial pH value of the bulk liquid and the size of the acid/base pulse, a yellow liquid will appear only in those regions where mixing is achieved within a specified degree. Delaplace et al. (2004) extended this method with colorimetric analysis of digital images captured from a video shot during the mixing process and showed how the time to 90% mixing could be obtained.

Quantitative stimulus/response experiments

When quantitative measurement of mixing time is performed by the injection of tracer a number of issues have to be considered. The ideal technique for obtaining mixing times should fulfill the following

- The measuring volume should be as small as possible to avoid averaging effects.
- The probe should have negligible response time.
- Disturbance of the bulk flow by probes and probe supports should be minimized.
- Physical parameters (e.g. viscosity) of the system should not be changed by the tracer.
- It should be applicable to systems containing gas.

- The technique should ideally be applicable to biological media.
- Ideally, the method can be used repeatedly without changing the bulk liquid.

In reality none of the techniques commonly used fulfill all these points. In the following sections the different techniques are reviewed and their strengths and weaknesses are highlighted.

The conductivity method

The most commonly used method for determination of mixing time is based on measurement of conductivity after injection of a concentrated salt pulse.

The advantages of the conductivity method are that conductivity probes have very low response times, and that probes can be designed with very small measuring volume. A number of types of electrodes have been used for measurements of mixing time. Khang and Fitzgerald (1975) developed a probe with a point electrode shielded by a coiled wire electrode, which is recommended by e.g. Brown et al. (2004) for mixing time studies.

One disadvantage of the method is that it is not suited for systems containing gas unless special precautions are taken. This is due to occurrence of non-conductive gas between the electrodes, which will give rise to a high noise to signal ratio which renders it more or less impossible to determine mixing time. Pinelli et al. (2001) and Otomo et al. (2003b) showed that the conductivity method can be used with success in systems containing gas if the probe is shielded by a cage containing holes with a diameter 0.5 mm. Experiments without gas showed that the cage does not influence the measurements significantly. However, the level of noise was reduced significantly since only very small bubbles will be entering the cage.

Another drawback of the method is that only a limited amount of experiments can be performed before the liquid needs to be changed due to the accumulation of salt which will decrease the sensitivity of the probe. If mixing time is to be measured in fermentation media the sensitivity will also be poor since most fermentation media are good conductors.

The pH method

Mixing time has been determined in a number of studies (e.g. Singh et al. (1986); Marten et al. (1997)) by following the response in pH after injection of acid or base tracer.

An advantage of using pH probes is that they are not sensitive to gas bubbles. The technique can also be used during a fermentation without affecting the process significantly (Marten et al., 1997). However, if acid is produced in the fermentation, the mixing time needs to be much smaller than the char-

acteristic time for acid production, unless a model is set up which includes acid production.

The major disadvantage of using the pH method is that pH probes have long response times (on the order of some seconds) compared to e.g. conductivity probes. Thus pH probes should not be used for mixing time measurements in laboratory-scale systems where the mixing time can be a few seconds or in other systems with very low mixing time. Another disadvantage of the method is that large pulses of acid and base are required to get good sensitivity if the method is used in fermentation media which typically have high buffer capacity.

The thermal method

In the thermal method a liquid pulse with a temperature different from that of the bulk liquid is added, and the temperature is measured by thermocouples (e.g. Hoogendoorn and den Hartog (1967); Masiuk (2000)).

A disadvantage of this technique is that it is not suitable if e.g. the viscosity of the bulk liquid is sensitive to the temperature. Furthermore very large pulses are needed for production scale equipment to achieve good sensitivity.

The radiotracer method

In the radiotracer method a radioactive isotope is used as tracer and the radioactivity is measured by scintillation counters (e.g. Pedersen (1992); Pedersen et al. (1994); Dominguez et al. (1999)).

An obvious advantage of using radioactive tracers is that the method is noninvasive since the scintillation counters will be placed on the outside of the reactor wall. Other advantages of the method are that it is insensitive to gas bubbles, it can be used repeatedly without changing the liquid, and it can be used during fermentations with the right choice of tracer.

A major disadvantage of the method is that the fraction of the working reactor volume 'seen' by the scintillation counter can be quite large, especially in small-scale systems with a small aspect ratio. This will lead to considerable averaging effects. In the study by Pedersen (1992), which was performed in a tank with a working volume of 10 L and with an aspect ratio of 1.72, the liquid volumes seen by the detectors were between 4.72 and 7.54 liters depending on the position of the scintillation counters (the largest of these volumes is seen by the counter placed in the middle of the tank). Thýn et al. (1976) performed mixing time experiments using conductivity electrodes with different measuring volumes and showed that the measured mixing time decreases with increasing fraction of probe measuring volume to vessel volume due to averaging. In a geometrically similar vessel with a diameter of 0.2 m and with a 6-bladed Rushton turbine revolving at 300 RPM, the time to 95% homogeneity was shown to decrease from 13.6 s when

the fraction was 10^{-3} to 5.6 s when the fraction was equal to 0.754, the fraction found for one of the scintillation counters used in the work by Pedersen (1992). Another disadvantage is the concern in production facilities about working with radioactive isotopes.

The fluorophor method

Mixing time measurements with a fluorophor as tracer has also been reported in the literature. An example is the study by Einsele et al. (1978) who obtained mixing times by measuring fluorescence after injection of a tracer of quinine in a culture of *S. cerevisiae*.

The advantages and disadvantages of the fluorophor method are much the same as with the conductivity method. Advantages are low response time and the possibility of very small measuring volume. However, as with the conductivity method, the sensors are very sensitive to bubbles. Furthermore, the method cannot be used repeatedly without changing the liquid due to high background fluorescence. If mixing time is measured during fermentations the high background fluorescence of many fermentation media will also result in poor sensitivity.

Processing of mixing time data

Data obtained by the conductivity, pH, fluorophor, radiotracer or thermal method must be processed to obtain a mixing time for the investigated system.

Normalized concentrations/outputs E are obtained by the following equation

$$E = \frac{c(t) - c_0}{c_{\text{final}} - c_0} \tag{1.1}$$

Mixing is often postulated to be a first order process (e.g. Pedersen et al. (1994); Marten et al. (1997)). If that is indeed the case there will be an exponential relationship between the difference in concentration to the final level and t

$$|E - 1| = \left| \frac{c(t) - c_{\text{final}}}{c_{\text{final}} - c_0} \right| = \exp\left(-k_{mix} t\right) \tag{1.2}$$

k_{mix} is the characteristic mixing constant which is equal to the reciprocal of mixing time for 63.2 % mixing. k_{mix} can be obtained as the slope of a logarithmic plot of $|E-1|$ versus t, and it can be used to calculate the mixing time, t_{mix}, for any arbitrary degree of mixing m if mixing is indeed a first order process

$$t_{mix,m} = -\frac{1}{k_{mix}} \ln\left(1 - m\right) \tag{1.3}$$

If the method mentioned above is used to find mixing time, the time between injection of tracer to the initial probe response will be neglected since it

will only be the linear part of a plot of $\ln(|E-1|)$ which will used to find k_{mix}. Some authors find the mixing time as the mixing time found by linear regression plus the time between injection and the initial response (e.g. Li et al. (1990)).

Brown et al. (2004) propose that the 95% mixing time should instead be found as the time from injection of tracer until the normalized output is within ±5% of the final equilibrium value. In some cases this can be difficult to find directly from a plot of E versus t because of the fine scale around the endpoint. Brown et al. (2004) suggest that the data should be plotted in terms of a log variance as a function of time

$$\log(\sigma^2) = \log([E-1]^2) \tag{1.4}$$

and the 95% mixing should be read where $\log(\sigma^2)$ equals $2\log(0.05) = -2.60$. This graph is more accurate for obtaining the 95% mixing time. If more than one probe is used the responses of all the M probes can be combined and weighed towards the probe showing the largest deviation from equilibrium. This is achieved using an RMS variance which again is plotted versus time to find the time to 95% mixing

$$\log(\sigma^2_{RMS}) = \log\left(\frac{1}{M}\sum_{i=1}^{M}[E_i-1]^2\right) \tag{1.5}$$

1.1.2 Mixing in mechanically stirred vessels

The most important type of bioreactor in use in the bioindustry today is the stirred tank bioreactor. The reactor is typically cylindrical with an aspect ratio H/T of 2-5. The reactor is equipped with a stirrer, consisting of a shaft onto which one or more impellers are mounted. The reactor is equipped with baffles to break the vortex that would otherwise form in the reactor, and thereby decrease the mixing efficiency. Typically 4 equally spaced baffles are used (Nielsen et al., 2003) having a width of 1/10 or 1/12 of the tank diameter. Air is introduced via a sparger, which is located below the lowest of the impellers. The sparger may be a point sparger, i.e. a single open tube, or a ring with fine orifices. The ring sparger typically has a diameter slightly smaller than the impeller. Figure 1.2 shows the inside of a bioreactor which in this case is equipped with coils for cooling.

Several different impellers are available (see figure 1.3). They can essentially be divided into two groups: radial flow impellers and axial flow impellers. Examples of radial flow impellers are the Rushton turbine, the Chemineer CD6, the Chemineer BT6 (all depicted in figure 1.3) and the Scaba 6SRGT. The 3 last mentioned are all rather similar in shape. Examples of axial flow impellers are the Lightnin A315 and the Chemineer Maxflo W (see figure

Figure 1.2. The inside of a stirred tank bioreactor. The impeller shaft with two 6-bladed Rushton turbines, baffles and internal cooling coils are seen in the picture. The picture was adopted from Nielsen et al. (2003)

1.3). Both of these impellers are known as high-solidity (solidity refers to the degree of occlusion of an impeller's swept circle by its blades) hydrofoil impellers. The axial flow impellers can be used in either down-pumping or up-pumping mode. The 45° pitched blade turbine can be considered a mixed flow impeller since the flow is neither radial nor axial.

The radial flow Rushton turbine used to be the impeller of choice in the bioindustries but more modern impellers offer a number of advantages which will hopefully become apparent later in this section.

Figure 1.3. Selected impeller types. In the top row three different radial flow disc turbines are shown: A 6-bladed Rushton turbine (left), a Chemineer CD6 (middle) and a Chemineer BT6 (right), which is very similar in shape to the Scaba 6RSGT. In the bottom row a pitch blade turbine (left) and a Chemineer Maxflo W impeller (a high-solidity hydrofoil impeller) are shown.

A number of features are important for mechanically stirred systems and

determines which kind of impeller(s) to install. Amongst others they are Nienow (1998)

- Power drawn and torque.
- Air dispersion capabilities and the effect of gassing on power drawn.
- Bulk fluid and gas phase mixing.
- Volumetric oxygen transfer coefficients.

In this section the first and second item in the list will first be treated shortly to introduce certain important concepts. The primary focus of the section is, however, liquid mixing which will be treated in detail. Finally some recommendations are given concerning which impeller types should be chosen in a given situation. A review of oxygen transfer correlations will be given later in the chapter

The literature on the subject is extensive. A very good review that covers most aspects of importance for mechanically stirred bioreactors is found in Nienow (1998) and a good and short review by the same author is found in Nienow (2000). Another good reference is Grenville and Nienow (2004) that only deals with blending of miscible liquids.

Power drawn and torque

Some fundamentals will be described first. The Reynolds number for a stirred system, Re is found from

$$Re = \frac{\rho_l N D^2}{\mu} \tag{1.6}$$

where ρ_l is the liquid density, N is the impeller speed, D is the impeller diameter, and μ is the dynamic viscosity (in any consistent set of units). According to Nielsen et al. (2003) the flow is fully turbulent if $Re > 10,000$, laminar for $Re < 10$, and transitional in between. Nienow (1998) states that Re should be above $\sim 20,000$ to be fully turbulent.

The dimensionless power number, Po, is defined as (Nielsen et al., 2003)

$$Po = \frac{P}{\rho_l N^3 D^5} \tag{1.7}$$

where P is the power drawn (and again in consistent units). The power number is dependent on the flow regime, see figure 1.4. For laminar flow the power number is inversely proportional to Re, while it is constant in the turbulent range. In the transitional range the relationship is more complex since both inertial and viscous effects are of importance. In the following I

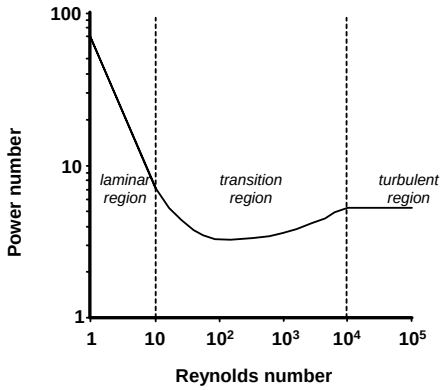

Figure 1.4. Schematic representation of the power number, Po, with Reynolds number, Re, for a 6-bladed Rushton turbine in a baffled tank. The picture was adopted from Nielsen et al. (2003).

Table 1.1. Selected power numbers for single impellers in the turbulent regime. Adopted from Nienow (1998).

Type	Po
6-bladed Rushton turbine	5.00
Scaba 6SRGT	1.45
4-bladed, 45° pitch turbine	1.27
6-bladed, 45° pitch turbine	1.70
Lightnin A315	0.84

will only deal with the turbulent regime. A selection of power numbers for single impellers in baffled tanks are shown in table 1.1.

Power is also related to torque M in the following way

$$P = 2\pi NM \tag{1.8}$$

By manipulation of Eq.(1.8) and (1.7) it can be inferred that for two impellers of equal impeller diameter (referred to by indices 1 and 2) drawing the same power, the relative torque of the two impellers is given as

$$M_1 = M_2 \left(\frac{Po_1}{Po_2} \right)^{1/3} \tag{1.9}$$

Thus the Rushton turbine requires a low speed and a high torque compared to the other impellers listed in table 1.1. The torque determines the size of shafts, mechanical seals, gearboxes etc., and it is consequently cheaper to install a low power number impeller (Nienow, 1998).

In multiple impeller systems the power number is dependent on impeller spacing. For dual Rushton turbines Hudcova et al. (1989) found that the

power number was 2 times the power number for a single impeller when the impeller spacing was equal to or above the tank diameter and smaller when the spacing was lower. According to Nienow (1998) the same applies for e.g. the axial flow hydrofoil impeller Lightnin A315.

Air dispersion capabilities and the effect of gassing on power drawn

The power drawn is affected by aeration. When gas is sparged beneath an impeller gas bubbles are drawn to regions of low pressure. With e.g. Rushton turbines this results in the formation of gas filled areas (called cavities) behind the impeller blades. The formation of these cavities depends on the ratio between the volumetric gas flow rate and the stirrer speed. The cavities will grow with increasing gas flow rate at a given stirrer speed until eventually the impeller becomes fully immersed in gas, a condition called flooding (Nielsen et al., 2003), see figure 1.5. Flooding is not desired since it will give poor gas dispersion and will be followed by a drop in the volumetric mass transfer coefficient, $k_l a$.

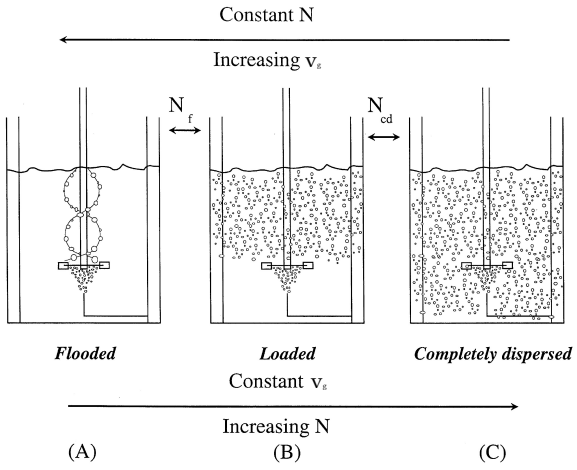

Figure 1.5. Schematic representation of the transition between the conditions (A) flooded (B) loaded (C) completely dispersed. The picture was adopted from Paglianti et al. (2000).

In low viscosity systems the power drawn at constant impeller speed generally falls with increasing gassing rate due to the growing cavity size. This is a severe problem with Rushton turbines where the power drawn can easily drop to 40-50 % of the unaerated power drawn at a given stirrer speed (for an in depth discussion of this phenomenon see Nienow et al. (1985); Nienow (1998)). In case the motor is sized for the full-speed unaerated situation the installed power of the motor will be poorly utilized at aerated conditions.

With radial flow disc turbines shaped like the Chemineer CD6, the Chemineer BT6, and the Scaba 6SRGT the decrease in power drawn upon gassing is much smaller, essentially because cavities do not form behind the blades (Nienow, 1998). In water Saito et al. (1992) found that the 6-bladed disc turbine Scaba 6RSGT essentially maintained the same power number in the gassed situation as in the ungassed until flooding occurred. Compared to a 6-bladed Rushton turbine the Scaba 6RSGT was able to disperse a little less than 3 times the amount of gas at equal power drawn and equal impeller diameter before flooding occured. Vasconcelos et al. (2000) studied a number of 6-bladed disc turbines with different blade shapes. They found the power number upon gassing remained more or less unchanged when the blade shape was similar to the one of the Chemineer BT6 and Scaba 6SRGT or to that of the Chemineer CD6. The blade shape similar to that of the Chemineer CD6 did, however, lead to a little more decrease in power drawn upon gassing than the shape similar to the Chemineer BT6 and the Scaba 6SRGT.

Down-pumping pitched-blade turbines flood easily and they are not recommended for gas dispersion tasks (Nienow, 1998). Down-pumping high-solidity hydrofoil impellers like the Lightnin A315 do not flood as easily as down-pumping pitched-blade turbines or hydrofoils of low solidity. The power drawn at aerated conditions is, however, dependent on the choice of sparger (Otomo et al., 2003a). Otomo et al. (2003a) studied a down-pumping Lightnin A315 hydrofoil and showed that a transitions in the aerated power characteristics took place when the impeller went from what is known as indirectly loaded (with axial downwards flow and small cavities) to what is known as directly loaded (with radial flow and large cavities formed). With a ring sparger this transition took place at a higher aeration rate than when a point sparger was used. At low impeller speed the power number remained virtually unchanged on gassing until the transition occurred. At higher impeller speeds the power number gradually declined before the transition. Thus it is very difficult to predict gassed power characteristics of a down-pumping high-solidity hydrofoil impeller, even more so than for a Rushton turbine. Furthermore, the down-pumping high-solidity hydrofoil impellers give rise to torque instabilities upon gassing (McFarlane and Nienow, 1996). This can decrease the life time of the stirrer system. Hari-Prajitno et al. (1998) showed that the maximum torque instability was found at the transition point between indirectly and directly loading, and for a down-pumping Lightnin A315 torque fluctuations of up to 25 % were reported.

Up-pumping high-solidity hydrofoils are much less prone to torque fluctuations than their down-pumping counterparts. Furthermore, the power drawn on gassing remains virtually unchanged. This has been shown with the up-

pumping B2 high-solidity hydrofoil impeller[1] (Hari-Prajitno et al., 1998) and also with up-pumping Lightnin A315 impellers (Nienow and Bujalski, 2004). Thus up-pumping high-solidity hydrofoil impellers are very suited for gas dispersion.

Single impeller systems

Most studies with a single impeller operating in the turbulent range have been performed in unaerated tanks with an aspect ratio of 1, i.e. with liquid height H equal to the tank diameter T and the results of those studies will be reported and explained here. Ruszkowski (1994) investigated mixing in a tank with a diameter of $T = 0.609$ m and $H = T$ with a range of different impellers (a 6-bladed Rushton turbine, a propeller, and a variety of pitched blade turbines with different D/T ratios, blade angles, and number of blades). He found that the mixing time could be written as

$$t_{mix,95\%} = 5.3\frac{Po^{-1/3}}{N}\left(\frac{D}{T}\right)^{-2} \tag{1.10}$$

in any consistent set of units.

Cooke et al. (1988) obtained mixing time data in $H = T$ tanks of two different scales (20 L and 4.3 m^3) using two different radial flow impellers, the 6-bladed Rushton turbine and an ICI gasfoil and with different D/T ratios. They correlated the data by the following equation

$$t_{mix,90\%} \propto \frac{Po^{-1/3}}{N}\left(\frac{D}{T}\right)^{-2.2} \tag{1.11}$$

From this information it appears that the mixing time for a single impeller system can be written as

$$t_{mix} \propto \frac{Po^{-1/3}}{N}\left(\frac{D}{T}\right)^{-2} \tag{1.12}$$

Two different theories have been suggested to explain turbulent mixing with a single impeller. One is the bulk flow model while the other is known as the turbulence model. Since the latter agrees better with experimental results than the former, only the latter will be presented here (see Nienow (1997) for a thorough explanation of both concepts).

In the turbulence model mixing time is taken to be inversely proportional to the turbulent energy diffusion, i.e.

$$t_{mix} \propto \left(\frac{\varepsilon}{L^2}\right)^{-1/3} \tag{1.13}$$

[1]The B2 impeller was developed by the group of Alwin Nienow at the University of Birmingham in collaboration with Hayward-Tyler.

where L is the integral scale of the turbulence fluctuations and ε is the local turbulent kinetic energy dissipation rate (measured per unit mass, i.e. with unit length^2 time^{-3}). The primary question in this approach is what values of ε and L one should use. The turbulent kinetic energy dissipation rate varies with position and is at the maximum close to the impeller. In the analysis by Nienow (1997) it is assumed that the slowest mixing will be where ε is at the lowest value, i.e. close to the wall where $\varepsilon = \varepsilon_T$. Furthermore it is assumed that the integral scale is proportional to the tank diameter T and it is used that $\varepsilon_T = R\frac{P}{\rho_l V}$ where R is the ratio of turbulent kinetic energy dissipation at the wall to the mean energy dissipation rate per unit mass. Thus Eq.(1.13) can be written as

$$t_{mix} \propto \left(\frac{P}{\rho_l V}\right)^{-1/3} T^{2/3} R^{-1/3} \tag{1.14}$$

Impellers with a large D/T ratio are known to distribute the energy dissipation more evenly than impellers with small D/T ratio. On this ground it is assumed that $R \propto (D/T)^{\alpha}$ which is inserted in 1.14 to give

$$t_{mix} \propto \left(\frac{P}{\rho_l V}\right)^{-1/3} T^{2/3} \left(\frac{D}{T}\right)^{-\alpha/3} \tag{1.15}$$

Using the relation between power and power number and the geometry of a $H = T$ tank this equation can be written in the form

$$t_{mix} \propto \frac{Po^{-1/3}}{N} \left(\frac{D}{T}\right)^{-5/3} \left(\frac{D}{T}\right)^{-\alpha/3} \tag{1.16}$$

The results of Ruszkowski (1994) and Cooke et al. (1988) suggest that α should be equal to 1 giving the overall equation

$$t_{mix} \propto \frac{Po^{-1/3}}{N} \left(\frac{D}{T}\right)^{-2} \tag{1.17}$$

When this equation is rewritten is terms of power input per unit mass and using the results of Ruszkowski (1994) the following equation emerges

$$t_{mix,95\%} = 5.9 \left(\frac{P}{\rho_l V}\right)^{-1/3} T^{2/3} \left(\frac{D}{T}\right)^{-1/3} \tag{1.18}$$

where the variables are in SI-units.

The following conclusions can now be drawn for single impellers in tanks of $H = T$ operating in the turbulent regime

- All impellers of equal diameter give the same mixing time at a given power input.

- A larger impeller diameter will for the same power input result in a shorter mixing time.
- When scaling up at constant specific power input the mixing time increases with the tank diameter raised to the power of 2/3 or stated differently with the volume to the power of 2/9.

The first conclusion may seem counterintuitive but is supported by a large amount of experimental data.

Much less work has been done on the effect of gassing on the mixing time and the literature may seem rather confusing. This may in part be due to the fact that erroneous conclusions have been drawn from measurements with conductivity probes which are not suited for measurements in gassed systems unless special precautions are taken (Pinelli et al., 2001; Otomo et al., 2003b). The subject is, however, also often presented as more or less a body of unrelated facts (see e.g. the review of multiple impeller systems by Gogate et al. (2000), pp. 115-117 to get an impression). According to Nienow (1998) the presence of air may lead to a reduction in mixing time when the impeller is flooded. This is, however, not desired. Several studies have shown - provided that the impeller is not flooded - that for a given impeller and at equal energy dissipation rates there is no difference between the mixing time obtained in the aerated and unaerated case (e.g. the previously cited studies of Cooke et al. (1988); Pinelli et al. (2001); Otomo et al. (2003b) and the study of Haß and Nienow (1989) who obtaining mixing times using the decolorization technique with iodine and thiosulphate). Thus Eq. (1.18) can still be used. The effect of gassing will for e.g the Rushton turbine lead to a decrease in the power number and in this situation the stirrer speed used to reach a certain power input will be larger in the aerated case than in the unaerated.

Multiple impeller systems

In systems of high aspect ratio H/T multiple impellers are needed. It is known that when multiple radial flow impellers are used the mixing time increases significantly compared to a $H = T$ tank with similar volume. This is due to zoning (Nienow, 1998; Cronin et al., 1994). Vasconcelos et al. (2000) tested various designs of 6-bladed disc turbines in a dual impeller system and found that the mixing time was independent of blade shape and it can be concluded that all impellers of this type will give rise to zoning. Cooke et al. (1988) found that the mixing time increased with H/T when comparing data obtained in two tanks of $H = T$ (20 L and 4.3 m^3 volume) stirred by a single impeller with a tank of $H = 3T$ (60 L) stirred by 3 impellers. They gave the

following equation for multiple Rushton turbines or ICI gasfoils

$$t_{mix,90\%} = 3.3\frac{Po^{-1/3}}{N}\left(\frac{D}{H}\right)^{-2.43} \tag{1.19}$$

in any consistent set of units. They did not elaborate on whether the increase in mixing time was due to the increase in H/T or in the number of impellers used. With combinations of radial and axial flow impellers (radial impeller as bottom impeller with one or two down-pumping axial flow impellers above) the mixing time decreased by approximately 50%. The equation can also be used in aerated systems if no impellers are flooded.

With axial flow impellers much less zoning occurs than with radial flow impellers. Otomo et al. (1995) studied different dual impeller systems in a vessel with $H/T = 2$ and a volume of 0.59 m^3 using the conductivity technique. At identical power drawn a decrease in the mixing time of 50% was observed when two down-pumping Lightnin A315 hydrofoil impellers were used instead of two 6-bladed Rushton turbines or two 6-bladed hollow blade turbines. Hari-Prajitno et al. (1998) investigated mixing using different impeller systems in a tank with a liquid volume of 0.276 m^3 and $H/T = 2$ using the iodine/thiosulphate decolorization technique. Dual impeller configurations with two up-pumping or one up-pumping and one down-pumping B2 high-solidity hydrofoil impeller were compared to a dual Rushton turbine configuration and a set-up with two down-pumping Lightnin A315 impellers. The B2 impellers have either 30° or 45° angle of attack. Most of the work was done on the impeller with 30° angle of attack and only results for this impeller will be reported here. With two up-pumping B2 impellers the mixing time was lowered with approximately 40-45% compared to a dual Rushton system represented by Eq.(1.19). The best combination in terms of mixing was the combination of one up-pumping and one down-pumping B2 impeller with a reduction in mixing time of a little more than 60%. This combination did, however, loose more power on gassing than the combination of two up-pumping B2 impellers. Vrábel et al. (2000) studied mixing in two scales, a tanks with a liquid volume of 8 m^3, aspect ratio 1.59, and with 3 impellers and another with liquid volume 22 m^3 with aspect ratio 3.13 and using 4 impellers. Two different impeller systems were studied: one with Rushton turbines and another with the radial flow disc turbine Scaba 6RSGT as bottom impeller and the axial hydrofoil impellers Scaba 3HSP in up-pumping mode as the upper impellers. At equal power drawn the mixing time was reduced approximately 50% with the axial flow/radial flow combination compared to the case with Rushton turbines.

Choosing the right impellers

All impellers of the same D/T ratio are equally energy efficient for bulk blending in the turbulent range in single impeller systems with $H = T$. If liquid mixing is the only thing to consider in such a system the choice of impeller may therefore seem of no importance. However, the power number of the impeller determines the torque and consequently an impeller with a low power number would be preferred since for a given D/T ratio the price of installation will be lower. Alternatively for retrofitting at equal torque, power and impeller speed, the mixing time can be lowered by installing a large diameter impeller with small power number instead of a small diameter impeller with high power number. For a multiple impeller system axial flow impellers - whether up-pumping or down-pumping - give much lower mixing time than radial flow impellers.

In a multiple impeller system where both gas dispersion and liquid mixing is of importance the right choice of impellers seems to be to use high-solidity hydrofoil impellers in the up-pumping mode or to use a modern radial flow disc turbine (like e.g. the Chemineer BT6 or the Scaba 6SRGT) as the bottom impeller in combination with high-solidity hydrofoil impellers in the up-pumping mode.

1.1.3 Mixing by stationary jets

Various reviews on mixing by jets are available. The book chapters by Revill (1992) and Grenville and Nienow (2004) can be recommended.

Mixing by turbulent jets is common in the chemical process industries and if a transport pump is already available it is a very cheap mixing solution. In jet mixing a fast moving stream of liquid is injected into the bulk. The difference in velocity between the jet and the bulk liquid creates a mixing layer at the jet boundary, which grows in size in the direction of the flow, entraining and mixing bulk liquid into the jet (Revill, 1992). An example of a jet mixed tank is illustrated in figure 1.6. Side entry jets or axial jets are typically used. If placed near the tank floor the jet should point towards the liquid surface and vice versa.

According to Revill (1992) a jet can be considered to be fully turbulent above a Reynolds number Re of about 1000-2000 and laminar below a Re of about 100 and transitional in between. Fox and Gex (1956) observed a change in mixing time functionality at a Re of 2000. Likewise, Lane and Rice (1981) correlated their mixing time data with separate equations for $100 < Re < 2000$ and for Re above 2000. Other authors (e.g. Grenville and Nienow (2004) do, however, state that Re should be above 10,000 to get a fully turbulent jet.

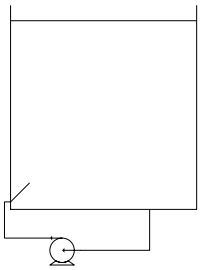

Figure 1.6. Example of a jet mixed tank.

One of the earliest studies of jet mixing in the turbulent range is the study of Fossett and Prosser (1949) who injected a tracer solution into the recirculation loop of a tank of diameter $T = 1.524$ m with an inclined side entry jet. The mixing time was defined as the time from the start of injection to the time when there was no difference between the concentration measured by a probe in the tank and the concentration measured by a probe immersed in a solution of the final concentration. The solution was usually injected as a very long pulse. When the total injection time was around half of the total time for mixing they correlated their data by

$$t_{mix} = 9.0\frac{T^2}{u_d d} \tag{1.20}$$

where u_d is the jet velocity at the nozzle outlet and d is the nozzle diameter (SI units are used in all Eqs. 1.20 - 1.30). For a short pulse addition it was proposed that the constant should be changed from 9.0 to 4.5. The work by Fossett and Prosser (1949); Fossett (1951) is presently of little qualitative use. It does for example not seem likely that an equation of this type should be able to predict mixing times for a tank of arbitrary aspect ratio H/T.

A number of other studies have been performed in the turbulent regime where the authors correlated their data by expressions similar to that of Fossett and Prosser (1949) but with a factor to account for liquid depth (e.g Okita and Oyama (1963) who studied side entry jets), i.e.

$$t_{mix} \propto \frac{T^{1.5}H^{0.5}}{u_d d} \tag{1.21}$$

For $Re < 5000$ Okita and Oyama (1963) correlated their data with an expression in the following form

$$t_{mix} \propto \frac{T^{1.5}H^{0.5}}{Re\, u_d d} \tag{1.22}$$

Fox and Gex (1956) used mixing visualization with a colorimetric acid/base method to obtain mixing times in tanks with diameters of 0.30 m and 1.52

m using water, glycerol and vegetable oil as model liquids, while mixing time was determined in a tank with diameter 4.27 m by iodometry (the tank contained oil, and a small amount of saturated oil was injected in the bulk containing unsaturated oil. Samples were then taken during an experiment and analyzed). In the study they changed both tank diameter T, liquid height H, jet diameter d, jet velocity u_d, dynamic viscosity μ and density ρ_l. The data for the single inclined side entry jet configuration studied were correlated by the following equations depending on whether the flow was fully turbulent or in the transitional range

$$\begin{aligned} t_{mix} &= \frac{ATH^{0.50}}{(u_d d)^{0.67} g^{0.17}} \qquad (1.23) \\ A &= \frac{7.8 \cdot 10^5}{Re^{1.33}} \quad \text{for} \quad 250 < Re < 2000 \\ A &= \frac{120}{Re^{0.17}} \quad \text{for} \quad 2000 < Re < 1.6 \cdot 10^5 \end{aligned}$$

where g is the gravitational acceleration. Note that with this correlation and for a given liquid and tank geometry the mixing time in the turbulent regime is not correlated by $t_{mix} \propto {}^{1}/_{(u_d d)}$ but with $t_{mix} \propto {}^{1}/_{(u_d d)^{0.83}}$, while in the transitional regime $t_{mix} \propto {}^{1}/_{(u_d d)^2}$

Lane and Rice (1981) measured mixing times in vessels with both side entry jets and axial jets and correlated their results in a form similar to that used by Fox and Gex (1956).

Using the same approach as Nienow (1997) but for turbulent stationary jets instead of impellers, Grenville and Tilton (1996) proposed that the mixing time is governed by the turbulent kinetic energy dissipation rate at the end of the free path of the jet where the velocities and the turbulent kinetic energy dissipation rate are much smaller than at the nozzle outlet. As with impellers, the analysis relies on the premises that in low viscosity fluids the mixing time follows

$$t_{mix} \propto \left(\frac{\varepsilon}{L^2}\right)^{-1/3} \qquad (1.24)$$

Again the problem is to determine which values of ε and L to use. The turbulent kinetic energy dissipation rate is high near the jet and much lower in other regions of the tank as for an agitator, but the variation in ε is larger for a jet. Grenville and Tilton (1996) used the jet free path length Z as the integral scale and the turbulent kinetic energy dissipation rate at the end of the jet free path as ε. The turbulent kinetic energy dissipation rate at the end of the jet free path ε_Z was set proportional to

$$\varepsilon_Z \propto \frac{u_Z^3}{d_Z} \qquad (1.25)$$

where u_Z is the jet velocity at the end of the free path and d_Z is the jet diameter at the end of the jet free path. A momentum balance gives a

relationship between the velocity and jet diameter at the nozzle outlet and at the end of the jet free path

$$u_d d = u_Z d_Z \tag{1.26}$$

The entrainment of liquid as the jet moves away from the nozzle leads to a reduction in the velocity. Thus the centerline velocity of the jet u_Z can according to Revill (1992) be written as

$$u_Z = 6u_d \frac{d}{Z} \tag{1.27}$$

When Eqs. (1.25) to (1.27) are substituted into Eq. (1.24) with $L = Z$ and $\varepsilon = \varepsilon_Z$ the following equation emerges

$$t_{mix} \propto \frac{Z^2}{u_d d} \tag{1.28}$$

Grenville and Tilton (1996) found that this equation correlated well with data obtained in 3 different scales and with data from another source. They suggested the following equation for 99% mixing

$$t_{mix,99\%} = 3.0 \frac{Z^2}{u_d d} \tag{1.29}$$

with all variables in SI units. The equation is suggested to hold for the following conditions (Grenville and Nienow, 2004) for $Re > 10,000$: $0.2 < H/T < 2.0$, $0.178\ \mathrm{m}^3 < V < 1200\ \mathrm{m}^3$, $1.32 \cdot 10^{-2}\ \mathrm{m\ s}^{-1} < u_d d/Z < 0.137\ \mathrm{m\ s}^{-1}$, $86 < Z/D < 753$. The data were obtained in systems where the jet was angled so that it intercepted the liquid surface at the opposite tank wall in order to maximize the jet path length, which maximizes liquid entrainment as is recommended by Revill (1992). Thus Z should be calculated from the aspect ratio H/T

$$Z = \sqrt{1 + \left(\frac{H}{T}\right)^2} \left(\frac{4VT}{\pi H}\right)^{1/3} \tag{1.30}$$

Yianneskis (1991) investigated the effect of tracer insertion time in a vessel with $H = T = 0.294$ m using the technique based on conductivity. It was found how the constant in the equation proposed by Fossett and Prosser (1949) was dependent on the tracer insertion time. Furthermore, it was found that the position of the probe and the tracer injection point did not have a significant effect on the mixing time. Simon and Fonade (1993) studied steady and unsteady turbulent jets and found that with alternating jets the mixing time was reduced by 15% compared to steady jets.

Recently, jet mixing in the turbulent regime has been studied by the use of computational fluid dynamics (CFD). When compared to experimental

results Patwardhan (2002) found that the overall mixing time could be predicted fairly well by CFD (using the 'k-ε' model for turbulence modeling) while the concentration profiles at various locations in the tank were not predicted well. Jayanti (2001) investigated the use of axial upward-pointing jets in cylindrical vessels by CFD, and found that a conical base gave rise to lower mixing time than a hemispherical or ellipsoidal base due to elimination of dead zones.

To summarize the above results, it can be concluded that for a stationary jet in a tank of fixed geometry and with a given liquid, all studies show that $t_{mix} \propto 1/(u_d d)^{\alpha}$ where α is between 0.83 and 1.0 for a turbulent jet and 2.0 for a jet in the transitional range[2].

1.2 Mass transfer

Good mass transfer is essential for obtaining high productivity in many cultivations. Examples of mass transfer problems are transfer of oxygen from the gas to the liquid and diffusion of substrates into pellets, immobilized cells etc. The most important mass transfer problems are gas-liquid mass transfer and molecular diffusion of substrates into pellets or cell aggregates. The latter is outside the scope of this thesis, while the former will be reviewed in some detail[3].

1.2.1 Basic mass transfer theory

Gas-liquid mass transfer transfer is often modeled by the two-film theory introduced by Whitman (1923), see figure 1.7.

For steady state mass transfer of component A from gas bubble to the bulk liquid the following equations for the flux J_A through each of the two films can be written as the product of the concentration difference across the layer and a mass transfer coefficient k

$$J_{A,g} = k_g(p_A - p_{A,i}) \tag{1.31}$$

$$J_{A,l} = k_l(c_A - c_{A,i}) \tag{1.32}$$

where p_A is the partial pressure of A, c_A is the concentration of A, and index i indicates the concentration at the interface.The equilibrium concentration

[2]As will be discussed in chapter 2 rotary jet heads are fundamentally different from stationary jets in that the jet is injected into constantly changing parts of the bulk volume. The stationary flow pattern found with a stationary jet is therefore not found with a rotary jet head.

[3]The following subsection 1.2.1 on mass transfer fundamentals was inspired by Nielsen et al. (2003) while the remaining subsections are based on an extensive literature survey.

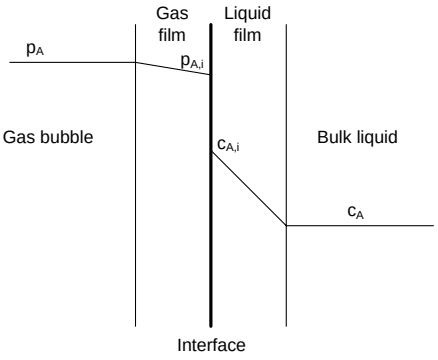

Figure 1.7. Concentration and partial pressure profiles in gas and liquid films for the transfer of the gaseous compound A into the liquid phase. The compositions of the gas bulk and of the bulk liquid are assumed to be constant.

found at each side of the interface can be related through Henry's law

$$p_{A,i} = He_A c_{A,i} \tag{1.33}$$

where He_A is Henry's constant for component A. Concentrations at the interface are not directly measurable, and thus the flux of component A is now written as the overall mass transfer coefficient times the driving force in the liquid phase

$$J_A = K_l(c_A^* - c_A) \tag{1.34}$$

with c_A^* being the saturation concentration in the bulk liquid obtained with the bulk gas phase

$$c_A^* = \frac{p_A}{He_A} \tag{1.35}$$

At steady state the fluxes are equal, i.e. $J_{A,g} = J_{A,l} = J_A$ and by inserting Eq.(1.35), (1.33), and (1.32) in Eq.(1.31) and rearranging we find the following relationship between the overall mass transfer coefficients and the coefficient for gas and liquid phase

$$\frac{1}{K_l} = \frac{1}{He_A k_g} + \frac{1}{k_l} \tag{1.36}$$

k_g is typically considerably larger than k_l and for gases with low or moderate solubility (and thus high He_A) such as oxygen or carbon dioxide the gas-phase resistance is negligible compared the liquid-phase resistance. Consequently, the overall mass transfer coefficient, K_l, is approximately equal to the mass transfer coefficient of the liquid film, k_l. In practise only K_l can be measured. In the literature there is therefore no clear distinction between K_l and k_l for oxygen transfer.

The volumetric rate of mass transfer, OTR, i.e. the mass transfer per unit reactor volume can be found from the flux J_A times the gas-liquid interfacial area per unit liquid volume a

$$OTR = J_A a = k_l a(c_A^* - c_A) \tag{1.37}$$

$k_l a$ is known as the volumetric mass transfer coefficient. This parameter is most often used to quantify gas-liquid mass transfer in aerated systems due to the difficulties associated with determining k_l and a separately.

It should be noted that especially in the older literature on mass transfer the gas-liquid interfacial area is often measured per unit dispersion and not per unit liquid volume V. If a is the gas-liquid interfacial area per unit liquid volume and a_d is measured per unit volume of dispersion, the relationship between them is

$$a_d = a(1 - \epsilon) \tag{1.38}$$

where ϵ is the fractional gas holdup in the dispersion $V_g/(V_g+V)$ where V_g is the volume of gas in the dispersion. Thus when inspecting the literature one needs to consider whether it is $k_l a$ or $k_l a_d$ which is reported. The definition in which the interfacial area is measured per unit liquid volume is undoubtedly the most convenient when the volumetric rate of the mass transfer process is to be used together with mass balances for dissolved oxygen.

1.2.2 Methods for $k_l a$ determination

Various methods have been proposed for measuring volumetric oxygen transfer coefficients in aerated systems. In the following sections some of these methods will be discussed.

The direct method

The name of this method is due to the fact that measurements are performed directly on an aerobic cultivation (or on another oxygen consuming reaction). In the method an oxygen analyzer is used to measure the oxygen content of the gas streams entering and leaving the reactor. At steady-state the volumetric rate of oxygen transfer (OTR) is equal to the volumetric oxygen uptake rate. A simple mass balance gives

$$OTR = \frac{1}{V}\left[\left(\frac{p_O v_g}{RT}\right)_{in} - \left(\frac{p_O v_g}{RT}\right)_{out}\right] \tag{1.39}$$

where R is the gas constant, T is the absolute temperature, p_O is the partial pressure of oxygen and v_g is the gas flow rate.

When the oxygen transfer is measured the volumetric transfer coefficient can be calculated by the governing equation for mass transfer

$$OTR = k_l a(c_l^* - c_l) \tag{1.40}$$

where c_l is the liquid oxygen concentration and c_l^* is the saturation concentration of oxygen obtained with the gas phase. If a well mixed liquid phase is assumed c_l can be measured by a single oxygen probe. In large-scale it is advised to measure the dissolved oxygen concentration various places in the tank to test this assumption. In a small-scale system with low height to diameter ratio c_l^* can be estimated by assuming well mixed gas phase, and thus c_l^* is calculated from the partial pressure of oxygen measured in the outlet. In large-scale reactors it is a good approximation to use a logarithmic mean value for the driving force, which corresponds to plug flow of the gas phase

$$\overline{(c_l^* - c_l)_L} = \frac{(c_{l,in}^* - c_l) - (c_{l,out}^* - c_l)}{\ln \frac{(c_{l,in}^* - c_l)}{(c_{l,out}^* - c_l)}} \tag{1.41}$$

If the difference in the partial pressure of oxygen in the inlet and outlet is small the assumptions regarding the gas phase will have a very small impact on $k_l a$. However, too small a difference will result in poor sensitivity of the gas analyzer used to measure the OTR.

The direct method is of course suited for obtaining volumetric oxygen transfer coefficients during cultivations but it is not particularly suited for finding $k_l a$-values as a function of a large set of operating conditions.

Dynamic methods

The dynamic oxygen electrode method

In the dynamic oxygen electrode method, the oxygen concentration in the inlet gas is changed stepwise and the dissolved oxygen tension is measured. The time varying concentration of oxygen in the liquid phase is given by the following equation if there is no reaction

$$\frac{dc_l}{dt} = k_l a(c_l^* - c_l) \tag{1.42}$$

In the original method (Bandyopadhyay and Humphrey, 1967) only the liquid phase dynamics was considered, c_l^* was assumed constant and electrode dynamics was not considered. In that case it is seen from integration of Eq.(1.42) that $k_l a$ can be found as the slope of $\ln(c_l^* - c_l)$ versus time.

However, for accurate determination of $k_l a$ with the dynamic oxygen electrode method complete system dynamics needs to be considered and consequently electrode dynamics and gas and liquid phase dynamics should be included.

With rapid changes in the dissolved oxygen concentration an oxygen probe response lag arises, and the electrode output is not directly related to the instantaneous value of dissolved oxygen. The response lag of a membrane-covered oxygen electrode is related to the time required for oxygen to diffuse through an outer liquid diffusion film and through the membrane. Different models have been used to account for the response lag. These range from simple first order models (e.g. Aiba and Huang (1969)) to two first order lag models in series to include the resistance in the outer liquid diffusion layer (e.g. Dunn and Einsele (1975)) to more complicated diffusion models based on an unsteady state molecular diffusion equation for the membrane (e.g. Heineken (1970, 1971); Linek (1972)).

Even though complete system dynamics should in principle be known in the dynamic oxygen electrode method, the method has most often been used in combination with simple models for gas and liquid phase mixing, and $k_l a$ has often been obtained by using the moment method (Dang et al., 1977; Shioya and Dunn, 1979).

The start-up method

The start-up method is merely a variant of the dynamic oxygen electrode method in which aeration is initiated into a deoxygenated liquid without gas hold-up and thus the entering gas does not mix with the gas used for deoxygenation. This will to some extent suppress the effect of non-ideal mixing of the gas phase on $k_l a$.

However, other problems arise with the start-up method. Linek et al. (1981) showed that the start-up method gave incorrect $k_l a$-values in 1 M KCl if nitrogen transport in the liquid film was neglected as is the case when moment analysis is applied. Ideally, nitrogen transport should also be considered with the normal dynamic oxygen electrode method where gas is continuously fed to the reactor and a shift in oxygen concentration performed. However, the influence on the calculated value of $k_l a$ is larger for the start-up method. Consequently, Linek et al. (1989b) proposed a version of the start-up method where pure oxygen is absorbed in the liquid from which all other gas components were previously removed. Nocentini (1990) on the other hand suggests that the start-up method can give reasonable estimates of $k_l a$ in vessels stirred by multiple impellers if the liquid phase is assumed to be fully backmixed while plug flow is assumed for the gas and the oxygen tension is measured at the middle of the vessel height.

As outlined above the main drawback of the dynamic methods are associated with the assumptions concerning gas phase dynamics and the fact that nitrogen transport is often neglected even in cases where it should not. It appears that these drawbacks are of higher importance for non-coalescing batches than for coalescing batches.

The dynamic pressure method

The dynamic pressure method, which was introduced by Linek et al. (1989a), is also based on measuring the transient in dissolved oxygen. However, the transient is induced by a small change (up to 20%) in the total pressure of the system, and therefore the partial oxygen pressure in all bubbles is changed simultaneously. Consequently, the influence of non-ideal mixing on the k_la value is suppressed.

It is advised only to use shift-ups in pressure since shift-downs may be accompanied by spontaneous nucleation of bubbles which will result in increased mass transfer. Linek et al. (1989a, 1994) showed that in coalescing batches the difference in k_la between a shift-down and a shift-up in pressure was within the experimental error. However, in non-coalescing batches, the k_la-values obtained with a shift-down in pressure were much higher than with a shift-up. The increase in k_la observed with a shift-down decreased with increasing values of k_la. Thus in sulphate solution at a k_la of 0.36 h^{-1} the enhancement of k_la was 100% while it was 17% at a k_la of 360 h^{-1}.

In the method first published by Linek et al. (1989a) the pressure change was ideal, i.e. it was immediate. However, in a later article Linek et al. (1993) showed that the method can also be used if the pressure step is non-ideal, which is expected in large tanks, and the method has been used in 1 m^3 scale (Linek et al., 1994).

Linek et al. (1989a) compared the dynamic pressure method to the variant of the start-up method where pure oxygen is absorbed in the liquid from which all other gas components were previously removed by e.g. vacuum desorption and to a steady-state sulphite method (Linek et al., 1990). For coalescing batch (pure water) the modified start-up method and the dynamic pressure method gave similar results. This was not the case for non-coalescing sulphate solution. This was explained by the fact that with the variant of the start-up method the transient in dissolved oxygen tension was completed before a steady bubble size distribution was reached. For non-coalescing sulphate solution the steady-state sulphite method and the dynamic pressure method gave similar results.

Linek et al. (1989a, 1994) showed that the k_la-values obtained in the dynamic pressure method by absorption of pure oxygen and air are identical, something which is not the case for the steady-state sulphite method. Furthermore, Linek et al. (1993) showed that the error caused by neglecting simultaneous nitrogen transport is less than 10% for $k_la < 720$ h^{-1}.

In conclusion, the dynamic pressure method has been shown to give correct values of k_la for coalescing, non-coalescing and viscous systems (Linek et al., 1989a). The main advantage is of course, that the method can be used without complex models for the gas phase.

The sulphite method

The sulphite method relies on on the oxidation of sulphite to sulphate in the presence of a catalyst (Cu^{2+} or Co^{2+})

$$SO_3^{2-} + \tfrac{1}{2}\ O_2 \rightarrow SO_4^{2-}$$

The liquid phase oxidation of sulphite to sulphate is almost instantaneous and the reaction rate is 0 order even for very low concentrations of the sulphite concentration and the oxygen concentration (e.g. Linek and Vacek (1981)).

One drawback of the sulphite method is that the sulphate oxidation may enhance the oxygen absorption due to rapid chemical reaction not only in the bulk liquid but also in the liquid film. Denis et al. (1990) investigated the influence of catalyst concentration on k_la and found that k_la was unaffected when the Cu^{2+}-concentration was below 10^{-3} M. With Co^{2+} as catalyst there was a clear enhancement of k_la with concentrations above 10^{-6} M.

In the traditional use of the sulphite method, sulphite was added to the reactor prior to reaction. During the reaction samples were taken out and analyzed for unreacted sulphite by iodometry. Thus the rate of oxidation could be found, and k_la was obtained by the following equation

$$k_la = \frac{r(SO_3^{2-})}{2(c_l^* - c_l)} \tag{1.43}$$

where $r(SO_3^{2-})$ is the volumetric rate of sulphite oxidation. With this method c_l would normally be close to zero, and the equation reduces to

$$k_la = \frac{r(SO_3^{2-})}{2c_l^*} \tag{1.44}$$

Apart from the risk of having reaction in the liquid film, the sulphite method traditionally used has a number of drawbacks. First of all the high absorption rates leads to a considerable shrinkage of the bubbles. The shrinkage affects the specific surface area and thereby k_la.

Steady-state versions of the sulphite method have been proposed, which eliminates this effect by lowering the absorption rate (e.g. Imai et al. (1987); Linek et al. (1990)). In the version suggested by Linek et al. (1990) a 0.5 M Na_2SO_3 solution is slowly fed into a continuous reactor containing a 0.5 M Na_2SO_4 solution so that the dissolved oxygen concentration is between 90-95 % of the saturation value. Thus, the absorption rate is lowered 10-20 times compared to the traditional method. The dissolved oxygen concentration is measured by an oxygen electrode, and the k_la-value can be calculated from

$$k_la = \frac{v_{in}[SO_3^{2-}]_{in}}{2V(c_l^* - c_l)} \tag{1.45}$$

where v_{in} is the inflow rate of sulphite and $[SO_3^{2-}]_{in}$ is the concentration of the sulphate fed to the reactor. Linek et al. (1990) did not obtain the same values of $k_l a$ when air was used instead of pure oxygen in the steady-state sulphite method. The authors assumed a fully back-mixed gas phase. Deviations from this will have a larger negative impact on the calculated $k_l a$-value when air is used instead of pure oxygen, and probably this can explain the differences. As mentioned earlier Linek et al. (1989a) showed that the dynamic pressure method and the steady-state sulphite method does give the same in sulphate-solution when pure oxygen is used.

Compared to fermentation systems, a major drawback of both the traditional sulphite method and the steady-state method by Linek et al. (1990) is that sulphite solutions are very non-coalescing. This will give a large specific surface area and thereby a high $k_l a$ compared to e.g. pure water. Even though fermentation broths do often have a rather low coalescence due to excretion of surfactants and due to the composition of the medium the $k_l a$ obtained by these methods will most often be larger than those found in fermentations or other bio-reactions. In the steady-state method proposed by Imai et al. (1987) sulphite is fed to a reactor containing water, and since the amount of sulphate accumulated during an experiment is very small, the $k_l a$-values obtained with the method are comparable to those obtained in pure water.

The hydrogen peroxide method

The hydrogen peroxide method is a chemical method like the sulphite method, but it reverses the usual pattern of oxygen transfer (Hickman, 1988). Oxygen is produced in the liquid by decomposition of hydrogen peroxide in the presence of catalase according to the following reaction

$$2\ H_2O_2 \rightarrow 2\ H_2O + O_2$$

This oxygen is transferred to the gas phase at a rate that depends on the mass transfer coefficient. The reaction is first order with respect to catalase and hydrogen peroxide over a wide range of concentrations

$$r = k[H_2O_2][\text{catalase}] \tag{1.46}$$

At steady state the volumetric rate of reaction, r, is equivalent to the amount of hydrogen peroxide added to the reactor per unit volume

$$r = \frac{v_{in}[H_2O_2]_{in}}{V} \tag{1.47}$$

Similarly, at steady state the oxygen transfer rate is equal to the rate of oxygen production. Assuming ideal mixing of the liquid phase the following

equation can be written

$$OTR = \frac{r}{2} = k_l a(c_l - c_l^*) \tag{1.48}$$

Combining Eqs. 1.48 and 1.47 gives an equation for $k_l a$

$$k_l a = \frac{v_{in}[\mathrm{H_2O_2}]_{in}}{2V(c_l - c_l^*)} \tag{1.49}$$

The value of c_l^* can be found from an oxygen balance for the gas phase. In practise the difference in $k_l a$ between assuming a fully backmixed gas phase or plug flow is very small. Thus the method does not require complex models of gas phase mixing like some of the dynamic methods.

The hydrogen peroxide method is easy to implement, and it has been used by e.g. Novozymes A/S in production-scale equipment (Pedersen, 1997). It is only necessary to know the concentration and flow rate of H_2O_2, the liquid volume, the gas flow rate (to estimate c_l^*) and the dissolved oxygen tension at steady state.

One requirement of the method is that the reaction is indeed first order in hydrogen peroxide. If there is insufficient catalase the time to reach a steady state will be very long. If the rate of reaction ultimately becomes zero order (which would require very large concentrations of hydrogen peroxide) Eqs. 1.46 and 1.47 are not equal and the $k_l a$-value will be overestimated. It is therefore crucial to keep the amount of catalase above a certain level (for directions see Cooke et al. (1991)). Thus the loss of catalase activity over time needs to be considered. The decrease in activity is accelerated by departure from neutral pH and by the ionic strength of the medium, particularly in sulphate solutions (Vasconcelos et al., 1997). It is also well known that catalase deactivates at a rate which is proportional to the hydrogen peroxide concentration (Ghadermarzi and Moosavi-Movahedi, 1996), and large standing concentrations of H_2O_2 in the tank should therefore be avoided. Vasconcelos et al. (1997) showed how activated manganese dioxide can replace catalase in strong electrolyte solutions where the catalase deactivates fast.

Finally, it should be noted that the production of water and the presence of hydrogen peroxide can alter the rheological properties of some fluids (Cooke et al., 1991).

Linek et al. (1996a) speculated that the hydrogen peroxide method can lead to overestimation of the $k_l a$-value due to spontaneous nucleation of gas bubbles due to supersaturation of oxygen in the liquid phase (as with the dynamic pressure method with a shift-up in pressure). Based on the data published by Cooke et al. (1991), Linek et al. (1996a) concluded that the enhancement of $k_l a$ due to spontaneous nucleation is only occurring in non-coalescing solutions, and that the enhancement is most evident for small values of $k_l a$.

The hydrogen peroxide method is claimed by Gogate et al. (2000) (figure 20) and by Gogate and Pandit (1999) to give low values of the mass transfer coefficient - especially at high specific power input and at low superficial gas velocity - compared to e.g. the dynamic pressure methods, the method they recommend. Their analysis is, however, based on data obtained in the literature. Thus, no experiments have been performed to support their hypothesis, and they offer no explanations in support of why the hydrogen peroxide method should lead to underestimation of $k_l a$.

Common best practise

In the recently published book 'Handbook of Industrial Mixing', Brown et al. (2004) recommends to use the the hydrogen peroxide method for obtaining values of $k_l a$ in stirred vessels. The large German manufacturer of agitators EKATO GmbH does, however, still use either the classical sulphite method (with a dissolved oxygen tension in the liquid of virtually zero) or the dynamic start-up method for determination of $k_l a$ (Niefenthaler, 2000). In my opinion none of these methods are ideal for the reasons described above.

1.2.3 Empirical correlations for $k_l a$ in stirred vessels

For stirred vessels the volumetric mass transfer coefficient $k_l a$ (or the volumetric mass transfer coefficient based on dispersion volume $k_l a_d$) is typically correlated in terms of the specific stirrer power input P/V and superficial gas velocity, u_g, i.e.

$$k_l a = k \left(\frac{P}{V}\right)^{\alpha} u_g^{\beta} \tag{1.50}$$

Some authors include the gas buoyancy power in the correlation, see e.g. the expression of Linek et al. (1996b) in table 1.2. It has been shown by Pedersen (1997) that correlations using u_g are better for prediction of $k_l a$ upon scale-up than correlations using the specific gas flow rate in vvm. The same has been shown by Whitton and Nienow (1993), who studied two geometrically similar tanks with diameters of 0.61 m and 2.67 m. The square of the correlation coefficient R^2 was 0.933 when data for the two tanks were combined and $k_l a$ was correlated in terms of u_g. When $k_l a$ was correlated in terms of vvm R^2 was 0.188.

A correlation that is still often cited is the correlation by van't Riet (1979) who proposed correlations based on extensive analysis of the literature. For water he found

$$k_l a_d = 93.6 \left(\frac{P}{V}\right)^{0.4} u_g^{0.5} \tag{1.51}$$

while for noncoalescing strong salt solution, he found

$$k_l a_d = 7.2 \left(\frac{P}{V}\right)^{0.7} u_g^{0.2} \tag{1.52}$$

with $k_l a_d$ in h^{-1}, u_g in m s^{-1} and for $500 < P/V < 10,000$ W m^{-3} where P only contains shaft power. The correlations of van't Riet (1979) are today known to underestimate the volumetric mass transfer coefficient, especially at noncoalescing conditions and at large specific power input. Tables 1.2 and 1.3 contains some newer correlations together with a description of the equipment in which they were obtained. It can be seen that the dependence on the specific power input is larger than in the correlations proposed by van't Riet (1979). In multiple-impeller systems values of $k_l a$ have mostly been obtained for the entire system. Linek et al. (1996b) and Moucha et al. (1995) did, however, measure $k_l a$-values in individual stages of a reactor stirred with 4 Rushton turbines using the dynamic pressure method. While $k_l a$ was found to be equal for the 3 upper stages at equal values of the specific power input and the superficial gas velocity, a different value of $k_l a$ was found in the bottom stage, which was higher than the values found in the upper stages.

It appears from the literature that $k_l a$ is largely independent of the impeller type used (Nienow, 1996) at least in low-viscosity systems. Vasconcelos et al. (2000) tested various designs of 6-bladed disc turbines in a dual impeller system and found for the air/water system that the volumetric mass transfer coefficient obtained at a given specific power input and superficial gas velocity was independent of blade shape. Zhu et al. (2001) tested the Lightnin A310 and A315 hydrofoil impellers, a 4-bladed 45° pitched blade turbine, a 6-bladed Rushton turbine, a 6-bladed Rushton turbine with a hole in each impeller blade, and a 6-bladed hollow blade turbine. They found that the different impellers largely gave the same value of $k_l a$ at equal values of P/V and u_g in the air/water system even though the data indicated that the radial flow impellers gave slightly higher volumetric mass transfer coefficients. Vasconcelos et al. (1997) also found no difference in $k_l a$ in the air/water system when an up-pumping B2 hydrofoil impeller was compared to a 6-bladed Rushton turbine at equal values of the specific power input and the superficial gas velocity. The same conclusion was drawn by Martin et al. (1994) who compared a Rushton turbine with the down-pumping high-solidity hydrofoil Prochem Maxflo T. Still Chemineer (http://www.chemineer.com) claims that their hollow blade CD6 impeller is able to almost double $k_l a$ compared to a Rushton turbine operating at the same values of specific power input and superficial gas velocity. This statement is, however, not supported by evidence available in the open literature. Thus the most important factors for a gas dispersing impeller becomes whether it looses power upon gassing and when the transition to flooding occurs.

Table 1.2. Selected empirical correlations for $k_l a$ in water. $k_l a$ is in h^{-1} while P is in W, V in m^3, u_g in $\mathrm{m\ s}^{-1}$, ρ_l in $\mathrm{kg\ m}^{-3}$ and g is equal to $9.81\ \mathrm{m\ s}^{-2}$.

Reference	Method	Correlation	Conditions
Vasconcelos et al. (1997)	Hydrogen peroxide with catalase or MnO_2	$k_l a = 13.3(P/V)^{0.66} u_g^{0.34}$	Single B2 impeller ($D = 0.46T$) or 6-bladed Rushton ($D = T/3$) $H = T$, $T = 0.61$ m $250 \leqslant P/V \leqslant 4000$ W m^{-3} $0.0025 \leqslant u_g \leqslant 0.02$ m s^{-1} Temperature 20°C
Linek et al. (1991)	Dynamic pressure	$k_l a = 13.8(P/V)^{0.654} u_g^{0.4}$	Single 6-bladed Rushton ($D = T/3$) $H = T$, $T = 0.29$ m $74 \leqslant P/V \leqslant 8812$ W m^{-3} $0.00212 \leqslant u_g \leqslant 0.00424$ m s^{-1} Temperature 20°C
Moucha et al. (1995)	Dynamic pressure	1st stage: $k_l a = 52.6(P/V)^{0.611} u_g^{0.554}$ 2nd-4th stage: $k_l a = 63.7(P/V)^{0.580} u_g^{0.588}$	Four 6-bladed Rushtons ($D = T/3$) $H = 4T$, $T = 0.19$ m $\sim 100 \leqslant P/V \leqslant \sim 5000$ W m^{-3} $0.00212 \leqslant u_g \leqslant 0.00848$ m s^{-1} Temperature 20°C
Linek et al. (1996b)	Dynamic pressure	1st stage: $k_l a = 23.3(P/V + u_g \rho_l g)^{0.675} u_g^{0.494}$ 2nd-4th stage: $k_l a = 31.0(P/V + u_g \rho_l g)^{0.637} u_g^{0.54}$	Four 6-bladed Rushtons ($D = T/3$) $H = 4T$, $T = 0.19$ m $\sim 100 \leqslant P/V \leqslant \sim 5000$ W m^{-3} $0.00212 \leqslant u_g \leqslant 0.00848$ m s^{-1} Temperature 20°C
Nocentini et al. (1993)	Start-up method	$k_l a_d = 54(P/V)^{0.59} u_g^{0.55}$	Four 6-bladed Rushtons ($D = T/3$) $H = 4T$, $T = 0.232$ m P/V up to approximately 6000 W m^{-3} $0.00155 \leqslant u_g \leqslant 0.0108$ m s^{-1} Temperature 25°C
Vasconcelos et al. (2000)	Hydrogen peroxide	$k_l a = 22.3(P/V)^{0.66} u_g^{0.51}$	Dual 6-bladed disc turbines ($D = T/3$) $H = 2T$, $T = 0.392$ m $125 \leqslant P/V \leqslant 4000$ W m^{-3} u_g up to 0.013 m s^{-1} Temperature 25°C

Table 1.3. Selected empirical correlations for $k_l a$ in 0.5 M Na_2SO_4. $k_l a$ is in h^{-1} while P is in W, V in m^3, u_g in m s^{-1}, ρ_l in kg m^{-3} and g is equal to 9.81 m s^{-2}.

Reference	Method	Correlation	Conditions
Linek et al. (1991)	Dynamic pressure/ steady state sulphite	$k_l a = 1.12(P/V)^{1.24} u_g^{0.4}$	Single 6-bladed Rushton ($D = T/3$) $H = T$, $T = 0.29$ m $74 \leqslant P/V \leqslant 8812$ W m^{-3} $0.00212 \leqslant u_g \leqslant 0.00424$ m s^{-1} Temperature 20°C
Moucha et al. (1995)	Dynamic pressure	1st stage: $k_l a = 2.08(P/V)^{1.20} u_g^{0.439}$ 2nd-4th stage: $k_l a = 9.07(P/V)^{1.03} u_g^{0.554}$	Four 6-bladed Rushtons ($D = T/3$) $H = 4T$, $T = 0.19$ m $\sim 100 \leqslant P/V \leqslant \sim 5000$ W m^{-3} $0.00212 \leqslant u_g \leqslant 0.00848$ m s^{-1} Temperature 20°C
Linek et al. (1996b)	Dynamic pressure	1st stage: $k_l a = 0.464(P/V + u_g \rho_l g)^{1.32} u_g^{0.331}$ 2nd-4th stage: $k_l a = 1.89(P/V + u_g \rho_l g)^{1.17} u_g^{0.459}$	Four 6-bladed Rushtons ($D = T/3$) $H = 4T$, $T = 0.19$ m $\sim 100 \leqslant P/V \leqslant \sim 5000$ W m^{-3} $0.00212 \leqslant u_g \leqslant 0.00848$ m s^{-1} Temperature 20°C

$k_l a$ is amongst other things dependent on viscosity and medium composition. According to Nienow (1998) $k_l a$ is dependent on viscosity in the following way

$$k_l a \propto \mu^{-0.5} \tag{1.53}$$

Electrolytes and low molecular weight alcohols both act as bubble coalescence inhibitors and the bubble size is consequently reduced, see figure 1.8, thereby leading to an increase in $k_l a$. On the other hand addition of antifoams drastically reduce $k_l a$ (see e.g. Arjunwadkar et al. (1998)).

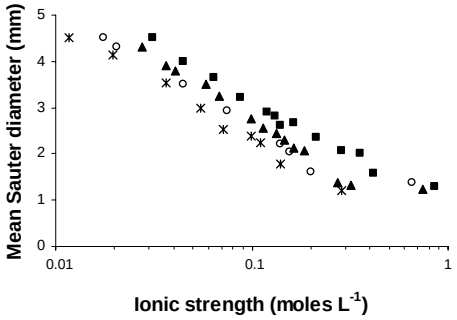

Figure 1.8. Mean Sauter bubble diameter as a function of ionic strength for aqueous solutions of the salts $Al_2(SO_4)_3$ (■), Na_2SO_4 (▲), NaCl (○) and NaOH (∗). The data are from an air water system in a bubble column (Keitel and Onken, 1982). The figure was adopted from Nielsen et al. (2003).

1.3 Outline of experimental work

Chapter 2 of this thesis presents a characterization of the investigated rotary jet head system in terms of mixing and mass transfer using some of the methods described in this chapter.

Chapter 3 and 4 deals with enzymatic oxidation of lactose to lactobionic acid, a process where both mixing and mass transfer is of importance. In chapter 3 the kinetics and operational stability of the enzyme is investigated and it is shown how mixing is important even in a stirred laboratory reactor. Chapter 4 deals with experiments performed in a pilot-scale rotary jet head reactor.

In chapter 5 some rather preliminary results for continuous aerobic cultivation of *S. cerevisiae* in the pilot-scale rotary jet head reactor are presented.

The thesis concludes with a summary and a number of suggestions for future work.

For the interested reader the thesis contains an appendix presenting an outline of experimental studies of the use of rotary jet heads in other industrial

applications.

Chapter 2

Characterization of the rotary jet head system

In this chapter the rotary jet head system will be described and results of mixing time experiments and mass transfer experiments will be presented. The experimental data were originally published in Nordkvist et al. (2003), but the discussion in that paper has been critically reviewed.

2.1 Introduction

In order to increase the productivity of large-scale bioreactors and at the same time to curtail capital costs and energy costs, and to facilitate cleaning in place (CIP) continued research in the area of bioreactor design is imperative. An efficient industrial bioreactor should ideally satisfy the following criteria

- High concentration feed should be rapidly mixed into the bulk volume - otherwise undesired byproduct formation may well occur.
- A high rate of mass transfer should be achieved at the vvm used in industrial operation, and at a modest power input. Insufficient mass transfer may curtail the process intensification that is sought by using high feed concentration and/or cell recirculation.
- Heat exchange must be efficient when the heat of reaction is high, and especially in large scale a good option would be to perform it outside the reactor. Otherwise, the productivity may become limited by heat transfer and not by mass transfer or by the rate of the bioreaction.

These requirements to an efficient, industrial scale bioreactor suggest that a design with external, forced flow and with feed inlet at some point in the loop of both liquid phase and gas phase substrates is an attractive design if in this way the feed and gas can be dispersed efficiently in the tank. Metabolic heat is easily removed in the recirculation loop if the flow is fast and efficient heat exchangers of the plate-type are used.

With these considerations in mind we have characterized a pilot plant reactor with forced flow in a recirculation loop where the circulated liquid is injected into the tank reactor as liquid jets through one or more rotary jet heads as described in the following. In this design the reactor vessel becomes just a shell for containment of the medium, without baffles and heat exchangers, and it is therefore both cheap and easy to clean. Mixing time results will be compared to mixing in stirred vessels and to mixing by stationary liquid jets, while the mass transfer results will be compared with those of mechanically stirred tank reactors.

2.2 Process and equipment description

2.2.1 The rotary jet head

Rotary jet heads (RJH) were originally developed as tank cleaning machines for maritime use, e.g. in oil tankers. They have now found use in the chemical industry and in the food industry (e.g. beer and beverage production) to ensure an efficient and fast cleaning of vessels between batches. The Toftejorg series of tank cleaning machines (previously manufactured by Toftejorg A/S, Ishøj, Denmark, which is now part of Alfa Laval) TZ79, TZ74 and TJ20G were recently (Hummer, 2004) modified for efficient mixing of liquids and for mass transfer from a gas to the liquid phase. The trade names for the three modified RJH, which have been commercialized by the company ISO-MIX A/S, are IM20 (nozzle diameter 8.0 to 10.0 mm), IM15 (6.0 to 8.0 mm) and IM10 (3.5 to 5.5 mm). We used the largest capacity IM20 machine shown in figure 2.1 in most of our experiments, but the smaller capacity machines IM15 and IM10 were also studied.

In the hub of the IM20 machine the liquid passes through a guide and a turbine, which is set into rotation. Through a gearbox this rotation is transformed into a combined horizontal rotation of the entire machine body and a rotation in the vertical plane of the four distributor arms. In this way the liquid jets from the four nozzles efficiently sweep the tank. After 45 rotations in the vertical plane and 43 in the horizontal plane the sweeping pattern is repeated. The liquid flow rate through the nozzles depends on the applied pressure, and the time to sweep a complete pattern can be varied

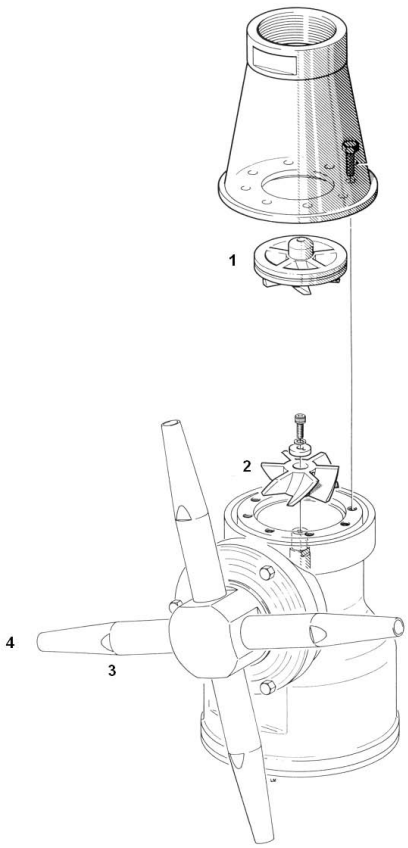

Figure 2.1. Schematic view of the IM20 rotary jet head. The recirculated liquid enters at the top and flows past the guide, 1, to the turbine, 2, whereby the RJH is set into a slow horizontal rotation via a gearing system (not shown). The four distributor arms, 3, are simultaneously set into a slow rotation in the vertical plane, and the liquid jets that leave the machine through the nozzles, 4, uniformly sweep the reactor volume. The total length of the machine (top to bottom) is 356 mm. The diameter of the distributor wheel is 268 mm. Total weight of the machine is 12.2 kg (ISO-MIX A/S, 2004).

by controlling the liquid flow rate. In our application of IM20 (d = 10 mm) 1.7 revolutions min^{-1} was obtained at a gauge pressure of Δp = 3 bar and a volumetric flow rate of v_l = 25 m^3 h^{-1}. At 10 bar gauge pressure and v_l = 46 m^3 h^{-1} the frequency increased to 3.5 revolutions min^{-1}. The distributor arms (3 on Figure 1) are interchangeable and nozzle diameters d = 8.0, 9.0, and 10.0 mm are standard for the IM20 rotary jet head. In the present study d = 8.0 and 10.0 mm were used. For IM15 the diameter was d = 7.0 mm. For the small machine, IM10, nozzle diameters of 3.9 and 5.5 mm were used.

2.2.2 Experimental system

The experimental system was centered around the tank depicted in figure 2.2. In order to use the system for mixing, liquid from the tank was recirculated in a loop as depicted in the figure and reinjected through the rotary jet head.

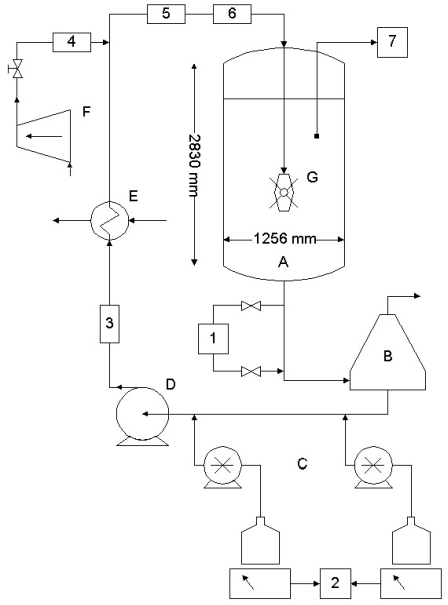

Figure 2.2. Pilot plant reactor (maximum liquid volume V = 3.4 m^3) and recirculation loop (volume 70 L when the degasser B is bypassed). A: Tank. B: Degasser. C: Positive displacement pumps. D: Centrifugal pump. E: Heat exchanger. F: Compressor. G: Rotary jet head. 1: pH electrode. 2: Balances. 3: Mass flowmeter (liquid). 4: Mass flowmeter (air). 5: Temperature sensor. 6: Pressure transmitter. 7: Oxygen electrode.

Liquid was withdrawn from the bottom of the tank, A, and transferred to the degasser, B, where larger air bubbles were removed. The degasser was bypassed during mixing experiments. The liquid was circulated with a centrifugal pump, D, operated at constant pressure. Operating temperature and pressure were measured at 5 and 6 after the air inlet. The volumetric flow rate of the liquid was measured with a mass flowmeter, 3, positioned right after the pump. In all experiments the liquid was cooled in a plate-type heat exchanger, E, to a temperature of 25°C. The liquid was finally re-injected into the tank through the rotary jet head, G. During oxygen transfer experiments atmospheric air was supplied from the compressor, F, and injected into the loop through three micro-porous polymer diffusers. A valve was adjusted manually to give the desired airflow measured on a mass flowmeter, 4.

The RJH can be placed at different vertical positions in the tank. We report only on results obtained when the machine(s) were placed in the middle of the liquid volume. In some experiments 2 RJH were used to disperse the circulating liquid (+injected gas) into the tank. Here the liquid was distributed through a manifold to two identical machines placed at the same vertical position in the tank.

2.3 Experimental procedures and data evaluation

2.3.1 Mixing

The tank reactor system, figure 2.2 with bypass of the degasser, has been characterized for mixing time at un-aerated conditions both in pure water and in 0.75 wt% and 1.50 wt% CMC solutions (Aqualon Blanose CMC 7MF). Mixing with two different addition methods were investigated

1. Addition of tracer to liquid surface: The tracer slug is added to the top of the tank and mixing is performed by the continuous injection of liquid through the RJH.

2. Addition of tracer in loop: The tracer is added to the recirculation loop and efficiently distributed to the bulk liquid via the rotary jet heads before mixing is completed by dissipation of the initially distributed tracer by the liquid jets.

Unless stated otherwise, the total liquid volume V of the system was 3.4 m^3 in all the experiments. Experiments were initially performed with the RJH IM10 (d = 5.5 mm), IM15 (d = 7.0 mm), and IM20 (d = 10.0 mm) at different locations in the tank. We found that a location in the middle of the liquid volume was best, and the results reported were all obtained for this configuration.

Characterization of mixing with tracer addition to the liquid surface

Dissipation of a tracer slug has often been characterized by a single rate constant, which can be related directly to mixing time, e.g. Pedersen et al. (1994); Marten et al. (1997). We have used an analysis approach similar to that of Marten et al. (1997) because it allows us to disregard the location of the probe relative to the tracer addition point and furthermore, it is not necessary to know the exact time of tracer addition. A conventional pH tracer technique was used, where either acid (HNO3, 13.8 M) or base (NaOH, 9 M)

was added to the liquid surface. The pH was monitored with a frequency of ~ 800 min^{-1}. For all experiments the pH step was between 0.2 and 0.3 pH units. For each pH measured a normalized pH was calculated according to

$$E = \frac{\mathrm{pH}(t) - \mathrm{pH}_0}{\mathrm{pH}_{\mathrm{final}} - \mathrm{pH}_0} \tag{2.1}$$

In our experiments the normalized pH profile followed first order kinetics as in Marten et al. (1997)

$$|1 - E| = \exp\left(-k_{mix} t\right) \tag{2.2}$$

k_{mix} is the mixing constant, which is equal to the reciprocal of $t_{mix,63.2\%}$, the time to reach 63.2% of the final pH change. In practice, k_{mix} was found by plotting $\ln\left(|1 - E|\right)$ versus t and performing a linear regression to obtain the slope. The time required for any specific degree of mixing, m can be calculated from

$$t_{mix,m} = -\frac{1}{k_{mix}} \ln\left(1 - m\right) \tag{2.3}$$

All results in this work are given as 95% mixing times. At least 4 independent measurements were performed for each set of operating conditions.

It should be noted that with this technique the lag time before an initial response is observed is neglected. While the mixing time obtained will be different with the two methods, the functionality does not normally change whether one or the other method is used.

It might be argued that E should be calculated on the basis of concentrations rather than pH as stated in section 1.1.1 in the introductory chapter. However, for small pH steps the discrepancy between the two methods is negligible, and the method based on concentrations is sensitive to small offsets in the pH measurements. To illustrate that the measurements based on pH give the same results as if based on concentration, we have made simulations of a first order mixing process with $t_{mix,95\%}$ based on the concentration of H^+ equal to 60 s. In a simulated step-up experiment (pH 3.50 to 3.80) $t_{mix,95\%}$ based on pH was determined to 64 s, while in the step-down experiment (pH 3.80 to 3.50) $t_{mix,95\%}$ based on pH was determined to 57 s. Thus, a step-up experiment overestimates the mixing time when based on pH measurements, while a step-down experiment underestimates the mixing time. When the average is used as in our experiments, the results for the mixing time based on concentration measurements and pH measurements are almost the same. However, this method can only be applied if the pH steps used are small.

Marten et al. (1997) showed that hydration of aqueous carbon dioxide influences the pH dynamics. To avoid the process of deconvoluting the responses of mixing and buffering, the CMC-solutions were completely free of carbonate, and during the experiments with tap water the pH was kept below 4,

where the carbonic acid buffer system is inactive. This was the case in both types of mixing experiments performed.

Characterization of mixing with tracer addition in the loop

In the experiments performed to characterize mixing with tracer addition in the recirculation loop, 45 mL of either 9 M HNO_3 or 9 M NaOH was added via positive displacement pumps (at C on figure 2.2) over a time interval of 4 seconds. From the monitored pH profile, a normalized profile was calculated according to Eq.(2.1). Since this mixing process involves more than one time constant - mixing is a consequence of both distribution of the tracer via the rotary jet head and of further dissipation - it is not possible to use Eqs.(2.2) and (2.3) to calculate the mixing time. Instead the mixing time, $t_{mix,95\%}$, was calculated as the time interval between an initial response in the normalized pH profile and a mixing degree, m, of 95%. At least 4 independent measurements were performed for each set of operating conditions.

Again the lag time before an initial response is observed is neglected with this method.

2.3.2 Rheology

The viscosities of the CMC solutions were measured at 25°C using a prototype StressTech rheometer (similar to StressTech AB2000) from Reologica Instruments AB equipped with a cylinder rotating in a concentric cylindrical cup. The shear stress was measured as a function of the shear rate. In general there was a tendency to get a lower viscosity for shear rates higher than the maximum values given in table 2.1, i.e. the CMC used was slightly pseudo-plastic.

Table 2.1. Rheological characterization of CMC solutions. The viscosity was constant between the minimum and maximum value of the shear rate.

CMC concentration (wt%)	Shear rate (s^{-1})		Viscosity (10^{-3} Pa s = cp)
	min	max	
0.75	1.0	300	27
1.50	0.3	32	137

The behavior was almost identical to the one observed by Pedersen et al. (1993) who also measured the viscosity of different CMC solutions, and found that the viscosity was largely independent of the shear rate for a 1 wt% solution in the shear rate range studied. For a 2 wt% solution the viscosity was independent of the shear rate for shear rates up to 20 s^{-1} after which

the viscosity declined. The behavior could not be correlated adequately by the power law.

2.3.3 Oxygen transfer

Oxygen transfer coefficients were obtained for the air/water system using the hydrogen peroxide steady state technique proposed by Hickman (1988), one of the methods reviewed in the introductory chapter.

The experiments were carried out according to Pedersen (1997). Initially catalase (Catazyme 25L, donated by Novozymes A/S) was added to the water in the tank. For each experimental condition (fixed value of volumetric gas flow rate v_g, liquid flow rate v_l, gauge pressure Δp, and temperature equal to 25°C) the aerated reactor was operated until a steady state in the dissolved oxygen tension was reached. The dissolved oxygen tension was measured by an Ingold polarographic oxygen sensor placed approximately 30 cm below the liquid surface (at 7 on figure 2.2). A constant flow, determined indirectly by weight measurements at position 2 on figure 2.2, of 35 wt% H_2O_2 (exact concentration determined by titration with $KMnO_4$) was then added in the recirculation loop via a positive displacement pump (at C on figure 2.2) and a new steady state in dissolved oxygen was reached and kept for about 30 min (figure 2.12). The addition of H_2O_2 was then stopped, and it was ensured that the dissolved oxygen tension stabilized at the level obtained before H_2O_2 addition. As described in section 1.2.2 in the introductory chapter, under the assumption of ideal mixing in the liquid phase, the k_la value can be calculated from the steady state measurements

$$k_la = \frac{v_{in}[H_2O_2]_{in}}{2V(c_l - c_l^*)} \tag{2.4}$$

where c_l^* is the saturation concentration of oxygen in water for the gas phase at the pressure at the position of the oxygen electrode. In the calculations of c_l^* the gas phase was assumed to be fully backmixed, and thus c_l^* is slightly higher than for air due to the production of oxygen in the tank.

Measurements of k_la values will be inaccurate if there are point-to-point variations in the hydrogen peroxide concentration in the tank, since this will give rise to point-to-point variations in the dissolved oxygen tension. Figure 2.12 with measurements of dissolved oxygen tension every 15 s for 18 min shows that the oxygen tension is virtually constant. If there were point-to-point variations in the hydrogen peroxide concentration due to inadequate liquid mixing, we would expect changes in the dissolved oxygen concentration when the liquid jets, that dispense the hydrogen peroxide, are close to the electrode.

Experiments were conducted with one IM20 (d = 10 mm) placed in the

middle of the tank reactor, and with two IM20 RJH placed in the middle of the tank. The working volume was 3.4 m^3 during all experiments with one IM20. During the experiments with two IM20 RJH the working volume decreased to 3.05 m^3 due to increased gas hold-up. The specific power input delivered by the pump P/V was varied from 248 to 2023 W m^{-3}. The superficial gas velocities u_g - based on the tank diameter of 1.256 m - ranged from 0.0052 to 0.043 m s^{-1}.

Attempts were also made to determine the oxygen transfer coefficient in a 0.2 wt% xanthan solution (Donated by CP Kelco, Lille Skensved, Denmark), a model liquid that simulates the properties of a penicillin fermentation broth (Pedersen et al., 1993). However, the degasser was not able to degas the solution sufficiently and the centrifugal pump could not handle the liquid-air dispersion even at volumetric air flow rates below 10 Nm^3 h^{-1}. Another pump, less sensitive to cavitation, is needed in order to make mass transfer experiments with high viscosity liquids.

2.4 Results

2.4.1 Flow characteristics of rotary jet heads

The RJH have been characterized both at un-aerated and aerated conditions to obtain relations between gauge pressure in the recirculation loop and the volumetric liquid flow rate.

If friction is neglected, the mechanical energy equation for an un-aerated liquid flow through N RJH simply states that the difference in pressure energy between the pressure transmitter (6 on figure 2.2) and the exit of the nozzles is transformed into kinetic energy (kinetic energy at the transmitter is neglected). For a volumetric flow rate v_l of circulating liquid, a liquid density ρ_l, a pressure difference Δp, and a total cross sectional area of the nozzles A_d (in consistent units), the equation reads

$$v_l \Delta p = \frac{1}{2} \rho_l v_l \left(\frac{v_l}{A_d} \right)^2 \tag{2.5}$$

where the total cross sectional area of the nozzles A_d can be written as

$$A_d = 4N \left(\frac{\pi}{4} d^2 \right) = \pi N d^2 \tag{2.6}$$

when 4 distributor arms are used as shown in figure 2.1. For $\rho_l = 1000$ kg m^{-3}, Δp in bar, v_l in m^3 h^{-1} and d in mm one obtains the following equation when the liquid is distributed through N identical RJH

$$v_l = 0.1599 d^2 N \sqrt{\Delta p} \tag{2.7}$$

The power input P (in W) to obtain a liquid flow rate v_l ($m^3\ h^{-1}$) at a given gauge pressure Δp (bar) is given by

$$P = \frac{v_l \Delta p}{0.036} = 1086 v_l^3 d^{-4} N^{-2} \tag{2.8}$$

again with d in mm. Eq.(2.8) shows that the power input to obtain a given v_l is strongly dependent on the nozzle diameter d, and that the distribution of a given liquid flow rate between several jet heads significantly reduces the power input.

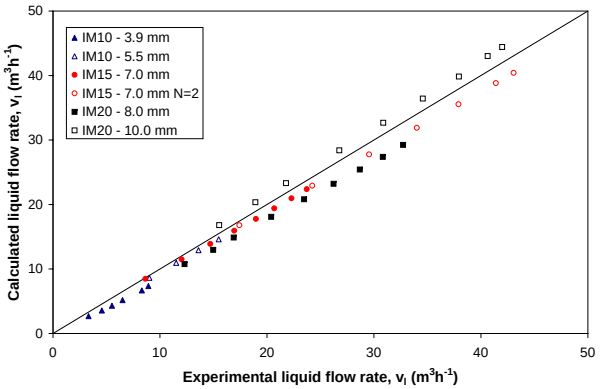

Figure 2.3. Volumetric liquid flow rate at un-aerated conditions calculated by Eq.(2.7) versus the experimentally determined flow rate.

Figure 2.3 shows experimental values of v_l (abscissa) and calculated v_l according to Eq.(2.7). Considering that the results are obtained with industrially manufactured machines the fit of the experimental data to the fundamental energy relation Eq.(2.5) is remarkably good. The difference between values calculated from Eq.(2.7) and experimental values can be explained by leak flows and friction losses. The rotary jet heads are designed to clean themselves. Thus, a certain part of the total liquid flow does not leave the machine from the nozzles. This is the reason why the experimental flow rate is up to 20% higher than the flow rate determined by Eq.(2.7) in the case of the IM10 with 3.9 mm nozzles. The relative importance of the leak flow is higher with small nozzles than with larger ones. As the flow rate increases for a particular RJH friction losses become more important. This is probably the reason why the experimental values are smaller than the values determined by Eq.(2.7) for the IM20 with 10.0 mm nozzles.

When the liquid is aerated by injection of air in the loop, the equation of motion for flow through N identical RJH gives the following equation if only the momentum terms are significant

$$-\frac{dp}{dz} = G\frac{du}{dz} \tag{2.9}$$

where p is the pressure, G is the mass flux, u is the linear velocity, and z is the coordinate in the direction of motion. The mass flux can be written as

$$G \approx \rho_l \frac{u}{1+n} = \rho_l \frac{u}{1+n_0 \frac{p_0}{p}} \tag{2.10}$$

where n is the ratio of the volumetric flow rates of respectively gas and liquid at the pressure p, and n_0 and p_0 are the ratio and the pressure at the pressure transmitter. The last equation is written assuming that gas expansion through the nozzles is isothermal. Substitution of Eq.(2.10) into Eq.(2.9) gives

$$-\frac{dp}{dz}\left(1+n_0\frac{p_0}{p}\right) = \rho_l u \frac{du}{dz} \tag{2.11}$$

which is integrated from the conditions at the transmitter (subscript 0) to the end of the nozzles (subscript t), again neglecting the kinetic energy at the transmitter.

$$u_t^2 = \frac{2}{\rho_l}\left(p_0 - p_t + n_0 p_0 \ln\left(\frac{p_0}{p_t}\right)\right) \tag{2.12}$$

The linear velocity at the outlet of the nozzles u_t of the bubbly flow can be related to the volumetric flow rates of gas and liquid

$$u_t = \frac{v_l + v_g}{A_d} = \frac{v_l\left(1+n_0\frac{p_0}{p_t}\right)}{\pi N d^2} \tag{2.13}$$

which upon insertion in Eq.(2.12) gives the following equation for the liquid flow rate when it is used that $p_0 = p_t + \Delta p$

$$v_l = 0.1599 d^2 N \sqrt{\Delta p} \times \frac{\sqrt{1+n_0\frac{\Delta p+p_t}{\Delta p}\ln\left(\frac{\Delta p+p_t}{p_t}\right)}}{1+n_0\frac{\Delta p+p_t}{p_t}} \tag{2.14}$$

Here v_l is in $m^3\ h^{-1}$, the nozzle diameter d is in mm, the pressure difference between the loop and the tank Δp is in bar, and finally the absolute pressure at the nozzle outlet p_t is in bar.

Eq.(2.14) assumes that gas expansion is both reversible and isothermal. However, the sudden expansion through the rotary jet head and through the nozzles in particular is neither fully reversible nor fully isothermal, and the volumetric liquid flow rate estimated by the fundamental Eq.(2.14) is much lower than the experimentally determined liquid flow rate at a given air flow rate. Consequently, an equation with two correction parameters α and β

was constructed

$$v_l = 0.1599 d^2 N \sqrt{\Delta p} \times \frac{\sqrt{1 + \alpha n_0 \frac{\Delta p + p_t}{\Delta p} \ln\left(\frac{\Delta p + p_t}{p_t}\right)}}{1 + n_0 \left(\frac{\Delta p + p_t}{p_t}\right)^{\beta}} \qquad (2.15)$$

$$= 0.1599 d^2 N \sqrt{\Delta p} \times \frac{\sqrt{1 + \alpha \frac{n_t p_t}{\Delta p} \ln\left(\frac{\Delta p + p_t}{p_t}\right)}}{1 + \frac{n_t p_t}{\Delta p + p_t} \left(\frac{\Delta p + p_t}{p_t}\right)^{\beta}}$$

where n_t is the ratio between gas and liquid flow rates at the pressure of the tank. Eq.(2.15) should merely be considered a data fitter but with the attractive feature that it reduces to Eq.(2.7) when the ratio of gas to liquid is zero. By least squares regression the values of α and β were determined to $\alpha = 1.41$ and $\beta = 0.587$ for a mixture of water and air. Figure 2.4 shows experimental values of v_l at aerated conditions (abscissa) and calculated values of v_l according to Eq.(2.15). The agreement between experimental and calculated values is very good, especially for the IM20.

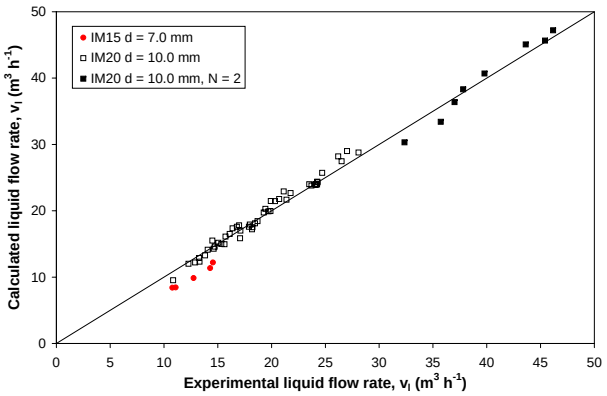

Figure 2.4. Volumetric liquid flow rate at aerated conditions calculated by Eq.(2.15) versus the experimentally determined flow rate.

The power input delivered by the pump P in W is again simply found as $v_l \Delta p / 0.036$, where Δp is in bar and v_l is in m^3 h^{-1}. For a given value of n_t, Eq.(2.15) can easily be solved for Δp at a certain value of v_l. The last factor is a weak function of Δp, and a good starting value for the iteration is obtained by inserting Δp calculated from Eq.(2.7) in the last factor.

2.4.2 Mixing

Figures 2.5 to 2.8 collect the experimental results for mixing with tracer addition to the liquid surface (figures 2.5 and 2.6) and for tracer addition to

the loop (figures 2.7 and 2.8) of 45 mL liquid into the bulk liquid (3.4 m^3) of the tank. Figures 2.5 and 2.7 show $t_{mix,95\%}$ (abbreviated to t_{mix} in the following) as a function of the volumetric liquid flow rate v_l while figures 2.6 and 2.8 use the specific power input P/V as abscissa.

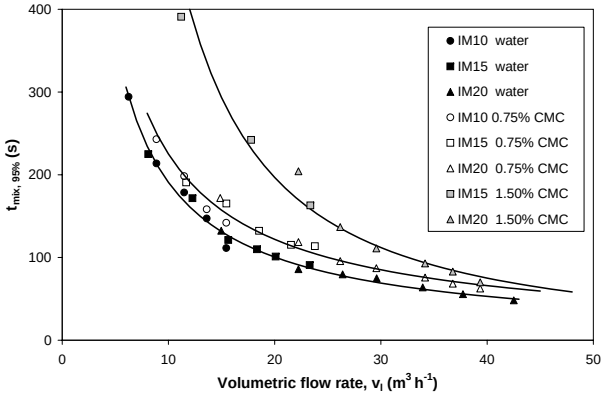

Figure 2.5. Mixing time versus volumetric flow rate for tracer addition to liquid surface for one rotary jet head placed in the center of the tank. The nozzle diameters were: IM10: 5.5 mm, IM15: 7.0 mm, IM20: 10.0 mm. Regression curves according to $t_{mix} = av_l^b$ are shown together with data points. (a, b) = ($1.60{\cdot}10^3$, -0.925), ($1.73{\cdot}10^3$, -0.885) and ($1.26{\cdot}10^4$, -1.39) for water, 0.75 wt% CMC and 1.50 wt% CMC, respectively.

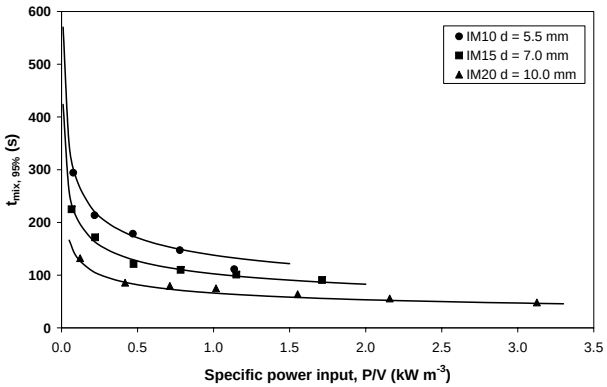

Figure 2.6. Mixing time in water versus specific power input for tracer addition to liquid surface. Curves are based on Eq.(2.17).

Figure 2.5 shows that t_{mix} is a unique function of v_l for each liquid (water and CMC solutions with viscosities of 27 and 137 mPa s) when tracer is added to the tank. A significant increase of t_{mix} is observed only at the highest value of the viscosity. The jet Reynolds number is fully turbulent for water and 0.75 wt% CMC (smallest Reynolds number higher than 4000, which is above the value of 2000 given by most authors (Revill, 1992; Fox and Gex,

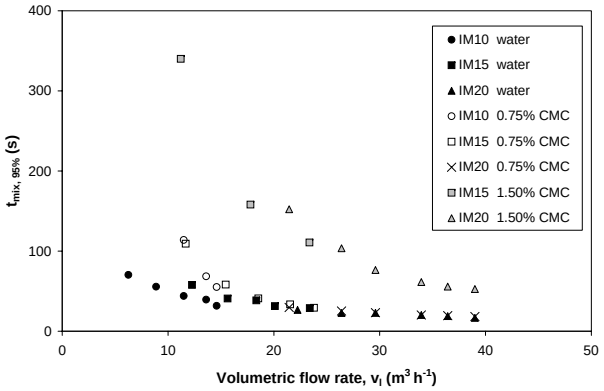

Figure 2.7. Mixing time versus volumetric flow rate for tracer addition in loop for one rotary jet head placed in the center of the tank. The nozzle diameters were: IM10: 5.5 mm, IM15: 7.0 mm, IM20: 10.0 mm.

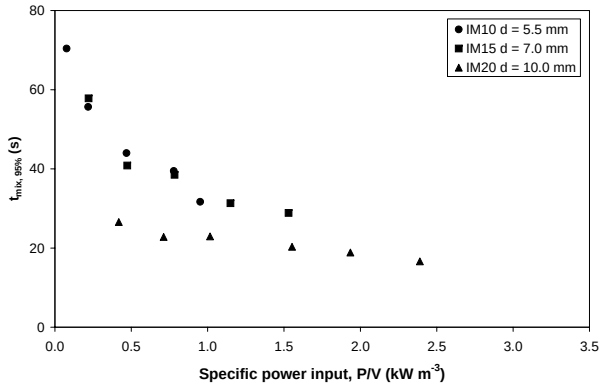

Figure 2.8. Mixing time in water versus specific power input for tracer addition in loop.

1956)), and the functionality is also alike, i.e. the exponent on v_l is the same within the experimental error. The increase in mixing time can probably be explained by the presence of relatively stagnant zones in the case of 0.75 wt% CMC. For mechanical stirrers an increase in mixing time has also been observed for a CMC solution compared to water, even though according to the Metzner and Otto approach (Metzner and Otto, 1957; Nienow and Elson, 1988) the flow was fully turbulent (Cronin et al., 1994). For the 1.50 wt% CMC solution (using a fixed viscosity of 137 mPa s) the Reynolds numbers are in the range 1032 to 2539, and the flow is consequently in the transitional range and in the range where a fully turbulent flow is realized (Revill, 1992). This explains both the much longer mixing times obtained and the change in functionality.

Figure 2.6 shows that the specific power input to reach a certain value of

t_{mix} decreases rapidly with the size of the nozzles of the RJH. The curves on figure 2.6 can in fact be derived from the curves on figure 2.5 as shown below. By least squares regression of the experimental results the following relation is derived for water

$$t_{mix} = 1.60 \cdot 10^3 v_l^{-0.925} \tag{2.16}$$

where t_{mix} is in s and v_l in $m^3\ h^{-1}$. When this expression is inserted into Eq.(2.8) one obtains for $N = 1$ in water and with tracer addition to the liquid surface

$$t_{mix} = 9.49 \cdot 10^3 d^{-1.23} \left(P/V\right)^{-0.308} \tag{2.17}$$

Since only one tank volume $V = 3.4\ m^3$ was used in the experiments reported here the inclusion of V in Eq.(2.17) is rather artificial and the equation should not be used with other volumes. In the equation P is measured in W, d in mm and t_{mix} in s.

The almost perfect agreement between experimental points and simulation according to Eq.(2.17) on figure 2.6 derives from the very good agreement of the volumetric flow data with the simple energy equation Eq.(2.5). The main features of mixing by RJH with tracer addition to the liquid surface are clearly exposed by the above formulas. The mixing time in a given medium is only a function of the volumetric flow rate v_l, and the power input needed to achieve the flow rate is given by Eq.(2.8). It is noted that the power input to achieve a given t_{mix} decreases drastically when d increases, and faster than with stationary nozzles. For media with viscosity different from that of water the two parameters in the relation between v_l and t_{mix} have different values from those shown in Eq.(2.16), but the power input can again be calculated using Eq.(2.8). Experimentally determined values of the two parameters for CMC solutions are given in the caption to figure 2.5.

Figures 2.7 and 2.8 show that for water and 0.75 wt% CMC injection of a tracer in the loop gives much smaller values for t_{mix} at a given volumetric flow rate v_l or specific power input P/V than when tracer is added to the liquid surface. Furthermore, with the data at hand it it not possible to ascertain whether the mixing time is still a unique function of v_l for a given liquid viscosity or whether it is rather inversely proportional to the product of the jet linear velocity in the nozzle outlet u_d times the nozzle diameter d (i.e. $t_{mix} \propto {}^1/_{(u_d d)} \propto \frac{d}{v_l}$) as is found with stationary turbulent jets (Grenville and Tilton, 1996). Thus, the values of the mixing time is lower for a given volumetric liquid flow rate with the IM10 with 5.5 mm nozzles than with the IM15 with 7.0 mm nozzles, but at the same time this is not observed when comparing the IM15 with 7.0 mm nozzles with the IM20 with 10.0 mm nozzles.

For the highest liquid viscosity the difference between the mixing times obtained with the two different injection methods is not nearly as large as is

found with water and 0.75% CMC. This is again ascribed to the difference in Reynolds numbers. Liquid feed addition to the recirculation loop is, however, always to be preferred. If the fermentation medium is a pseudo-plastic liquid (as is the case in penicillin fermentation, in xanthan gum production, or when making detergent enzymes) the liquid viscosity is extremely shear-rate sensitive and much better mixing of feed is to be expected via the rotary jet head than by direct addition to the tank.

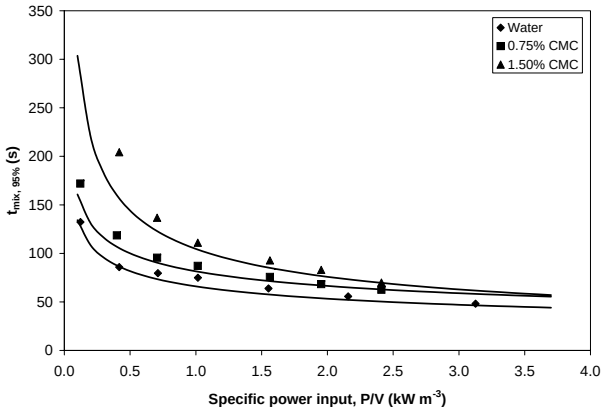

Figure 2.9. Mixing time for IM20 RJH ($d = 10$ mm) versus specific power input for tracer addition to liquid surface. The curves are based on equations similar to Eq.(2.17) using the values of a and b shown in the caption to figure 2.5.

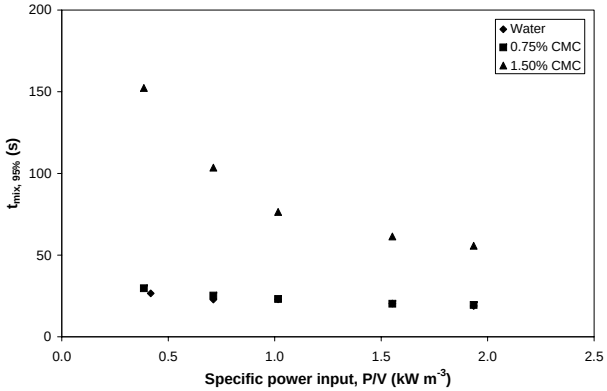

Figure 2.10. Mixing time for IM20 RJH ($d = 10$ mm) versus specific power input for tracer addition to the loop.

Figures 2.9 and 2.10 give some specific results for the IM20 machine which is the most interesting choice since a large liquid flow rate is obtained for a low power input. With tracer addition in the loop the mixing time is much lower than with addition to the liquid surface for the two low-viscosity liquids. For the high viscosity fluid it does not make much difference whether the pulse is injected into the recirculation loop or added directly to the tank.

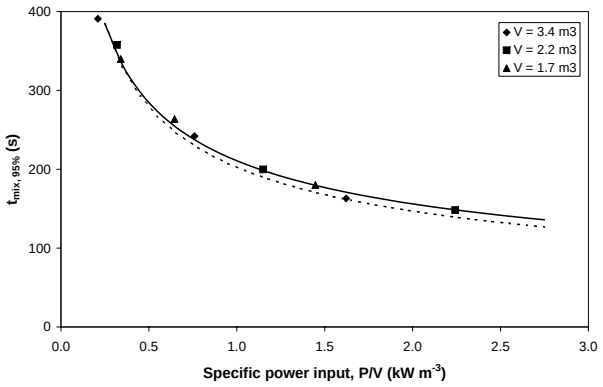

Figure 2.11. Specific power input P/V (kW m^{-3}) to obtain a given mixing time t_{mix} with one IM15 machine located in the middle of the liquid volume in 1.50 wt% CMC solution and with tracer addition to the liquid surface. Three different reactor volumes V = 1.7, 2.2 and 3.4 m^3 were used by varying the liquid height. The specific power input to obtain a given t_{mix} is seen to be independent of liquid height. Full line: Empirical correlation between t_{mix} and P/V according to Eq.(2.18). Broken line: Based on Eq.(2.19).

Figure 2.11 shows the mixing time as a function of the specific power input for mixing in 1.50 wt% CMC with one IM15 RJH placed in three different liquid volumes, and with tracer addition to the liquid surface. The volumes used were 3.4, 2.2, and 1.7 m^3, and they were obtained by adjusting the liquid height, always placing the RJH in the middle of the liquid volume. The figure shows that the power input P to achieve a certain mixing time t_{mix} with a given rotary jet head configuration is proportional to the liquid volume. Based on all the results on Figure 2.11 the following relation is obtained by regression for 1.50 wt% CMC solution mixed by one IM15 machine

$$t_{mix} = 4.22 \cdot 10^3 (P/V)^{-0.434} \tag{2.18}$$

which is shown on figure 2.11 together with the experimental data. An equally good fit of the experimental results is obtained from figure 2.5 with $a = 1.26 \cdot 10^4$ and b = -1.39 (1.50 wt% CMC), d = 7.0 mm for the IM15 machine and the liquid volume, V = 3.4 m^3. When these values are inserted in Eq.(2.8) one obtains

$$t_{mix} = 4.96 \cdot 10^3 (P/V)^{-0.463} \tag{2.19}$$

The excellent agreement between Eq.(2.19) and the experimental results of figure 2.11 could indicate that the equation will also hold for other volumes, i.e. that the power input P needed to obtain a given mixing time is, indeed, proportional to V when tracer is added to the liquid surface. It should be noted that the Reynolds numbers of the experiments were in the range 936 to 2154, and since the behavior is much different with the 1.50 wt% CMC

solution than with the other liquids it cannot be concluded that the results can be extrapolated to 0.75 wt% CMC and water. For a stationary jet in the transitional range the mixing time can according to Fox and Gex (1956) be written in the following way for a given liquid

$$t_{mix} \propto \frac{TH^{1/2}}{u_d^2 d^2} \propto \frac{TH^{1/2}d^2}{v_l^2} \tag{2.20}$$

where T is the tank diameter and H is the tank height. When this equation is written is term of specific power input the following is obtained

$$t_{mix} \propto \frac{T^{-1/3}H^{-1/6}}{(P/V)^{2/3}d^{2/3}} \tag{2.21}$$

Observe that the mixing time decreases for a stationary jet at scale-up at constant specific power input and nozzle diameter (the same is observed for an impeller in the transitional flow regime). However, when the liquid volume is changed by adjusting the liquid height as we did in the experiments, the effect is minor. In our experiments the liquid height was only changed by a factor of 2, and with a stationary jet operated at constant specific power input this would only lead to a change in mixing time by a factor of $2^{-1/6} = 0.89$. Consequently it is hard to say whether scale-up performs differently in the rotary jet head system than in systems based on stationary jets.

2.4.3 Oxygen transfer

Figure 2.12 is a typical DOT response curve in which $k_l a$ is determined at 25°C by the H_2O_2 method as described in the section on experimental procedures. The volumetric air flow rate v_g was constant at 39.5 ± 0.2 Nm^3 h^{-1} throughout the experiment. Addition of H_2O_2 started at 11.5 minutes, and after 4 minutes a steady state was reached at which the oxygen tension was 50 ± 1.7% higher than before addition of H_2O_2. The steady state was kept for 18 minutes and after cessation of the H_2O_2 injection the oxygen tension settled back to its original value. Using Eq.(2.4) with a flow of 93.2 mole h^{-1} H_2O_2 and $V = 3.4$ m^3 the value of $k_l a$ is calculated to 93 h^{-1}.

We tried to correlate the obtained $k_l a$ in terms of power input delivered by the pump and superficial gas velocity. For one IM20 RJH, we found

$$278(P/V)^{0.27}u_g^{0.63} \tag{2.22}$$

with P/V in W m^{-3}, the superficial gas velocity u_g in m s^{-1} and $k_l a$ in h^{-1} With the same exponents on u_g and P/V, the constant was changed from 278 to 413 when two IM20 RJH were used. Thus, we tried to correlate the

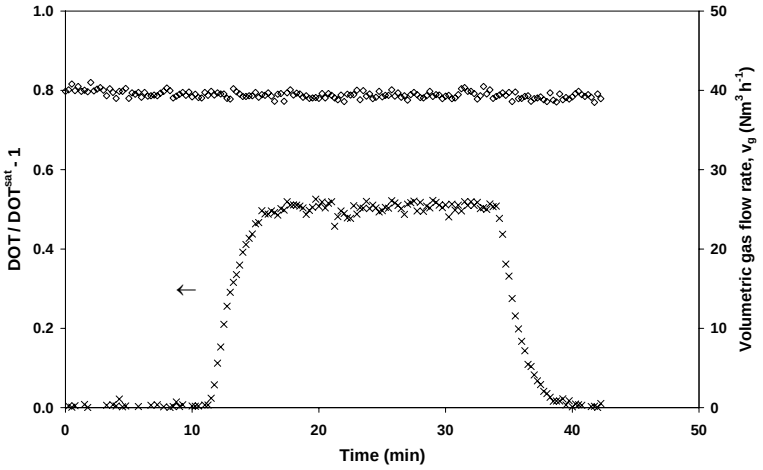

Figure 2.12. Typical mass transfer experiment using the hydrogen peroxide method in water at 25°C. One IM20 (d = 10 mm) machine was used. The steady state oxygen tension was 50% higher than when no peroxide was added.

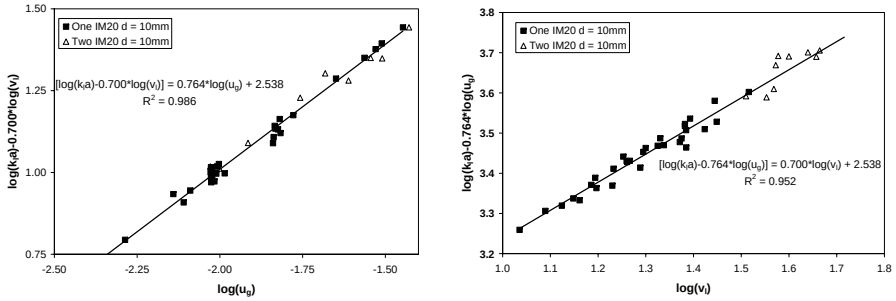

Figure 2.13. $k_l a$ data for one (black squares) and two (open triangles) IM20 (d = 10 mm) RJH. The regression lines are based on the data obtained with one IM20. The regression is given in Eq.(2.23).

data in terms of v_l instead of P/V. In figure 2.13 the data for $k_l a$ (in h^{-1}) with one or two IM20 RJH are regressed versus the volumetric rate of liquid circulation v_l ($\mathrm{m}^3\ \mathrm{h}^{-1}$) and the superficial gas velocity u_g, respectively. For $N = 1$ data the correlation of the figure is

$$k_l a = 345 u_g^{0.76} v_l^{0.70} \tag{2.23}$$

Using the same exponents to v_l and to u_g the numerical coefficient for the $N = 2$ regression line is 350 which shows that Eq.(2.23) gives the same prediction of the mass transfer coefficient whether a given v_l is dispensed through one or two jet heads. This result is unlikely to hold when N is large.

2.5 Discussion

For a classical engineering subject such as the mixing of one liquid into another the available literature concerning correlations between mixing time t_{mix} and operational or equipment specific variables is of course voluminous. The system studied here is, however, very different from conventional designs.

As in any type of mixing equipment, blending of two miscible liquids is the result of two processes: a convection process and an energy dissipation process. The liquid jets from the RJH move to ever changing parts of the bulk tank-volume, and do not create a stationary flow pattern in the tank, as is the case for a stationary turbulent jet. Thus when tracer is added to the liquid surface the mixing time is much longer than when tracer is added in the loop, in contradiction to what is observed with stationary jets where the mixing time is claimed to be independent of the addition point of the tracer Yianneskis (1991). This might explain why the mixing time was found to be a function of v_l alone when tracer was added to the liquid surface. The energy is simply utilized inefficiently for this type of mixing and the convection process alone determines the outcome of the mixing process. When tracer was added in the loop the mixing time declined significantly, and feed should of course always be distributed this way. With the data at hand it was not possible to ascertain whether the mixing time was a function of the nozzle diameter ($t_{mix} \propto (d/v_l)^{\alpha}$) in a fashion similar to that found for stationary jets when tracer was added in the loop.

In large-scale more than one RJH should of course be used both to ensure that no dead zones are formed and to operate at a low power input, see Eq.(2.8). The best location of the RJH is probably that in which the penetration of jets from the different RJH overlap to cover the entire tank volume and the feed should be equally divided between the RJH. If the total liquid flow is through one pipe, which is divided to the jet heads, only a single feed injection point is needed. Due to the non-stationary nature of the jet heads, zoning will probably not occur when more jet heads are used.

The mixing times obtained in this study can be directly compared with data from the literature. At a specific power input of 500 W m^{-3} we obtained mixing times of 81 s and 23 s for respectively tracer addition to the liquid surface and for addition in the loop in water with one IM20 (d = 10 mm).

Based on turbulence theory Nienow (1997) showed that with single impellers in tanks of aspect ratio 1 (i.e. $H = T$), the mixing time is independent of impeller type, and based on experimental work by e.g. Cooke et al. (1988) and Ruszkowski (1994) the following equation was proposed for turbulent mixing

$$t_{mix,95\%} = 5.9T^{2/3} \left(\frac{P}{\rho_l V}\right)^{-1/3} \left(\frac{D}{T}\right)^{-1/3} \tag{2.24}$$

where D is the impeller diameter and all variable values are in SI units. For a 3.4 m^3 tank with $D/T = 0.5$, Eq.(2.24) predicts a mixing time of 13 s at a specific power input of 500 W m^{-3}.

However, as discussed in the general introduction it is known that the mixing time increases in systems of high aspect ratio H/T where multiple impellers are needed. This is especially true when radial flow impellers are used since these give rise to zoning (Nienow, 1998; Cronin et al., 1994). Cooke et al. (1988) found that the mixing time increased with H/T when comparing data obtained in two tanks of $H = T$ (20 L and 4.3 m^3 volume) stirred by a single impeller with a tank of $H = 3T$ (60 L) stirred by 3 impellers. They gave the following equation for multiple Rushton turbines and ICI gasfoil impellers

$$t_{mix,90\%} = 3.3 N^{-1} Po^{-1/3} \left(\frac{D}{H}\right)^{-2.43} \tag{2.25}$$

where Po is the dimensionless power number, and N is the stirrer speed. The equation can be rewritten in the following way when the definition for the power number is used

$$\begin{aligned} t_{mix,90\%} &= 3.3 \left(\frac{P}{\rho_l V}\right)^{-1/3} V^{-1/3} D^{5/3} \left(\frac{D}{H}\right)^{-2.43} \\ &= 3.6 T^{2/3} \left(\frac{P}{\rho_l V}\right)^{-1/3} \left(\frac{D}{T}\right)^{-0.76} \left(\frac{H}{T}\right)^{2.10} \end{aligned} \tag{2.26}$$

again with all variables in SI units. For the tank under study with $T = 1.256$ m and $H/T = 2.18$, the equation gives a 90% mixing time of 46 s for $D/T = 0.5$ at a specific power input of 500 W m^{-3}. If it is assumed that mixing is a first order process a 95% mixing time can be calculated as

$$t_{mix,95\%} = \frac{\ln(1 - 0.95)}{\ln(1 - 0.90)} t_{mix,90\%} = 1.30 \cdot t_{mix,90\%} \tag{2.27}$$

Thus the 95% mixing becomes 60 s. It is well known that the mixing time decreases in multiple impeller systems if axial flow impellers are used instead of radial flow impellers (Nienow, 2000; Nienow and Bujalski, 2004). It has not been possible to find data in the literature for a reactor configuration with the exact same geometry as the the one used in our study, but I will try to give the reader a general idea of the expected mixing time in a system stirred by multiple axial flow impellers compared to that found in radial flow impeller systems.

Otomo et al. (1995) studied different dual impeller systems in a vessel with $H/T = 2$ and a volume of 0.59 m^3. For a specific power input of 460 W m^{-3} a 95% mixing time of 30 s was achieved with Rushton turbines ($D/T = 0.50$) while a mixing time of 14.9 s was found with Lightnin A315 impellers (D/T

= 0.42). Thus a reduction in mixing time of 50% was obtained with the axial flow impellers. Vrábel et al. (2000) studied a tank with a liquid volume of 8 m^3 and an aspect ratio of 1.59. Two different impeller systems were studied. With 3 Rushton turbines ($D = 0.41T$) a mixing time of around 80 s was found at a specific power input of 500 W m^{-3}. With the radial flow impeller Scaba 6RSGT ($D = 0.56T$) as bottom impeller and the axial up-pumping hydrofoil impeller Scaba 3HSP ($D = 0.61T$) as the 2 upper impellers, a mixing time of around 30 s for a specific power input of 500 W m^{-3} is to be expected if the results reported can be extrapolated. It is difficult to say whether the reduction in mixing time is only caused by less zoning, or whether the increased impeller diameter also contributes to the reduction in mixing time. Based on this information, it is probably safe to state that the mixing time in the tank investigated in this study at a specific power input of 500 W m^{-3} is smaller with an IM20 RJH than found with multiple radial flow impellers.

As discussed in the introductory chapter Grenville and Tilton (1996) proposed that the mixing time for turbulent stationary jets should be correlated by

$$t_{mix,99\%} = K_Z \frac{Z^2}{u_d d} \tag{2.28}$$

where Z is the jet's free path in m., u_d is the linear velocity of the jet at the nozzle outlet in m s^{-1}, and d is the nozzle diameter in m. Grenville and Tilton (1996) determined the constant K_Z to be equal to 3.0 from measurements in 3 different scales and by inclusion of data from another source. The equation is suggested to hold for the following conditions (Grenville and Nienow, 2004) in the turbulent range: $0.2 < H/T < 2.0$, 0.178 $m^3 < V <$ 1200 m^3, $1.32 \cdot 10^{-2}$ m $s^{-1} < u_d d/Z < 0.137$ m s^{-1}, $86 < Z/D < 753$. The mixing time for 95% mixing can be calculated as 0.65 times the mixing time for 99% if mixing is assumed to be first order. Thus for 95% mixing the constant K_Z is reduced to 1.95. The data were obtained in systems where the jet was angled so that it intercepted the liquid surface at the opposite tank wall in order to maximize the jet path length, which maximizes liquid entrainment as is recommended by Revill (1992). Thus Z should be calculated from the aspect ratio H/T

$$Z = \sqrt{1 + \left(\frac{H}{T}\right)^2} \left(\frac{4VT}{\pi H}\right)^{1/3} \tag{2.29}$$

Consider now one stationary nozzle with a nozzle diameter of 20.0 mm (same total cross sectional nozzle area as with an IM20 RJH with 4 nozzles of diameter 10.0 mm) aligned as recommended in the vessel investigated in this study. For this configuration the volumetric flow rate is $6.95 \cdot 10^{-3}$ m^3 s^{-1} at a specific power input of 500 W m^{-3}, and the linear velocity at the

nozzle outlet u_d is 22.1 m s^{-1}, and finally Z is equal to 3.01 m. Thus the mixing time determined by Eq.(2.28) is $t_{mix,95\%} = 1.95\frac{3.01^2}{22.1 \cdot 0.02} = 40$ s. The value of $u_d d/Z$ of 0.147 m s^{-1} is, however, outside the range for which the equation was derived as is H/T. Even though it can be difficult to apply this equation on the system studied here, it seems that the mixing time obtained with a single nozzle with a cross sectional area equivalent to that of the total cross sectional area of the 4 nozzles on an IM20 RJH with 10.0 mm nozzles is smaller than the mixing time obtained with the IM20 RJH when the tracer is added to the liquid surface, while the mixing time is larger for the stationary jet compared to the situation where tracer is added in the loop.

We have also tried to compare the results of the mass transfer study with the numerous studies on transfer of oxygen from air to water that are available in the open literature. Again it is difficult to make a relevant comparison between literature results and the results obtained with the RJH system since the concept of mass transfer by RJH is quite different from the concept of mass transfer by mechanical stirring of the medium, the standard operation in most bio-applications.

van't Riet (1979) obtained the following correlation by reviewing the literature for $k_l a$ in mechanically stirred reactors valid for water-like media and for P/V between 500 and 10,000 W m^{-3}

$$k_l a_d = 93.6 \left(\frac{P}{V}\right)^{0.4} u_g^{0.5} \tag{2.30}$$

where $k_l a_d$ is measured in h^{-1} while P/V and u_g again are in SI units. Vasconcelos et al. (2000) used the hydrogen peroxide method in a system stirred by two disc turbines with a liquid volume of 0.094 m^3 and $H = 2T$ and obtained a correlation similar to Eq.(2.30) but for $k_l a$ rather than $k_l a_d$. The numerical constant was 22.3, and the exponents 0.51 on u_g, 0.66 on P/V.

A comparison between the RJH system and a mechanically stirred system in a tank of the dimensions used in our study (volume 3.4 m^3, tank diameter of 1.256 m) can be made by the direct use of Eqs.(2.23) and (2.30). To compare the systems the power input to the liquid in the RJH system has to be calculated. This is done after solving for Δp at given values of u_g and v_l by the use of Eq.(2.15). Figure 2.14 shows values of $k_l a$ (broken line) for the rotary jet head configuration with 2 IM20 RJH and for mechanically stirred systems at different values P/V at a fixed value of P/V. The van't Riet (1979) and the Vasconcelos et al. (2000) correlations were used to exemplify the performance of mechanically stirred systems. It is seen that with this RJH configuration the volumetric mass transfer coefficients are not impressive compared to mechanically stirred systems when one considers that gas compression work is not considered in the calculation of P/V.

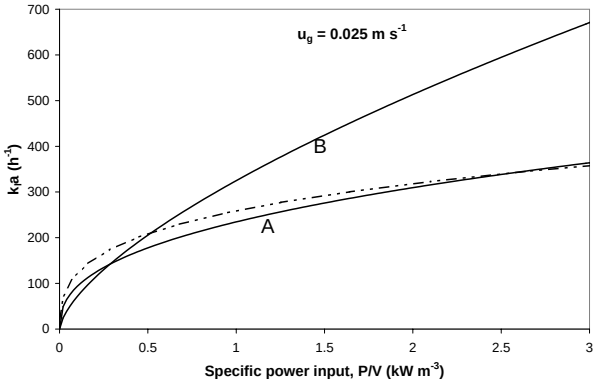

Figure 2.14. Comparison of the RJH system and mechanically stirred systems in a tank of volume 3.4 m^3 with a tank diameter of 1.256 m and height to diameter ratio 2.18. The superficial gas velocity used is 0.025 m s^{-1} corresponding to a volumetric gas flow rate of 0.55 vvm. Full lines: (A) van't Riet (1979), (B) Vasconcelos et al. (2000). Broken line: IM20 RJH $d = 10$ mm, $N = 2$. The correlations for mechanically stirred systems give very different results depending on the exponents to P/V and u_g proposed by the authors. Be aware that the volumetric mass transfer coefficient given by van't Riet (1979) is based on the volume of the dispersion and not on the liquid volume.

At this point it is not possible to say why $k_l a$ could be correlated in term of v_l rather than P/V, which is usually found to be the governing parameter, and it is therefore not possible to say whether the correlation can be extrapolated to systems with more rotary jet heads or different nozzle diameters.

Chapter 3

Enzymatic oxidation of lactose to lactobionic acid I: kinetics

3.1 Background

The Danish company Novozymes A/S investigates an enzymatic process for conversion of lactose to lactobionic acid. Since the process requires oxygen Novozymes expressed an interest in the rotary jet head system, and we agreed that part of the ph.d. project should be devoted to this application of the rotary jet head system.

We decided that an initial study should be conducted in small-scale to obtain the kinetics for the process prior to pilot-scale experiments in the rotary jet head system. As it turned out the kinetic investigation ended up being a project on it's own due to the many interesting facets of the kinetics.

3.2 Introduction

Lactose solution in the form of whey or whey permeate is a by-product of cheese production. The annual production of whey is 145 million tonnes of which only approximately 60% is utilized. Lactose can be crystallized as an α-lactose monohydrate by cooling of concentrated whey or whey permeate (Harju, 1991). Due to the huge amounts produced of this carbohydrate new methods for production of value-added products derived from lactose are desired. One such product is lactobionic acid.

Lactobionic acid (4-O-β-D-galactopyranosyl-D-gluconic acid) was first synthesized and described by Fischer and Meyer (1889). It is comprised of one molecule of galactose joined to a molecule of gluconic acid via a β-glucosidic

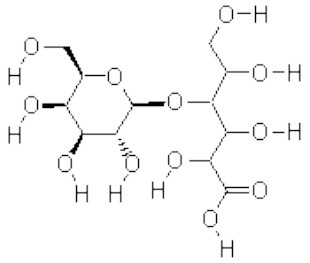

Figure 3.1. Structure of lactobionic acid.

Table 3.1. Properties of lactobionic acid according to the Merck Index.

Molecular weight (g mol^{-1})	358
pK_a	~ 3.8
Melting point (°C)	113-118
Solubility	Freely soluble in water, slightly soluble in methanol, ethanol, and glacial acetic acid
Other properties	Dehydration by distillation with dioxane yields lactobiono-δ-lactone

bond, see figure 3.1. The physicochemical properties of lactobionic acid are given in table 3.1.

3.2.1 Applications of lactobionic acid and its salts

At present lactobionic acid and its salts are mainly used in high-price speciality products. Lactobionate is e.g. used as an ingredient in solutions commonly used for stabilizing organs prior to organ transplantation (e.g. The University of Wisconsin (UW) solution and Celsior solution) (Southard and Belzer, 1995). Solutions containing lactobionate have been shown to suppress hypothermically induced cell swelling in all tissues tested. Furthermore, the metal-chelating properties of the substance leads to reduced oxidative damage to tissue during storage due to inhibition of the iron-catalyzed production of hydroxyl radicals (Shepherd et al., 1993; Charloux et al., 1995). The average wholesale price for UW solution was US$ 282 per liter in 2004 (Southard, 2004).

Lactobionic acid is also used to enhance the solubility of macrolide antibiotics such as erythromycin and to stabilize the solution (Hoffhine, 1956; Dutta and Basu, 1979; Shi et al., 1989). Erythromycin, a broad-spectrum antibiotic used for the treatment of infections caused by Gram positive bacteria, is mainly available in oral formulations. However, a small percentage of erythromycin is used as an injectable drug in the form of erythromycin

lactobionate. Hoffhine (1956) found that the solubility of erythromycin lactobionate in water is 200 mg mL^{-1} which should be compared to the solubility of erythromycin in water of 2 to 4 mg mL^{-1}. Furthermore, calcium lactobionate is used in human and veterinary medicine for stabilization of supersaturated solutions of calcium gluconate, the traditional form of calcium supplementation (Sen Gupta et al., 1967).

Other pharmaceutical applications involving lactobionic acid or its salts have been patented. Thus salts of sulphated lactobionic acid have been patented as inhibitors of the complement system (part of the immune response system) (Joseph and Bernstein, 1981) and lactobionic acid in an acetate glycine buffer has been claimed to stabilize γ-interferons (Goldstein and Thatcher, 1990). Recently lactobionic acid (and the lactose derivative lactitol) has been shown to inhibit trans-sialidase activity in the parasite *Trypanosoma cruzi* which causes Chagas' disease, one of the major health problems in Latin America with around 18 million people being infected and with no effective treatment being available (Agusti et al., 2004). Sialic acid bound to the surface of the parasite protects the parasite against lysis from the complement system and has a function in mammalian host cell invasion. To acquire sialic acid from host glucoconjugates *T. cruzi* expresses a trans-sialidase on its surface. It is this trans-sialidase which is inhibited by lactobionic acid.

Lactobionic acid (and its salts) has the potential to become a bulk chemical provided that the price becomes competitive with e.g. citric acid. It could be used as a biodegradable builder in washing or cleaning detergents (Gerling and Wilke, 1991; Gerling, 1998) and in various food technology applications. The primary function of builders in washing powder is to eliminate calcium and magnesium ions by complex formation or by ion exchange and to support the action of the surfactants. Also, builders should contribute substantially to the dispersion of dirt in washing solutions. Furthermore, they should inhibit greying and yellowing of the textiles and show good dirt-carrying capacity, preventing incrustation on textiles and deposits in washing machines. Lactobionic acid has as already mentioned excellent chelating power. Washing powder containing lactobionic acid does, however, also show better dispersing power and equally good washing ability as the builder STPP (containing polyphosphates) in comparative tests (Gerling and Wilke, 1991; Gerling, 1998). Furthermore, the greying of textiles is prevented just as well as with known builders, and less incrustation is observed.

In food technology the envisaged benefits of using lactobionic acid include reduction of souring and ripening time in cheese and yoghurt production, flavor enhancement and elimination of bitterness, improvement in the taste perception of sourness, and preservation of aroma freshness (Gerling, 1998). Furthermore, calcium lactobionate contributes to the improvement of crispness. Lactobionic acid still has considerable sweetening power and it can be

used as an acidulant with a milder and rounder flavor than lactic acid. This was noted by Booij (1985) who acidified milk with lactobionic acid to pH 4.2. The taste was described as the taste of cultured buttermilk sweetened with sugar.

Another possible application is found for the mineral salt complexes formed by lactobionic acid, which can be used to fortify functional drinks with essential minerals (Toshiaki et al., 1995a). As an example, milk may be used to deliver supplemental iron and copper, thus preventing anemia in infants, children, and adolescents. However, addition of these transition metals may cause oxidized flavors and odors in dairy products as a result of lipid peroxidation of milk fat. It was demonstrated by Hegenauer et al. (1979a,b) that lipid peroxidation was reduced significantly when iron and copper was added in the form of Fe(III) and Cu(II) chelates of lactobionate. It has also been proposed that lactobionic acid can be added to functional food due to its postulated potential as a prebiotic (a non-digestible food ingredient that beneficially affects the host animal by selectively stimulating the microbial activity of one or a limited number of probiotic bacteria in the colon) (Toshiaki et al., 1995b).

Presently lactobionic acid and its salts has no clearance in food technology in the EU. It needs to be registered and accepted as a novel food before it can be used. Registration as novel food involves submission of results of toxicology tests and animal studies. In the US, calcium lactobionate has been accepted by the FDA as a firming agent in dry pudding mixes (Code of federal regulations, 2004).

Lactobionic acid is also used as a new ingredient in skin care products due to its properties as an antioxidant and due to excellent humectant properties (Green et al., 2001). Lactobionic acid is a hygroscopic compound, binding moisture to the extent that a natural gel matrix forms. The gel matrix film contains approximately 14% water and may contribute to its skin conditioning benefits. Like other polyhydroxy acids, lactobionic acid provides anti-aging effects (Edison et al., 2004). Furthermore, clinical skin studies indicate that lactobionic acid is safe and non-irritating.

The lactone of lactobionic acid - obtained by dehydration - is an ideal raw material for amide synthesis (Gerling, 1998). Thus, Gerling et al. (1996) synthesized lactobionic acid amides from lactobionic acid and a mixture of primary fatty acid amines containing at least 30 w/w % fatty amines with chain length between 14 and 18 carbon atoms. The good surface active properties, the high solubility and the good foam stabilization properties in aqueous solution of the lactobionic acid amides make them suitable as softening, detergent, emulsifying, foam stabilizing and/or thickening agents in detergents, cleaning agents, fabric softeners and in cosmetic formulations.

Another application of lactobionic acid amides is in corrosion protection (Gerling et al., 1998a,b). In contrast to many of the conventional corrosion protection substances, lactobionic acid amides are neither toxic nor irritating, and they are biodegradable, non-allergenic and non-mutagenic. The corrosion protection properties of different lactobionic acid amides in aqueous solution (3 %) were tested on grey cast iron chips. While severe corrosion was detected when the chips were subjected to water for 2 hours, no corrosion or traces of corrosion was observed when the amides were added. Furthermore, it has been shown that corrosion of steel in water or brine can be reduced significantly by using lactobionic acid amides in low concentrations (0.1-0.5 %) (Gerling, 1998). Also, Schmitt and Saleh (2000) showed that lactobionic acid amides - in particular lactobionic acid oleylamide - were effective against localized corrosion of carbon steel under severe sour gas conditions (up to 4 MPa hydrogen sulfide) in brine/hydrocarbon mixtures. This type of corrosion is a problem in sour oil and gas production wells.

3.2.2 Production of lactobionic acid

Several chemical, electrochemical, and catalytical as well as microbial and enzymatic processes have been used for the production of lactobionic acid.

Chemical processes

Fischer and Meyer (1889) - the discoverers of lactobionic acid - used bromine for the oxidation of lactose to lactobionic acid. The yield was, however, only 30% due to the drop in pH and the resulting formation of hydrobromic acid which partly hydrolyzed lactose. The bromine oxidation process was improved by Hudson and Isbell (1929) by the use of buffering salts which prevented the formation of hydrobromic acid and gave a faster reaction with a yield in excess of 90%.

Electrochemical processes

The chemical oxidation of lactose can be further improved by the use of electrochemical cells. In the electrochemical method developed by Isbell and Frush (1931) bromine is used as oxidizing agent but only a small amount is needed because the bromide is reoxidized at the anode. Calcium carbonate is used as a pH-regulator. The electrochemical cell configuration was later improved by Sen Gupta et al. (1968) who found that yield and purity was improved when a rotating anode was used (Sen Gupta et al., 1968) instead of stationary electrodes (Sen Gupta et al., 1967). Druliolle et al. (1995) provided a new electrolytical method avoiding the use of bromine. In this

method lactose oxidation is performed in carbonate buffered solution on a platinum electrode modified with lead. Druliolle et al. (1995) reported a lactobionic acid selectivity of 90% when 87% of 10 mM lactose present initially had been converted. Further electrolysis did not result in the formation of higher concentrations of lactobionic acid.

Catalytical processes

Lactobionic acid can also be produced by subjecting a lactose solution to a dehydrogenation catalyst, thereby producing the lactone which is readily hydrolyzed to lactobionic acid. Platinum has proved to be an effective dehydrogenation catalyst in alkaline solution. Thus, de Wit et al. (1981) showed that the degree of conversion was more than 99% with a selectivity of 100% after 30 min when a 60 mL solution of 0.22 M lactose in 0.33 M KOH containing 0.60 g of a 5% Pt/C catalyst was stirred in a reaction vessel under a nitrogen atmosphere at 25°C. An equimolar amount of hydrogen gas was liberated. In the method used by Solvay Deutschland GmbH calcium lactobionate is produced by catalytical oxidation of lactose by continuously feeding an aqueous solution of lactose and calcium hydroxide into a reactor containing a special platinum catalyst (Gerling, 1998). Fuertes and Fleche (1991) patented a process where a catalyst containing 5% Pd and 3.5% Bi on carbon was used. They showed that a degree of conversion of 91% could be attained in 1.2 hours when 1 kg of 20% solution of lactose containing 6 g catalyst was treated at 35°C and pH was kept constant at 9.0 $\pm$ 0.5 by addition of NaOH. With the same amount of a commercially available 5% Pd/C catalyst the degree of conversion was less than 10% even after 4 hours.

Microbial processes

Stodola and Lockwood (1947) were the first to observe that several species of the genus *Pseudomonas* are able to oxidize lactose to lactobionic acid. Of the fifteen species examined *Ps. graveolens* was the most effective for the oxidation, which was performed in aerated rotating drums on a medium containing 9.3% lactose, corn steep liquor, urea, $CaCO_3$ for neutralization (insoluble but will dissolve as pH drops), and salts. After 165 h of fermentation all sugar was consumed and the yield was 75% mol mol^{-1}. Kluyver et al. (1951) studied the formation of lactobionic acid by *Pseudomonas* in more detail. Two species *Ps. calco-acetica* and *Ps. quercito-pyrogallica* were found to be good producers of lactobionic acid. In shake-flask cultures containing 10% lactose, yeast extract, $CaCO_3$, and salts yields of more than 90% mol mol^{-1} calcium lactobionate were obtained after 2-4 days before all lactose was depleted. Investigation of the later phases of the cultures showed that the lactobionate was then slowly consumed. Bentley and Slechta (1960) studied the lactose

oxidation by three of the *Pseudomonas* species (*Ps. quercito-pyrogallica*, *Ps. calco-acetica*, and *Ps. aromatica*) from the study of Kluyver et al. (1951) in further detail. Recently, Miyamoto et al. (2000) isolated a strain of genus *Pseudomonas* which was able to convert lactose to lactobionic acid. When $CaCO_3$ was added to the medium instead of using pH control 300 g L^{-1} lactose was converted to 290 g L^{-1} lactobionic acid in 155 h, giving a yield of 92% mol mol^{-1}.

Oxidation of lactose to lactobionic acid has been observed in other organisms. Thus, Tomlinson et al. (1978) observed that growing cells of *Halobacterium saccharovorum* oxidized lactose to lactobionic acid. Furthermore, a lactobionic acid producing strain of *Penicillium chrysogenum* (Cort et al., 1956) has been reported, and Eddy (1958) isolated two strains of paracolon bacteria which were able to oxidize lactose almost quantitatively to lactobionic acid. Recently, Murakami et al. (2002) screened for lactose-oxidizing microorganisms and isolated a strain of *Burkholderia cepacia* which was also able to give lactobionic acid yields of more than 90% mol mol^{-1}. The medium contained peptone and/or yeast extract. Murakami et al. (2002) showed that the biomass yield on the medium containing lactose was equivalent to the yield on a medium which only contained peptone and yeast extract, while it increased 2-fold with glucose, maltose or sucrose as sugar. Thus, in the microbial processes lactobionic acid is formed from lactose without generation of energy in the from of ATP, while biomass is probably formed from yeast extract and peptone (or other complex compounds present in the medium) which are used both to supply building blocks and energy through catabolism.

Enzymatic processes

Several enzymatic schemes for oxidizing lactose to lactobionic acid have been investigated, and during the last decade enzymatic methods have received increased attention.

Nishizuka and Hayaishi (1962) purified an enzyme from *Ps. graveolens* which they coined lactose dehydrogenase and characterized in detail. This enzyme catalyzes the dehydrogenation of lactose to lactobiono-δ-lactone, which is subsequently hydrolyzed to lactobionic acid. The enzyme was found to be a flavoprotein with pH-optimum at 5.6 and a K_m-value for lactose of 11 mM. 2,6-dichlorophenolindophenol, methylene blue, or ferrocyanide served as electron acceptors, but oxygen was not effective as electron acceptor. It was shown that the enzyme utilized several aldoses as substrates and that the activity was 4 to 5 times higher with glucose or galactose than with lactose. Furthermore, direct acidification of milk by lactose dehydrogenase has been studied (Wright and Rand, 1973; Rand and Hourigan, 1975). Best acidification results were obtained when lactase was added together with

lactose dehydrogenase due to the higher activity of the enzyme with glucose and galactose and due to the increased molar amount of sugar, but the yield of lactobionic acid will of course decrease.

Hexose oxidase, a carbohydrate oxidase capable of oxidizing several saccharides including glucose, galactose, maltose, cellobiose and lactose to their corresponding aldonic acids was first extracted from the red alga *Iridophycus flaccidum* (Bean and Hassid, 1956). The relative activity of the enzyme towards glucose, galactose, lactose, maltose and cellobiose was 100 : 100 : 49 : 47 : 30. The K_m-values for glucose and galactose were found to 2.5 mM and 5 mM, respectively. No kinetic parameters were given for the oxidation of lactose. Later, hexose oxidase was extracted from another red alga *Chondrus crispus* by Sullivan and Ikawa (1973), who found a molar weight of the enzyme of 130 kDa. Sullivan and Ikawa (1973) did not detect the presence of flavin in the enzyme but did detect Cu^{2+}. Furthermore it was found that the enzyme was a glucoprotein (70% carbohydrate). The relative activity of the enzyme towards glucose, galactose, lactose, maltose and cellobiose was 100 : 82 : 22 : 49 : 32. Again the K_m-value was not determined for lactose but only for glucose and galactose where it was found to 4 mM and 8 mM, respectively. In 1997 Groen et al. (1997) characterized hexose oxidase from *C. crispus* and found very different properties. Thus, a molar mass of 87 kDa was obtained. Furthermore, the glycoprotein was found to contain only 25% sugar and not 70% as obtained by Sullivan and Ikawa (1973), and the enzyme was found to contain flavin. The authors concluded that the large discrepancies probably originate from characterization of a contaminating protein in the case of Sullivan and Ikawa (1973). The oxidase was active over a broad pH range with pH optima at 6 and 10. At 25°C K_m for lactose was found to 1.7 mM. Furthermore, the maximum specific activity was 4.1 U/mg protein when the assay mixture was saturated with air. With glucose the K_m-value for oxygen was determined to 0.30±0.04 mM. In the assay Groen et al. (1997) measured the oxygen consumption with a Clark-type oxygen electrode. No information is given in the article concerning the measuring time of the assay. Commercially available Clark-type electrodes typically have a response time of around 1 min. Thus, if the time span of the assay is short, the results obtained are incorrect, and if this is indeed the case the K_m-value for oxygen is underestimated. Recently, Savary et al. (2001) purified the *C. crispus* hexose oxidase. These authors found a molecular mass of the enzyme of 117 kDa, which is far from the 87 kDa found by Groen et al. (1997). Also K_m for lactose was determined to 97 mM at 26°C using an assay coupled to peroxidase (i.e. the rate of hydrogen peroxide production is measured). Unfortunately, the specific enzyme activity for lactose was not given. Similar to the use of lactose dehydrogenase for direct acidification of milk this application of the enzyme has been studied (Rand, 1972; Rand and Hourigan, 1975). Better and faster acidification was also here achieved with

hexose oxidase when lactase was present in the system.

Lin et al. (1991) screened for soil-derived fungi producing oxidases capable of oxidizing oligosachharides on wheat bran solid culture and isolated a strain *Acremonium strictum* T1 which produced a flavin-containing carbohydrate oxidase which was coined glucooligosaccharide oxidase by the authors. This oxidase specifically oxidizes oligosaccharides with a glucose residue on the reducing end and with the sugar residue joined by an α or β-1,4 glucosidic bond. The relative activity of the enzyme toward maltose, maltotriose, maltotetraose, maltopentaose, maltohexaose, maltoheptaose, lactose, cellobiose and glucose was 100 : 94 : 74 : 46 : 66 : 56 : 64 : 47 : 59. Later Lin et al. (1993) subjected the strain *A. strictum* T1 to a strain improvement program and a hyper-producing strain was isolated. This strain produced 75 times more oxidase than the wild type strain resulting in a maximum titer of 6 units per g of culture medium (1 part wheat bran, 1 part water) after 4 days of cultivation. Batch conversion of lactose with partially purified enzyme from the mutant strain was investigated. The reaction was carried out at 35°C in a 3 L fermentor containing 2 L of 27.5 g L^{-1} lactose solution. 1000 units of partially purified glucooligosaccharide oxidase was added, and 100,000 units of catalase was added to eliminate the produced H_2O_2. pH was controlled in the range of 7-8 with 4 M NaOH. No information is given in the article concerning aeration and agitation. After 4 hours of reaction a degree of conversion of 98% was achieved at which point the enzyme activity was 60% relative to the initial value.

Satory et al. (1997) investigated conversion of lactose and fructose to sorbitol and lactobionic acid by glucose-fructose oxidoreductase from *Zymomonas mobilis*. There are two disadvantages of this method. First of all a mixture of sorbitol and lactobionic acid is produced, since the enzyme needs fructose as electron acceptor. Secondly, the K_m-value of the enzyme for lactose is 1.2 M (30°C, pH 6.2), which is an 80-fold increase in K_m relative to the physiological substrate glucose. Thus with lactose as substrate the reaction will be first order in lactose even for lactose concentrations close to the solubility of lactose which is 0.6 M at 30°C.

Baminger et al. (2001) used cellobiose dehydrogenase for the production of lactobionic acid. This flavoprotein shows negligible activity for direct oxidation with molecular oxygen. Thus different electron acceptors were used to re-oxidize the cellobiose dehydrogenase. The electron acceptors were regenerated by the enzyme laccase, a multi-copper oxidase which strongly prefers oxygen as oxidizing agent but is highly unspecific regarding the reducing substrate. Thus in this system cellobiose dehydrogenase, laccase, and a redox mediator is used for the production of lactobionic acid from lactose and oxygen. It was found that a number of benzoquinones, catechol, 2,6-dichloroindophenol (DCIP) and 2,2'-azino-bis(3-ethylbenzthiazoline-6-sulfonic acid)

(ABTS) were suitable as redox mediators. Ludwig et al. (2004) investigated the reaction further, and found that K_m for lactose of cellobiose dehydrogenase from *Sclerotium rolfsii* was 2.4 mM (30°C, pH 4.0) and that K_m of laccase LAP2 from *Trametes pubescens* for oxygen was 0.41 mM. The authors claim that this is a better way of performing the process than using the flavoproteins which utilize oxygen as the terminal electron acceptor, because the formation of hydrogen peroxide leads to inactivation of the enzyme, and this may - according to the authors - even be a problem when catalase is added to the system (e.g. Leitner et al. (1998)). However, during batch reactions in the cellobiose dehydrogenase/laccase-system both cellobiose dehydrogenase and laccase deactivated. The deactivation increased with increasing temperature and increasing dissolved oxygen tension, and it was more pronounced when air was used instead of pure oxygen to reach the desired dissolved oxygen concentration. The authors speculate that this could be due to the combination of aeration and shearing. One obvious disadvantage of the process is that the redox mediator needs to be removed by e.g. adsorption to produce lactobionic acid or a salt of lactobionic acid of food grade quality. This is due to the toxicity of most redox mediators.

The carbohydrate oxidase which is investigated in this study was recently cloned from *Microdochium nivale* and expressed in *Fusarium venenatum* (Xu et al., 2001). It is able to oxidize several mono-, oligo-, and polymeric saccharides and transfer their electrons to molecular oxygen or other electron acceptors. It has been shown that the enzyme can be considered as safe for use in the food industry (Ahmad et al., 2004).

3.3 Materials and methods

3.3.1 Enzymes

Lactose oxidase

The carbohydrate oxidase cloned from *M. nivale* and expressed in *F. venenatum* (Xu et al., 2001) was produced by Novozymes A/S. In the following it will be referred to as lactose oxidase or LOX.

The purity of the enzyme was analyzed by SDS-PAGE using a Criterion XT Precast Gel, 10% Bis-Tris gel in a XT MES buffer (BioRad Laboratories) according to the manufacturer's instructions. 10 μl of diluted enzyme solution was mixed with 9 μl of sample buffer (0.125 M Tris-HCl pH 6.8, 20% glycerol, and 4.6% SDS), and 1 μl of 1 M dithiothreitol, and heated to 96°C for 5 minutes. Following electrophoresis the gel was incubated for 60 minutes in a blotting solution consisting of 0.1% (w/v) Coomassie Brilliant Blue R-250 dissolved in 10% acetic acid, 40% methanol, and 50% water. Destaining of

the gel was performed in 10% acetic acid, 30% methanol, and 60% water. It was found that the enzyme was more than 95% pure.

The amount of pure enzyme protein was determined relative to an enzyme standard of known protein content by a colorimetric method in which the hydrogen peroxide formed by LOX acts as substrate for peroxidase which catalyzes the oxidative condensation of aminoantipyrine (AA) and N-ethyl-N-sulfopropyl-m-toluidine (TOPS) forming a purple product that can be measured spectrophotometrically at 540 nm.

Enzymes samples with unknown protein concentration were diluted with 100 mM phosphate/100 mM citrate buffer at pH 6 to a concentration of 4.38 -10.95 mg pure enzyme protein L^{-1}. Enzymatic assaying was performed automatically in a Konelab analyzer which performed the following operations: 30 μL of enzyme solution was added to 220 μL of a reagent with the following composition: 5 mM lactose, 5 mM TOPS, 2 mM AA, 2.88 U mL^{-1} peroxidase, 100 mM phosphate/100 mM citrate buffer, pH 6.0. The reaction temperature was 37°C. The rate of reaction was monitored at 540 nm for 200 s. 5 standards with known protein concentration were analyzed similarly and used to make a standard curve from which unknown protein concentrations were inferred.

Catalase

The catalase used was the commercially available catalase Catazyme 25 L from Novozymes A/S. According to Novozymes A/S the enzyme contains 25,000 U g^{-1}. One unit is defined as the amount of enzyme which, under a specific set of conditions, decomposes 1 μmol of H_2O_2 per minute. The conditions used by Novozymes A/S are pH 7.0 and 25°C. The enzyme was used without any further purification steps.

3.3.2 Set-up and operating conditions

The experimental set-up used in our enzymatic experiments is depicted in figure 3.2. It was inspired by the set-up used at Novozymes when we entered the project in the summer of 2004. At Novozymes reactions were carried out at constant pH by addition of 5 M NaOH and at constant temperature, stirring rate, and gas flow rate. However, compared to the Novozymes experiments, we ensured that the reaction was run a constant dissolved oxygen tension (DOT).

All reactions were performed in an MBR bioreactor with a working volume of 1.0 L. The bioreactor was fitted with two Rushton turbines rotating at 1000 rounds per minute (RPM). Temperature was kept constant to within ±0.5°C,

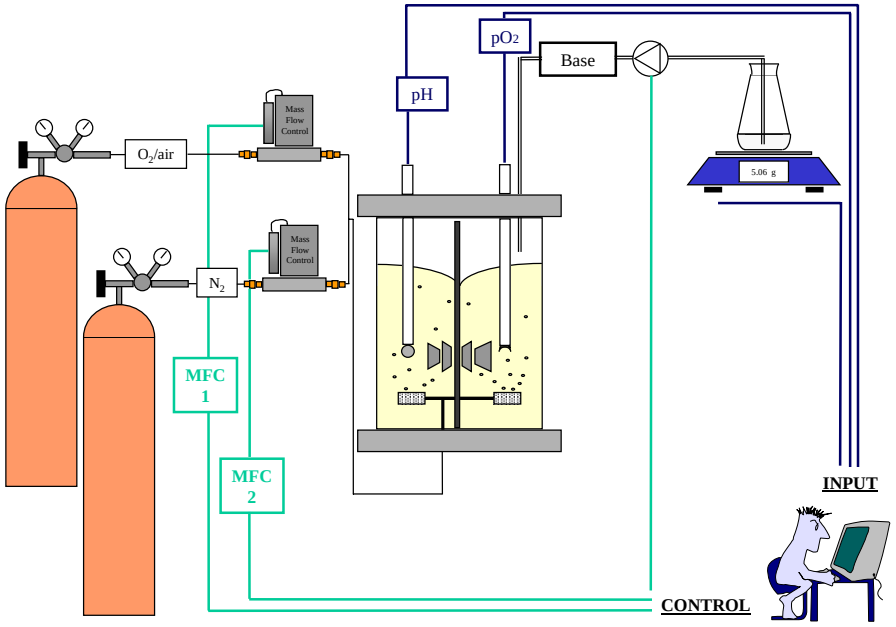

Figure 3.2. Set-up used for enzymatic experiments.

and unless stated otherwise it was 38°C. Also as standard, a constant pH of 6.4 was maintained by automatic addition of 2 M NaOH to the liquid surface. The rate of base addition was monitored during the reaction by weight measurements.

The bioreactor was equipped with a polarographic oxygen sensor from Mettler Toledo. The oxygen electrode was calibrated by sparging the medium with air and N_2. During the reaction the dissolved oxygen tension was controlled by sparging the reactor with 200 mL min^{-1} of gas composed of a mixture of N_2 and atmospheric air or pure oxygen. The ratio of N_2 and air or oxygen was adjusted by the use of two mass flow controllers from Bronkhorst and the DOT was kept constant by feedback regulation of the gas ratio.

Unless stated otherwise, the medium consisted of 1.00 L of a 50 g L^{-1} lactose solution containing 50 mM phosphate at pH 6.4, and 1.017 g LOX solution containing 59 mg enzyme protein mL^{-1} (i.e. 60 mg enzyme protein) was added to start the reaction. Furthermore, in experiments with catalase 0.25 g Catazyme 25 L was added initially unless stated otherwise in the text.

3.3.3 Measurement of hydrogen peroxide

The hydrogen peroxide concentration was determined spectrophotometrically with 2,2'-azino-bis(3-ethylbenzthiazoline-6-sulfonic acid) (ABTS) at 433 nm essentially as described in van Niel et al. (2002). This procedure is suited for measurements in the range of μM, and samples taken from the reactor were diluted if required.

To 3 mL of diluted sample, 75 μL of ABTS solution (28 g L^{-1}) and 15 μL of horseradish peroxidase (500 U mL^{-1}) were added and the absorbance was measured immediately.

3.4 Results

The kinetics of lactose oxidation was investigated by running reactions where the oxygen concentration was kept constant by gas-blending and pH was kept constant by titration with 2 M NaOH. The rate of base addition, and thus the formation of lactobionic acid, was recorded. The time course of two experiments performed at identical conditions is given in figure 3.3, which shows the rate of base addition for both experiments as well as the variation in dissolved oxygen tension during one of the experiments. It is seen that the reproducibility is good. Furthermore, the controller was able to keep the dissolved oxygen tension around the set-point of 44.1% except at the very beginning of the experiment where the ratio of air to nitrogen was adjusted to reach the set-point and at the very end of the reaction where the rate of base addition declined rapidly due to exhaustion of the lactose.

To verify that base weight measurements were appropriate for obtaining the kinetics an experiment was conducted where the accumulated hydrogen peroxide was measured during an experiment performed at 38°C without addition of catalase, see figure 3.4. The hydrogen peroxide concentration was determined during the experiment with the enzymatic method described above. The concentration of lactobionic acid, c_{lac}, in mol L^{-1} was calculated from base weight measurements from the following equation

$$c_{lac}(t) = \frac{\sum_{i=0}^{t/\Delta t} \frac{\dot{m}_{b,i} c_b}{\rho_b} \Delta t}{V_0 + \sum_{i=0}^{t/\Delta t} \frac{\dot{m}_{b,i}}{\rho_b} \Delta t} \tag{3.1}$$

In this equation $\dot{m}_{b,i}$ is the rate of base addition in g h^{-1} in the i'th time interval, c_b is the concentration of base in mol L^{-1}, ρ_b is the density of the base in g L^{-1}, V_0 is the initial volume of the reaction mixture in L, and Δt is the sampling interval in h.

It is seen from figure 3.4 that the agreement between measured values of the hydrogen peroxide concentration and calculated values of the lactobionic

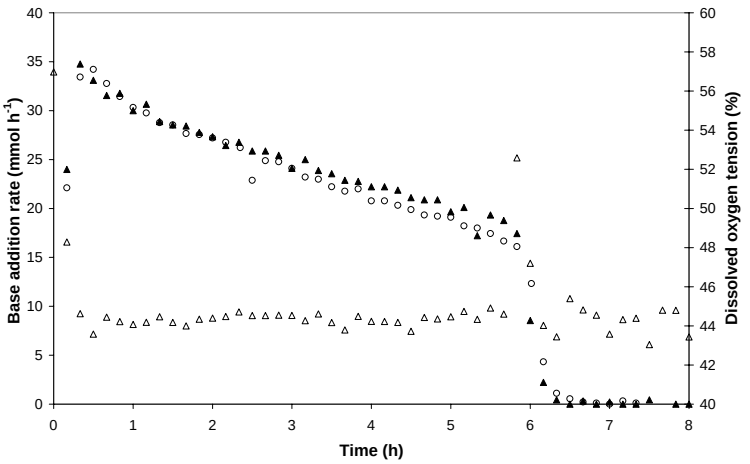

Figure 3.3. Rate of base addition versus time for two experiments (filled triangles and open circles) performed at 38°C and a dissolved oxygen tension of 44.1% relative to saturation of water with air at 38°C and 1 bar (corresponding to 50% saturation at 49°C and 1 bar). 60 mg pure LOX enzyme and 0.25 g catalase was added initially. The dissolved oxygen tension is shown for one of the experiments (open triangles).

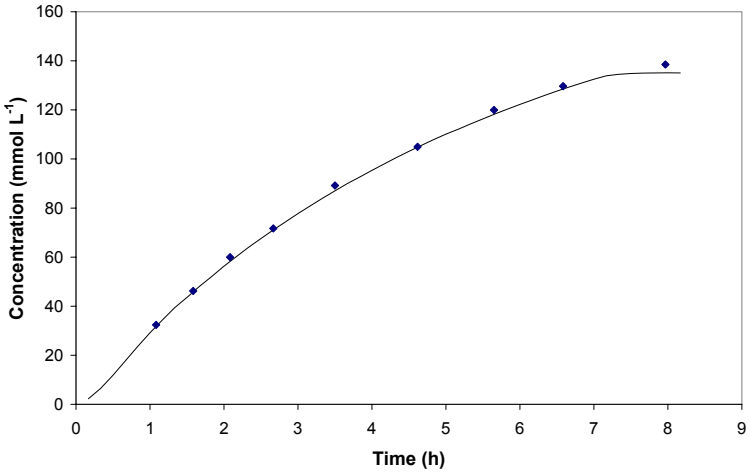

Figure 3.4. Concentration of H_2O_2 (points) measured with the enzymatic method versus time for an experiment performed without the addition of catalase. The line represents the concentration of lactobionic acid calculated from base weight measurements. The temperature was 38°C, and the dissolved oxygen tension was kept constant at 44.1% relative to saturation of water with air at 38°C and 1 bar (corresponding to 50% saturation at 49°C and 1 bar). 60 mg pure LOX enzyme, but no catalase was added initially.

acid concentration is very good. It was therefore concluded that base weight measurements are sufficient for obtaining the kinetics.

With reference to figure 3.3 it is seen that the base addition rate increases initially before a value is reached from which the rate of base addition declines. This is because the enzyme is operating in a transient state initially before a pseudo-steady state is obtained. Furthermore, during this transient the controller has not yet adjusted the dissolved oxygen tension to the set-point value. It is seen from the figure that the decline in the reaction rate after approximately 6 hours is abrupt. The carbohydrate oxidase follows the enzymatic ping-pong scheme. The simplest (deactivation as well as inhibition by H_2O_2 is neglected) ping-pong scheme is given below

$$E_{ox} + S \underset{k_{-1}}{\overset{k_1}{\rightleftarrows}} E_{ox}S \xrightarrow{k_2} E_{red} + P \tag{3.2}$$

$$E_{red} + O_2 \xrightarrow{k_3} E_{ox} + H_2O_2 \tag{3.3}$$

where E_{ox} is the oxidized form of the enzyme, S represents lactose, $E_{ox}S$ represents lactose bound to the oxidized form, E_{red} is the reduced form of the enzyme, and P is the product of the enzymatic reaction (the lactone form which is spontaneously hydrolyzed to lactobionic acid). The volumetric rate of reaction is

$$r = k_2[E_{ox}S] \tag{3.4}$$

The following two equations can be written when pseudo-steady state approximations are used for $[E_{ox}S]$ and $[E_{red}]$

$$0 = k_1[E_{ox}][S] - (k_{-1} + k_2)[E_{ox}S] \tag{3.5}$$

$$0 = k_2[E_{ox}S] - k_3[E_{red}][O_2] \tag{3.6}$$

These two equations can be supplemented by an equation expressing that the amount of active enzyme $[E]$ equals the sum of all the enzyme forms

$$[E] = [E_{ox}] + [E_{red}] + [E_{ox}S] \tag{3.7}$$

Combining Eqs.(3.5-3.7) yields the following expression for $[E_{ox}S]$

$$[E_{ox}S] = \frac{[E][S][O_2]}{[S][O_2] + \frac{k_{-1}+k_2}{k_1}[O_2] + \frac{k_2}{k_3}[S]} \tag{3.8}$$

which is inserted in Eq.(3.4) to give the final rate expression

$$r = k_{cat}[E]\frac{[S][O_2]}{[S][O_2] + K_{mS}[O_2] + K_{mO}[S]} \tag{3.9}$$

where $K_{mS} = \frac{k_{-1}+k_2}{k_1}$ and $K_{mO} = \frac{k_2}{k_3}$ are respectively the Michaelis constants for lactose and molecular oxygen, and $k_{cat} = k_2$. When $K_{mS} << [S]$ the equation can be simplified to

$$r = k_{cat}[E]\frac{[O_2]}{[O_2] + K_{mO}} \tag{3.10}$$

According to Feng Xu, Novozymes (unpublished results), the K_{mS}-value of lactose oxidase for lactose is 0.12 ± 0.04 mM at 20°C and in the range 0.2-0.5 mM at 50°C. This means that the reaction is essentially zero order in lactose until very small concentrations of lactose are reached. Thus, with a K_{mS}-value of 0.12 mM the rate of reaction at 2 g L^{-1} lactose would still be more than 98% of the value at 50 g L^{-1} lactose if the rate of reaction was not influenced by other parameters. The low K_{mS}-value explains the abrupt decline in the rate of base addition at the end of the reaction. However, the rate of reaction also declines significantly during the course of the reaction. The reason for this is investigated below in considerable detail.

Be aware that while r is a volumetric rate of reaction the figures presenting the data obtained show the base addition rate in mmol h^{-1}. While the volumetric rate of reaction, according to Eq.(3.10), will decrease due to the (small) dilution of the enzyme by base addition, the rate measured in e.g. mmol h^{-1} will remain constant - provided that deactivation and inhibition of the enzyme is not observed - because then the total amount of active enzyme is constant and because the oxygen concentration is controlled at a set-point value. Stated differently, the rates given in the figures are equivalent to the volumetric rate for the initial enzyme concentration since the initial volume is 1.00 L. This fact makes data analysis easy.

3.4.1 Effect of temperature

Initially, the effect of temperature was investigated, since it was found that the rate of reaction is heavily dependent on this parameter. In all experiments the DOT was controlled at 50% relative to saturation of water with air at 49°C. At temperatures other than 49°C the dissolved oxygen concentration corresponding to 50% DOT at 49°C was obtained from the following equation relating the solubility of oxygen in pure water at a partial oxygen pressure of 1 bar to the temperature:

$$c_l^* = 0.0270 \exp\left(\frac{1142}{T}\right) \tag{3.11}$$

In this equation, which was obtained by fitting tabular values of the oxygen solubility in the range 25-50°C, c_l^* is in mmol L^{-1} and T is in K.

The results of the experiments are given in figure 3.5. It is seen from the figure that the initial rate of reaction increases with increasing temperature. Furthermore, the decline in the rate of reaction increases with increasing temperature. At this particular set of operating conditions the optimal temperature (to give the smallest time to full conversion of the lactose) should be found around 38°C.

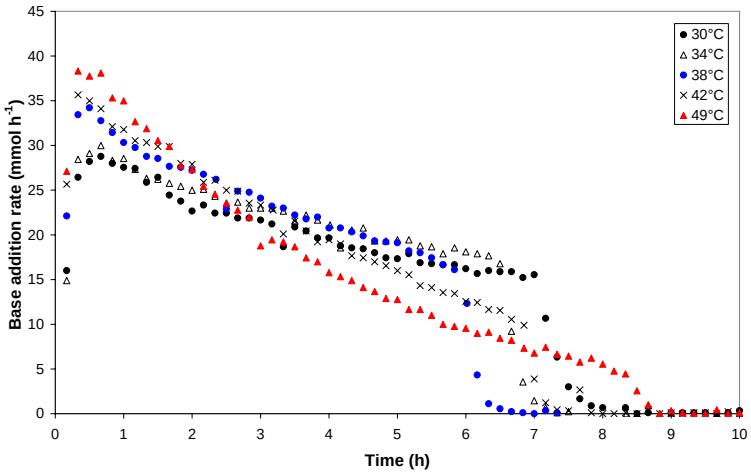

Figure 3.5. Effect of temperature on the rate of reaction. All reactions were performed with 50 g L^{-1} lactose at an oxygen concentration corresponding to 50% saturation of water with air at 49°C and 1 bar. 60 mg pure LOX enzyme and 0.25 g catalase was added initially.

An experiment was performed where LOX was incubated in oxygen free lactose solution (the solution was sparged with nitrogen) at 49°C for 3 hours and 5 minutes before catalase was added and the oxygen concentration was raised to 50% relative to saturation with air at 49°C. Furthermore, an experiment was performed where lactose was the missing component during incubation for 3 hours and 30 minutes. The results are given in figure 3.6. If the decline in reaction rate was only due to the effect of temperature, the initial rate of reaction should be around 20 mmol base h^{-1} (see figure 3.5) after 3 hours and 5 minutes incubation with N_2, which corresponds to a 50% decrease of initial rate compared to the case of no incubation. However, the initial rate was only around 12% lower. Furthermore, after the reaction was started the decline in the reaction rate was exactly as observed when the enzyme was not incubated. The same held true when the enzyme was incubated with air even though the enzyme had deactivated somewhat more.

Based on these experiments, it was concluded that the optimal temperature was around 38°C at the specific set of conditions, and that the decline in reaction rate was not caused by temperature alone. It was decided to perform the remaining experiments at 38°C.

3.4.2 Finding the reason for the decline in reaction rate

The decline in reaction rate could in principle be explained by either inhibition of the lactose oxidase enzyme by the product lactobionic acid or

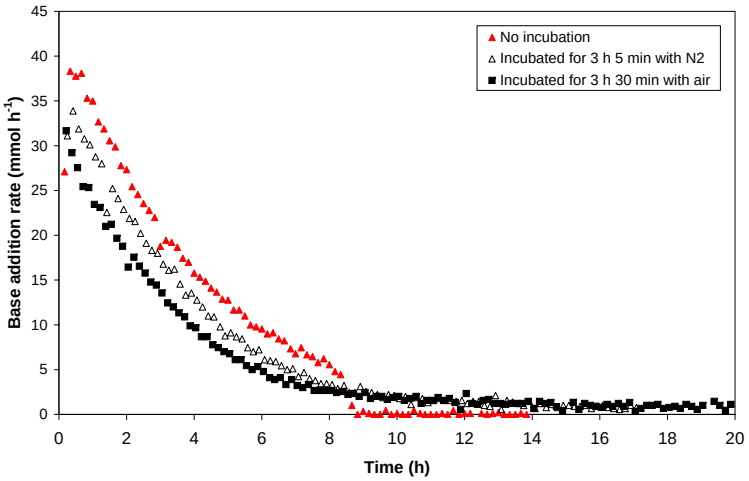

Figure 3.6. Rate of reaction versus time for the following reactions: Open triangles: Incubation for 3 h 5 min at 49°C with N_2 prior to reaction (missing component oxygen). Black squares: Incubation for 3 h 30 min with air (missing component lactose). Red triangles: No incubation prior to reaction. The reactions with incubation were not followed to completion. All reactions were performed with 50 g L^{-1} lactose at an oxygen concentration corresponding to 50% saturation of water with air at 49°C and 1 bar. 60 mg pure LOX enzyme and 0.25 g catalase were used.

by hydrogen peroxide if the amount of catalase used was not sufficient to sustain a very low concentration of hydrogen peroxide. An experiment was performed where 60 g of sodium lactobionate was added to the reactor during an experiment (data not shown). This did not result in a lowered reaction rate, and it was concluded that lactobionic acid does not act as an inhibitor. Furthermore, an experiment was performed where the amount of catalase added initially was increased by a factor of 10 to 2.5 g. There was no difference between an experiment performed with 0.25 g catalase and one with 2.5 g catalase (data not shown), and it was concluded that the hydrogen peroxide concentration was sufficiently low not to cause product inhibition or deactivation.

On the basis of these experiments we concluded that the decline in reaction rate was caused by deactivation of the lactose oxidase and not by product inhibition. A number of hypotheses were put forward to try to explain the deactivation of the enzyme.

Ludwig et al. (2004) observed that both the cellobiose dehydrogenase and the laccase used in their system for lactobionic acid production deactivated during the reaction. The rate of deactivation was higher when air was used than when pure oxygen was used. Consequently they ascribed the deactivation to the combined effect of shear rate and the presence of the air-liquid interface,

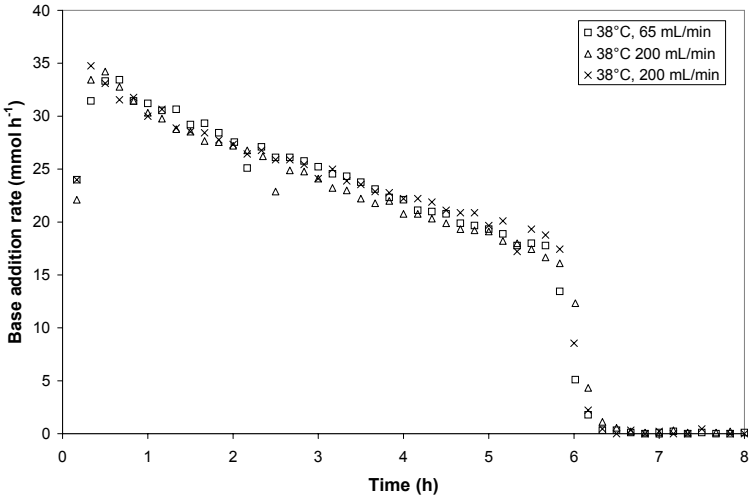

Figure 3.7. Rate of reaction versus time for two different gas flow rates: 65 mL min^{-1} and 200 mL min^{-1}. All reactions were performed at 38°C with 50 g L^{-1} lactose at an oxygen concentration corresponding to 44.1% saturation of water with air at 38°C and 1 bar (corresponding to 50% saturation at 49°C and 1 bar). 60 mg pure LOX enzyme and 0.25 g catalase were used.

a combination which has been shown to cause deactivation of some proteins due to irreversible aggregation of the proteins at the air-liquid interface (Maa and Hsu, 1997).

If the combined effect of shear rate and the air-liquid interface was the cause of deactivation of the lactose oxidase, the deactivation should be dependent on the total gas flow rate. This hypothesis was tested by doing an experiment with a total gas flow rate of 65 mL min^{-1} instead of 200 mL min^{-1}, the value usually used. The results are shown in figure 3.7. It is clearly seen that a decrease of the total gas flow rate does not change the rate of deactivation.

At this point it was speculated that maybe the deactivation could be caused by an oxygen metabolite, and it was decided to perform experiments with different oxygen concentrations.

3.4.3 Effect of oxygen tension

Initially, a set of experiments was performed at 38°C with an initial lactose concentration of 50 g L^{-1} and with different oxygen concentrations in the liquid. When a dissolved oxygen tension above 100% relative to saturation of pure water with air at 38°C was desired, pure oxygen and nitrogen instead of air and nitrogen was used to reach the oxygen concentration.

It was found that both the initial rate of reaction as well as the rate of deac-

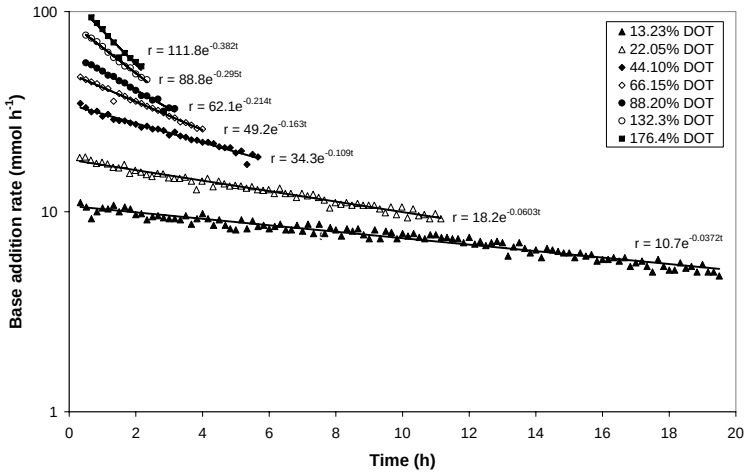

Figure 3.8. Effect of dissolved oxygen on the rate of reaction with an initial lactose concentration of 50 g L^{-1}. All reactions were performed at 38°C. The oxygen concentrations given in the legend are relative to saturation of water with air at 38°C and 1 bar. 60 mg pure LOX enzyme and 0.25 g catalase was added initially.

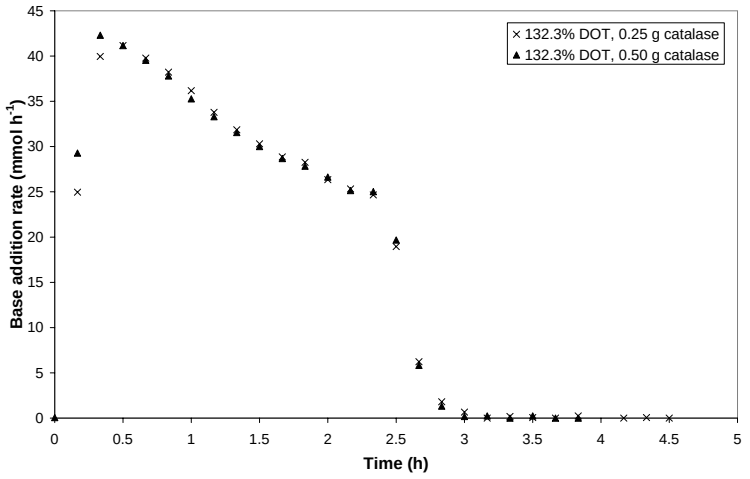

Figure 3.9. Effect of increasing the catalase dosage from 0.50 g to 0.25 g in experiments with a dissolved oxygen tension of 132.3% DOT relative to saturation of water with air at 38°C and 1 bar. The initial lactose concentration was 50 g L^{-1} and 60 mg pure LOX enzyme was added initially.

tivation increased with increasing oxygen concentration. Furthermore from logarithmic plots it appeared that the reaction rate declined exponentially, see figure 3.8. Notice that the initial transient phase (where the controller is adjusting the DOT to the set-point and the enzyme is not yet working in pseudo-steady state) and the phase with rapid decline in rate due to exhaus-

tion of lactose have been omitted.

To ascertain that the decline in rate was not caused by accumulating hydrogen peroxide at large dissolved oxygen concentrations an additional experiment was performed at 132.3% DOT with 0.50 g catalase instead of 0.25 g catalase, the amount normally used. There was no difference between experiments with 0.25 g and 0.50 g catalase, see figure 3.9.

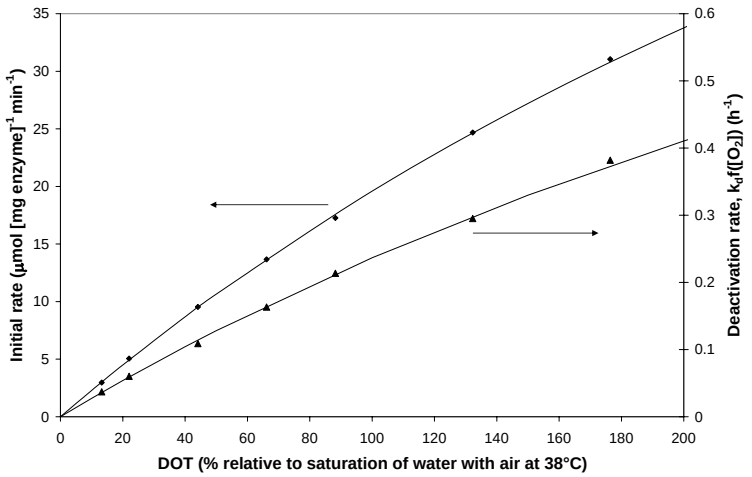

Figure 3.10. Initial rate of reaction and deactivation rate versus dissolved oxygen tension relative to saturation of water with air at 38°C and 1 bar using an initial lactose concentration of 50 g L^{-1}. The curves are based on the following parameters in Eqs.(3.14)-(3.15): k_{cat} = 122 μmol (mg protein)$^{-1}$ min^{-1}, K_{mO} = 524% DOT relative to saturation with air at 38°C or 1.17 mM, k_d = 1.55 h^{-1} and K_d = 554% DOT relative to saturation with air at 38°C or 1.23 mM.

The apparent exponential decline in reaction rate with time would imply that the enzyme is deactivating following a first order mechanism. Eq. (3.12) captures this observation and also that the rate of deactivation increases with increasing oxygen tension.

$$-\frac{d[E]}{dt} = k_d(f([O_2]))[E] \tag{3.12}$$

Here $f([O_2])$ (dimensionless) depends on the dissolved oxygen tension and k_d is the deactivation constant. The expression can be integrated to yield

$$[E] = [E]_0 \exp\left(-k_d f([O_2])t\right) \tag{3.13}$$

which upon insertion in the equation for the rate of reaction, eq.(3.10) gives

$$r = k_{cat}[E]_0 \frac{[O_2]}{[O_2] + K_{mO}} \exp\left(-k_d f([O_2])t\right) \tag{3.14}$$

The pre-exponential factor corresponds to the initial rate of reaction while the deactivation rate in the exponential captures the deactivation process.

Figure 3.10 - which is based on figure 3.8 - shows the normalized (i.e. per unit enzyme) initial rate $k_{cat}\frac{[O_2]}{[O_2]+K_{mO}}$ and the exponent $k_d f([O_2])$ versus the dissolved oxygen tension. The values of the initial rate were fitted to a Michaelis Menten type expression, Eq.(3.10) by weighted least squares analysis. Thus k_{cat} was found to be 122 μmol (mg protein)$^{-1}$ min^{-1} and the K_{mO}-value obtained was 524% DOT relative to saturation of water with air at 38°C or 1.17 mM. Furthermore it was found that the deactivation rate could be fitted adequately when the following expression for $f([O_2])$ was used

$$f([O_2]) = \frac{[O_2]}{[O_2] + K_d} \tag{3.15}$$

Again the parameters k_d and K_d were obtained by weighted least squares analysis with $k_d = 1.55$ h^{-1} and $K_d = 554\%$ DOT relative to saturation of water with air at 38°C or 1.23 mM. Note that K_d is practically the same as K_{mO} (considering that all experiments are conducted at $[O_2]$ far below K_m). This observation will shortly be used to derive a putative mechanism for the deactivation process.

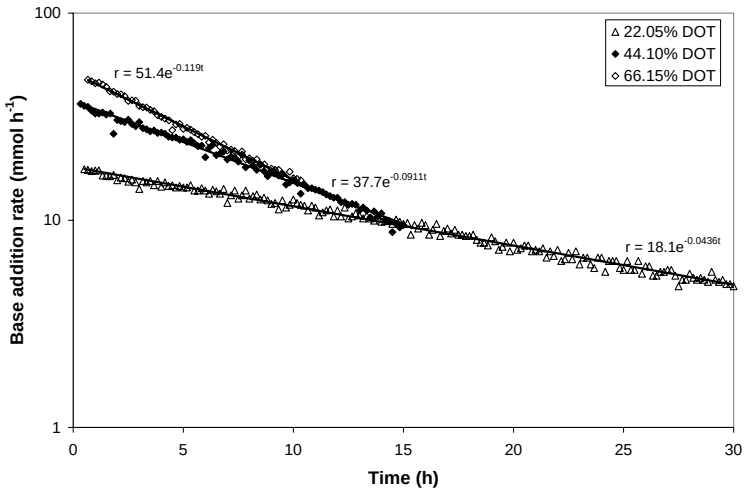

Figure 3.11. Effect of dissolved oxygen on the rate of reaction with an initial lactose concentration of 100 g L^{-1} and DOT-values in the interval 22.05% to 66.15% relative to saturation with air at 38°C and 1 bar. 60 mg pure LOX enzyme and 0.25 g catalase was added initially.

First is, however, investigated the effect of using a higher initial substrate concentration to see if substrate might somehow protect the oxidase from deactivation. Hence experiments were performed with an initial lactose concentration of 100 g L^{-1}. Again the decline in reaction rate appeared to be exponential, see figures 3.11 and 3.12. Graphs showing the initial rate of reaction and the deactivation rate is given in figure 3.13. Again the kinetic parameters were obtained by weighted least square analysis. The parameters

obtained were: $k_{cat} = 102$ μmol (mg protein)$^{-1}$ min^{-1}, $K_{mO} = 442\%$ DOT relative to saturation with air at 38°C or 0.98 mM, $k_d = 0.90$ h^{-1} and $K_d = 425\%$ DOT relative to saturation with air at 38°C or 0.95 mM. The hypothesis that K_{mO} and K_d are equal is strengthened, and it also appears that the kinetic parameters k_{cat} and K_{mO} are independent of the initial substrate concentration.

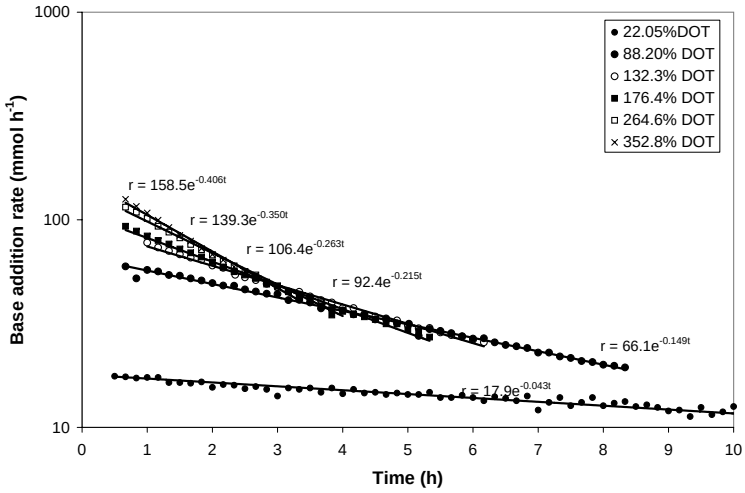

Figure 3.12. Effect of dissolved oxygen on the rate of reaction with an initial lactose concentration of 100 g L^{-1} and DOT-values in the interval 88.20% to 352.8% relative to saturation with air at 38°C and 1 bar. To emphasize the large increase in the initial rate of reaction and in the deactivation rate the data for a DOT of 22.05% are repeated from figure 3.11. 60 mg pure LOX enzyme and 0.25 g catalase was added initially.

Even though the kinetic parameters k_{cat} and K_{mO} may seem rather different in the experiments with respectively 50 g L^{-1} and 100 g L^{-1} lactose this can largely be explained by the very high correlation between the two parameters at oxygen concentration substantially below K_{mO}. The experimental values of the initial rate at the same oxygen concentration do in fact agree very well, see figure 3.14. Thus data for the two different initial values of lactose were analyzed together by weighted least squares analysis. Apart from forcing k_{cat} and K_{mO} to be similar for the two experimental series, K_d was forced to be equal for the two experiments. By doing so, the following parameter values were obtained: $k_{cat} = 103$ μmol (mg protein)$^{-1}$ min^{-1}, $K_{mO} = 439\%$ DOT relative to saturation with air at 38°C or 0.97 mM, $k_d = 0.90$ h^{-1} for 100 g L^{-1} lactose, $k_d = 1.23$ h^{-1} for 50 g L^{-1} lactose and $K_d = 425\%$ DOT relative to saturation with air at 38°C or 0.95 mM.

Figure 3.15 shows what happens when the initial lactose concentration is increased to 200 g L^{-1} at a dissolved oxygen tension of 66.15% DOT. For comparison data from experiments with initial lactose concentrations of 50 g

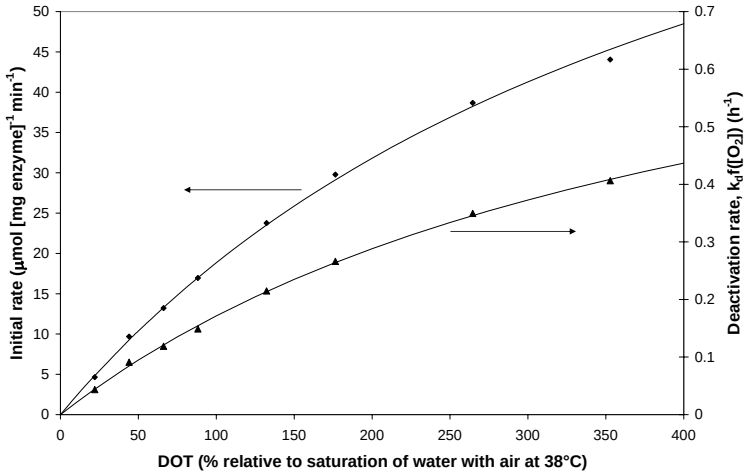

Figure 3.13. Initial rate of reaction and deactivation rate versus dissolved oxygen tension relative to saturation of water with air at 38°C and 1 bar using an initial lactose concentration of 100 g L^{-1}. The curves are based on the following parameters: k_{cat} = 102 μmol (mg protein)$^{-1}$ min^{-1}, K_{mO} = 442% DOT relative to saturation with air at 38°C or 0.98 mM, k_d = 0.90 h^{-1} and K_d = 425% DOT relative to saturation with air at 38°C or 0.95 mM.

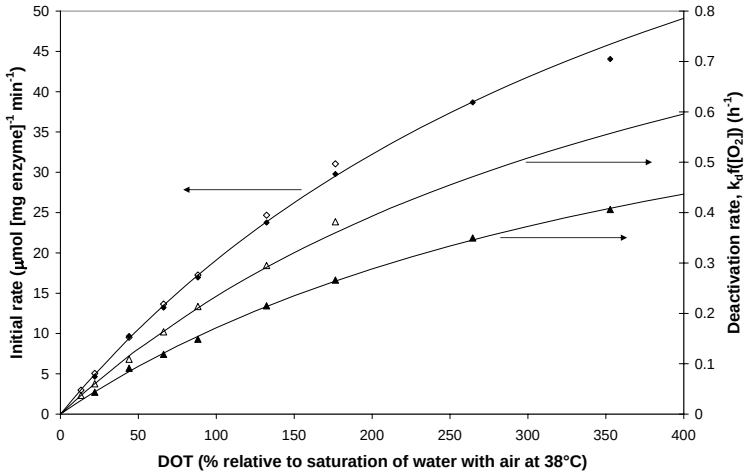

Figure 3.14. Initial rate of reaction and deactivation rate versus dissolved oxygen tension relative to saturation of water with air at 38°C and 1 bar with initial lactose concentrations of 50 g L^{-1} (open symbols) or 100 g L^{-1} (filled symbols). The curves are based on the consolidated parameters: k_{cat} = 103 μmol (mg protein)$^{-1}$ min^{-1}, K_{mO} = 439% DOT relative to saturation with air at 38°C or 0.97 mM, k_d = 0.90 h^{-1} for 100 g L^{-1} lactose, k_d = 1.23 h^{-1} for 50 g L^{-1} lactose and K_d = 425% DOT relative to saturation with air at 38°C or 0.95 mM. The initial rate of reaction is the same for the two different values of the initial lactose concentration while the deactivation rate is smaller for 100 g L^{-1} lactose.

L^{-1} and 100 g L^{-1} are included. Since the initial rate of reaction is constant for the same enzyme concentration and oxygen tension it can first of all be concluded that there is no substrate inhibition even at 200 g L^{-1} lactose, a value close to the saturation concentration of lactose. Furthermore, the rate of deactivation decreases with increasing initial lactose concentration, i.e. the same trend observed when experiments with 50 g L^{-1} lactose were compared with experiments with 100 g L^{-1} lactose. Apparently the enzyme is somewhat protected by a high initial substrate concentration. The almost exponential decrease of activity (with a rate that decreases a a higher initial substrate level) could indicate that substrate as well as product is able to protect the enzyme. The results for 50 g L^{-1} and 100 g L^{-1} lactose certainly support this hypothesis, but the curve for 200 g L^{-1} is downwards concave. Since the 200 g L^{-1} experiment lasts much longer than the 50 g L^{-1} and 100 g L^{-1} experiments one might speculate that the catalase had deactivated and hence that hydrogen peroxide accumulates and inhibits or deactivates the oxidase. However, addition of 0.50 g catalase instead of 0.25 g catalase did not give rise to an exponential decline of the rate, see figure 3.15. The positive effect of the high initial substrate concentration is clearly seen for the first 8-10 h, also at an initial lactose concentration of 200 g L^{-1}.

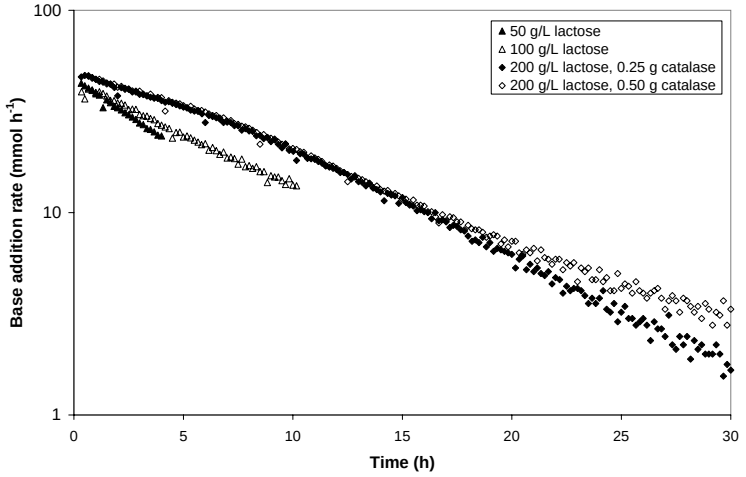

Figure 3.15. Effect of different initial lactose concentrations on the evolution in the rate of reaction. Experiments with 50 g L^{-1}, 100 g L^{-1}, and 200 g L^{-1} lactose present initially are shown. In all cases the dissolved oxygen tension was 66.15% relative to saturation with air at 38°C and 1 bar. In all experiments 60 mg pure LOX enzyme was added initially. 0.25 g catalase was added in the experiments with 50 g L^{-1} and 100 g L^{-1} lactose, while both 0.25 g and 0.50 g catalase were tried with 200 g L^{-1} lactose.

Figure 3.16 shows a semi-log plot of the rate of reaction versus time (again the initial transient and the phase just before depletion of lactose have been omitted) for two experiments performed with an initial lactose concentration

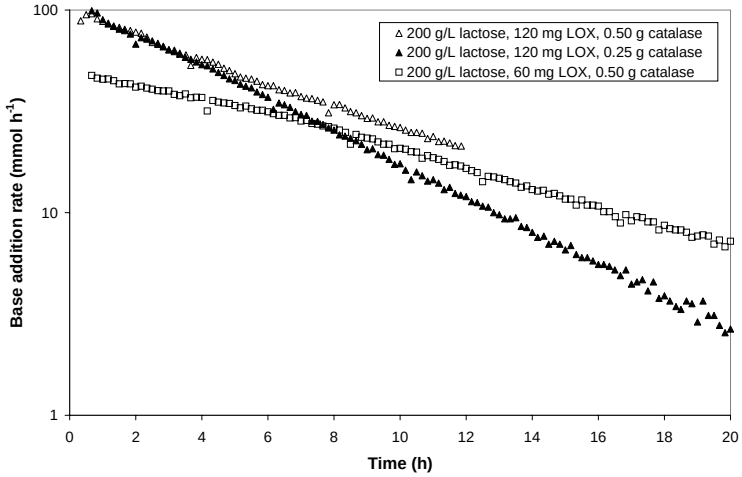

Figure 3.16. Rate of reaction versus time for reactions with an initial lactose concentration of 200 g L^{-1} and with addition of 120 mg LOX enzyme. In both cases the dissolved oxygen tension was 66.15% relative to saturation with air at 38°C and 1 bar. However, in one experiment 0.25 g catalase was added while 0.50 g was added in the other. For comparison the experiment with 200 g L^{-1} lactose, 60 mg LOX and 0.50 g catalase is included from figure 3.15.

of 200 g L^{-1} *but with twice the amount of oxidase* used in all the previously presented experiments and with two different catalase concentrations. Obviously the doubling of the oxidase concentration leads to doubling in the initial rate of reaction compared to an identical experiment with the only difference being the enzyme concentration from 49.2 to 102.6 mmol h^{-1}. When 0.25 g catalase is used the semi-log curve of rate versus time shows an increase in the deactivation rate with time. This was caused by accumulation of hydrogen peroxide since adding twice the amount of catalase gave almost an exponential decrease of rate with time. The deactivation rate was, however, higher than when an otherwise identical experiment was performed with 60 mg LOX instead of 120 mg LOX.

In the model leading to Eq.(3.14) it is assumed that the rate of deactivation is proportional to the enzyme concentration and dependent on the oxygen concentration. This corresponds to a situation where an oxygen metabolite produced from molecular oxygen (present at a concentration that depends on the molecular oxygen concentration) interacts with the carbohydrate oxidase and deactivates it. However, this model cannot explain why k_d - for the same initial lactose concentration increases with increasing enzyme concentration. If it was an oxygen metabolite that was responsible for the deactivation, then the fact that k_d decreased with decreasing enzyme concentration would imply that the oxygen metabolite was formed by interaction of molecular oxygen with the carbohydrate oxidase protein (whether active or not) whereby k_d

would be a function of the initial amount of active oxidase enzyme rather than a constant. This mechanism does not at all seem likely from a mechanistic point of view. Also, addition of additional protein in the form of BSA did not have an influence on the deactivation kinetics (data not shown). This made us speculate whether the increasing rate could in itself cause deactivation. This would also explain why the values of K_{mO} and K_d obtained by fitting were found to be similar, and it could maybe explain why k_d does not appear not be constant in the all the experiments with 200 g L^{-1} with the first order model. *A possible explanation for increased deactivation as a result of increased rate could be that the use of 2 M NaOH for titration causes high local concentrations of hydroxyl ions, thus denaturing the enzyme.* This hypothesis is pursued in the following.

3.4.4 Effect of using other bases for titration

If deactivation was caused by the use of a strong base one would probably avoid deactivation if a weak base was used. Thus a new series of experiments was started, the first with 0.5 M Na_2CO_3 as base. The results clearly showed that the total reaction time was lowered compared to using 2 M NaOH (4.66 hours compared to 6.33 hours with 2 M NaOH for conversion of 50 g lactose using 60 mg LOX at a DOT of 44.1% relative to saturation of water with air at 38°C). However, one disadvantage of using sodium carbonate is that the pK_a-value of H_2CO_3 is 6.37 (at 25°C), which is very close to the set-point pH-value of 6.4 used for the reaction. Thus, base weight measurements cannot easily be converted to a rate of reaction. In the next experiment 1.8 M NH_3 was used (pK_a for NH_4^+ equal to 9.25 at 25°C). The results are given in figure 3.17. It is seen that deactivation is largely avoided when NH_3 is used for titration.

3.4.5 Model for base deactivation and reevaluation of data

It is clear that the enzyme deactivates in the presence of a high local hydroxyl ion concentration. One possible way this can proceed is via a single step, two-state mechanism

$$E + OH^- \xrightarrow{k_d} I \tag{3.16}$$

Here E is the active enzyme (with this deactivation mechanism the different enzyme forms are treated as one), I is the completely deactivated enzyme, and k_d is the deactivation constant. From the mechanism it is seen that the decay must be proportional to the enzyme concentration and to the probability that the enzyme encounters a zone of high local pH. This probability must be proportional to rate of base addition and thus to the rate of reaction.

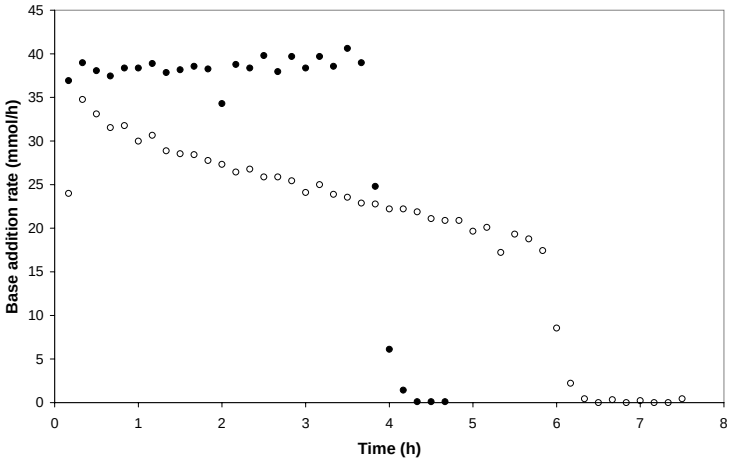

Figure 3.17. Effect on rate of reaction of using 1.8 M NH_3 for titration. For comparison an otherwise similar experiment with 2 M NaOH is included. The lactose concentration was 50 g L^{-1} and the oxygen concentration was 44.1% DOT relative to saturation of water with air at 38°C and 1 bar. 60 mg pure LOX enzyme and 0.25 g catalase was added initially.

The deactivation can therefore be written as

$$-\frac{d[E]}{dt} = k_d[E]r \tag{3.17}$$

Insertion of the expression for the rate of reaction, Eq.(3.10) gives

$$-\frac{d[E]}{dt} = k_{cat}k_d[E]^2\frac{[\mathrm{O_2}]}{[\mathrm{O_2}]+K_{mO}} \tag{3.18}$$

This deactivation model is second order in the enzyme concentration and not first order as suggested previously. When the dissolved oxygen concentration is constant the expression integrates to

$$\frac{1}{[E]}-\frac{1}{[E]_0} = k_{cat}k_d\frac{[\mathrm{O_2}]}{[\mathrm{O_2}]+K_{mO}}t \tag{3.19}$$

which upon insertion in Eq.(3.10) yields the following expression for the rate of reaction

$$r = \frac{k_{cat}}{k_{cat}k_d\frac{[\mathrm{O_2}]}{[\mathrm{O_2}]+K_{mO}}t+\frac{1}{[E]_0}}\cdot\frac{[\mathrm{O_2}]}{[\mathrm{O_2}]+K_{mO}} \tag{3.20}$$

Inversion gives

$$\frac{1}{r} = k_d t+\frac{1}{[E]_0k_{cat}}\cdot\frac{[\mathrm{O_2}]+K_{mO}}{[\mathrm{O_2}]} \tag{3.21}$$

Thus a plot of $\frac{1}{r}$ versus time should yield a straight line with slope k_d and intercept $\frac{1}{[E]_0k_{cat}}\cdot\frac{[\mathrm{O_2}]+K_{mO}}{[\mathrm{O_2}]}$, the inverse of the initial rate of reaction.

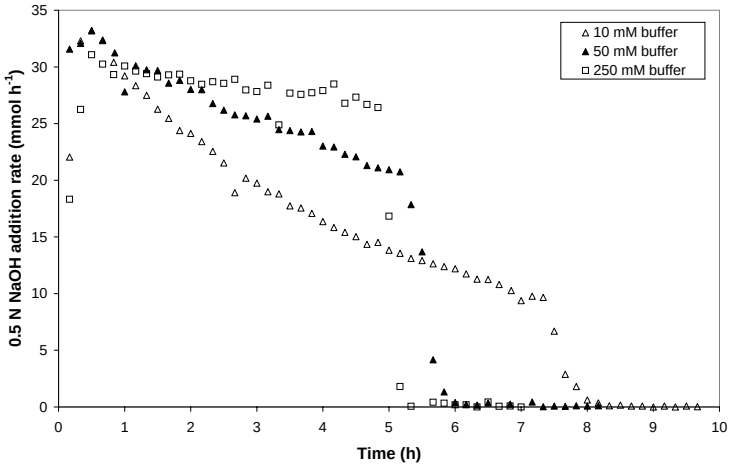

Figure 3.18. Effect of buffer concentration on the rate of reaction when 0.5 M NaOH was used for titration. Buffer concentrations of 10 mM, 50 mM, and 250 mM phosphate were used. The lactose concentration was 50 g L^{-1} and the oxygen concentrations was 44.1% DOT relative to saturation of water with air at 38°C and 1 bar. 60 mg pure LOX enzyme and 0.25 g catalase was added initially.

It is important to point out that in Eq.(3.17) $[OH^-]$ is *not* the average value of $[OH^-]$ in the reactor, but the local $[OH^-]$ value which is attained just after a drop of base is added. Due to the non-ideal mixing this value is always higher than the set-point $[OH^-]$. If NaOH is added to a heavily buffered solution the effect of non-inhomogeneity is less severe and the local $[OH^-]$ will not increase as much - hence the deactivating effect is smaller. Figure 3.18 clearly show the effect of buffering. With 250 mM phosphate buffer the rate of deactivation of the oxidase is small even with 0.5 M NaOH. Naturally the use of a weak base as in figure 3.17 is to be preferred.

Figure 3.19 shows inverse base addition rate versus time for experiments performed with 50 g L^{-1} lactose. This figure and especially figure 3.20 showing experiments with an initial concentration of 100 g L^{-1} lactose do, however, show that the model represented by Eq.(3.21) is not adequate: the lines are not straight. The slope of the curves increases with time. From figure 3.15 it is observed that the decline in rate is slower when more substrate is present initially. This indicates that the enzyme is being protected from base deactivation by a high substrate concentration. The following equation was proposed to include this effect.

$$\frac{1}{r} = k_d \frac{1}{1 + \frac{[S]}{K_p}} t + \frac{1}{[E]_0 k_{cat}} \cdot \frac{[O_2] + K_{mO}}{[O_2]} \tag{3.22}$$

The parameters K_{mO} and k_{cat} are taken to equivalent to the values obtained previously (k_{cat} = 103 μmol (mg protein)$^{-1}$ min^{-1}, K_{mO} = 439% DOT

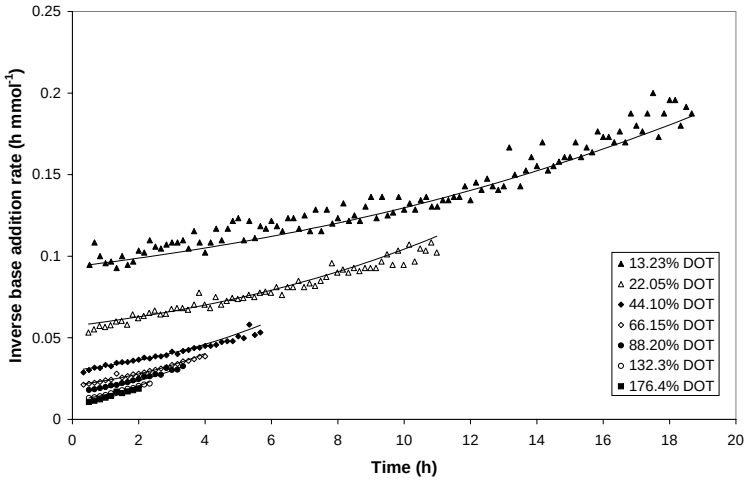

Figure 3.19. Inverse base addition rate versus time for experiments with an initial lactose concentration of 50 g L^{-1}. The oxygen concentrations given are relative to saturation of water with air at 38°C and 1 bar. 60 mg pure LOX enzyme and 0.25 g catalase was added initially. Lines are simulations based on Eq.(3.22) with parameters given below the equation.

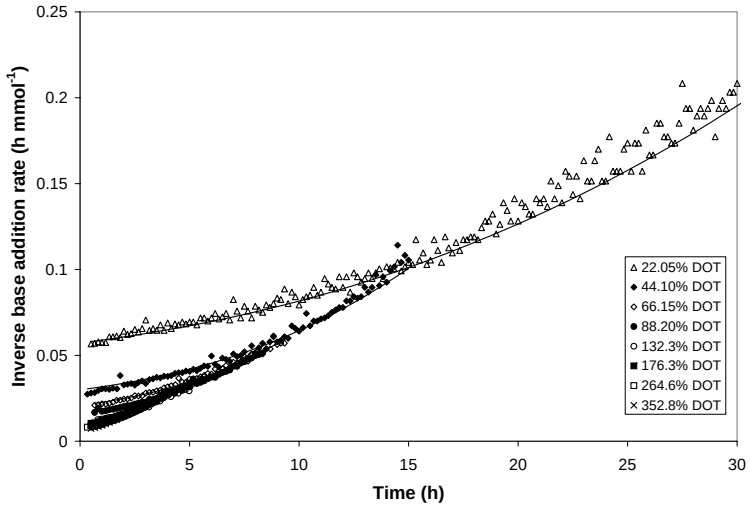

Figure 3.20. Inverse base addition rate versus time for experiments with an initial lactose concentration of 100 g L^{-1}. The oxygen concentrations given are relative to saturation of water with air at 38°C and 1 bar. 60 mg pure LOX enzyme and 0.25 g catalase was added initially. Lines are simulations based on Eq.(3.22) with parameters given below the equation.

relative to saturation with air at 38°C or 0.97 mM), while k_d and K_p are obtained by weighted least squares analysis of all data from experiments with initial lactose concentrations of 50 and 100 g L^{-1} lactose. The values were

found to $k_d = 0.00503$ L mmol^{-1} and $K_p = 141$ mmol L^{-1} (= 48 g L^{-1}).

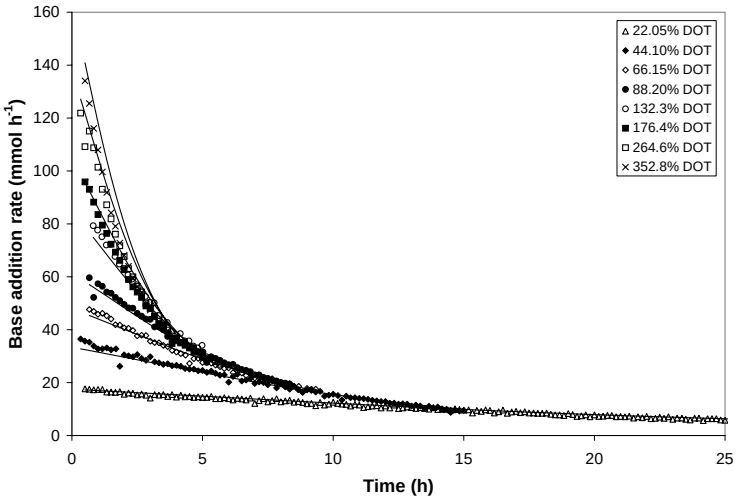

Figure 3.21. Base addition rate versus time for experiments with an initial lactose concentration of 100 g L^{-1}. Lines are based on Eq.(3.22). The oxygen concentrations given are relative to saturation of water with air at 38°C and 1 bar. 60 mg pure LOX enzyme and 0.25 g catalase was added initially. Lines are simulations based on Eq.(3.22) with parameters given below the equation.

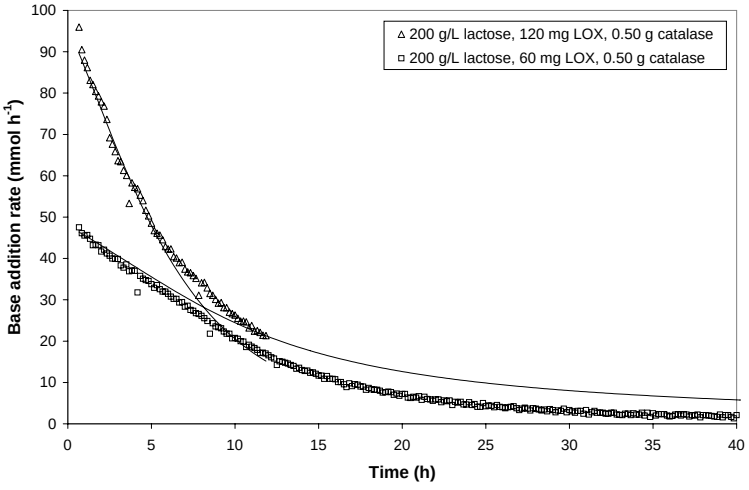

Figure 3.22. Rate of reaction versus time for the reaction with an initial lactose concentration of 200 g L^{-1} and with addition of 120 mg LOX enzyme or 60 mg LOX enzyme and with addition of 0.50 g catalase. The dissolved oxygen tension was 66.15% relative to saturation with air at 38°C and 1 bar. The line is based on Eq.(3.22). Lines are simulations based on Eq.(3.22) with parameters given below the equation.

Figure 3.21 shows experimentally obtained rates with 100 g L^{-1} lactose as the

initial concentration together with simulations according to Eq.(3.22). The agreement between experimental and simulated values is quite satisfactory. A significant difference between simulated values and experimental is only noted at the high dissolved oxygen tension of 352.4% DOT. The agreement between experimental and simulated values is even better in the case of an initial lactose concentration of 50 g L^{-1}.

Figure 3.22 shows that the model Eq.(3.22) is able to capture the experimental results adequately even in the experiment with 200 g L^{-1} where the enzyme amounts were doubled to 120 mg LOX protein and 0.50 g catalase. Only in the case of the experiment with 200 g L^{-1} and 60 mg LOX enzyme it seems that there is a large discrepancy, especially for times larger than 8 hours. Thus the experimental rates are smaller than the ones predicted by the model.

In the above analysis it was neglected that dilution changes the buffer strength of the solution.

3.4.6 Deactivation and inhibition by hydrogen peroxide

The deactivation by high local [OH^-] has been analyzed in some detail in the previous sections. H_2O_2 is, however, known to inhibit (competitively) and deactivate oxidases, e.g. glucose oxidase, see Kleppe (1966) and Bao et al. (2003). Hence a very brief discussion of the effect H_2O_2 will be given although the subject has not been pursued to any great length.

A single experiment is shown to illustrate that *M. nivale* carbohydrate oxidase is also both deactivated and inhibited by hydrogen peroxide, see figure 3.23. In the experiment where ammonia was used for neutralization hydrogen peroxide accumulated for 6.2 h until catalase was added. It is seen that the rate of base addition declined until catalase was added. After addition of catalase the rate of base addition increased almost as a jump. Hence the enzyme is inhibited by catalase. However, it is also being deactivated by hydrogen peroxide because the rate of base addition after addition of catalase did not increase to the initial level.

3.5 Discussion

In this study, the kinetic parameters for lactose oxidation by the *M. nivale* carbohydrate oxidase enzyme were obtained. First of all, the K_{mS}-value of 0.12 mM is low compared to K_{mS} found for other enzymes capable of oxidizing lactose to lactobionic acid. Compared to the very high K_{mS}-value of glucose-fructose oxidoreductase from *Z. mobilis* (Satory et al., 1997) of 1.2

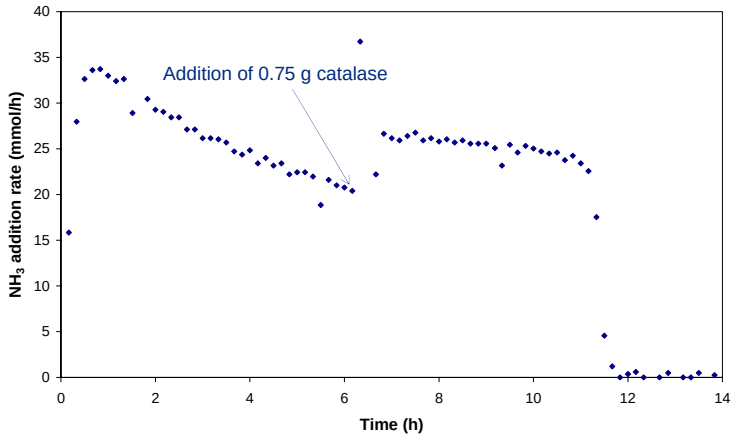

Figure 3.23. Rate of reaction versus time for a reaction with an initial lactose concentration of 100 g L^{-1} and with addition of 60 mg LOX enzyme but without addition of catalase at time zero. Consequently H_2O_2 accumulated until 0.75 g catalase was added after 6.2 h. 1.8 M NH_3 was used for titration. The dissolved oxygen tension was 44.1% relative to saturation with air at 38°C and 1 bar.

M, the value is minuscule. However, also compared to the K_{mS}-value of lactose dehydrogenase from *Ps. graveolens* of 11 mM (Nishizuka and Hayaishi, 1962), the value for hexose oxidase from *C. crispus* of 97 mM (Savary et al., 2001), and the value of cellobiose dehydrogenase from *S. rolfsii* of 2.4 mM (Ludwig et al., 2004), the value is small. The K_{mO}-value of the *M. nivale* carbohydrate oxidase of 0.97 mM found at 38°C is large compared to the saturation concentration of oxygen from air at 1 bar and 38°C of 0.22 mM. Unfortunately, the K_{mO}-value of the oxidases described in the introduction was only determined for hexose oxidase from *C. crispus* by Groen et al. (1997) (and only with glucose as substrate), who measured the consumption of oxygen using a Clark-type oxygen electrode. Thus, the value of 0.30 mM obtained by Groen et al. (1997) might be underestimated if the time for the experiment is comparable to the response time of the probe. In the cellobiose dehydrogenase/laccase system used by Ludwig et al. (2004), the K_{mO}-value of laccase LAP2 from *T. pubescens* was found to 0.41 mM. This is less than half the value found for the *M. nivale* carbohydrate oxidase used in the present study. Thus, a higher rate can probably be realized at low oxygen concentrations in a system where the *M. nivale* carbohydrate oxidase is coupled to laccase and a suitable redox mediator. This possibility is currently being investigated. Since *M. nivale* carbohydrate oxidase can use oxygen as terminal electron acceptor in contrast to cellobiose dehydrogenase it is still necessary to include catalase if deactivation and inhibition by hydrogen peroxide should be avoided.

It was found in this study that the operational stability of the *M. nivale* car-

bohydrate oxidase enzyme is heavily dependent on the strength of the base used for titration and on the buffer capacity of the reaction medium. The literature on operational stability of oxidases is scarce. Mostly enzyme stability is examined by incubating the enzyme in buffer at e.g. different values of pH and temperature and then measuring the residual activity after a certain incubation time. However, this may not reflect the stability at the actual operating conditions. One example of this concerns deactivation of glucose oxidase from *Aspergillus niger* by hydrogen peroxidase. Kleppe (1966) found that the reduced form of the enzyme is 1000 times more sensitive to hydrogen peroxide than the oxidized form. Thus, the stability towards hydrogen peroxide in an incubation assay will not reflect the stability during an actual process if the incubation assay is performed by incubating the enzyme with hydrogen peroxide for a certain period of time, removing the hydrogen peroxide and then measuring the remaining activity. In the incubation assay described above the oxidized form of the enzyme would be the only form present (unless the incubation solution is completely free of oxygen), while the more labile reduced form will also be present during an actual process.

The literature contains several examples of enzymatic processes where it may be speculated that enzyme deactivation is caused by addition of a strong base. As mentioned in the introduction Lin et al. (1993) investigated batch conversion of lactose by a partly purified glucooligosaccharide oxidase from *A. strictum*. The reaction was carried out in a reactor with a working volume of 2 L operated at 35°C and pH 7-8. 1000 units of partially purified glucooligosaccharide oxidase was added, and 100,000 units of catalase was added to eliminate the produced H_2O_2. 4 M NaOH was used for neutralization. After 4 hours of reaction 98% of the initial 27.5 g L^{-1} lactose was converted, but the enzyme activity had dropped to 60% relative to the initial value. It may very well be that this decrease in activity was caused by addition of the 4 M NaOH. Venugopal and Bradley (1993) examined the inactivation of glucose oxidase in a batch reactor system where glucose was added during the reaction. They found that the rate of deactivation was first order and that the rate constant was proportional to the oxygen concentration, and they speculated that deactivation was caused by an oxygen metabolite. The authors used 0.02 M NaOH for neutralization but only a 1 mM phosphate buffer. Even though the concentration of NaOH is 100 times lower than the one used in my study it might be that the deactivation found by Venugopal and Bradley (1993) was due to deactivation by base and not due to oxygen in itself or an oxygen metabolite.

A literature survey revealed that an effect similar to the one found in the present study was observed by Nidetzky et al. (1997) in production of sorbitol and gluconic acid from fructose and glucose by glucose-fructose oxidoreductase from *Z. mobilis* in a continuous ultrafiltration membrane reactor. The enzyme deactivation was lowered significantly by using 2 M

tris(hydroxymethylamino)methane or 2 M imidazol for titration instead of 2 M NaOH. However, Nidetzky et al. (1997) modeled the enzyme deactivation by the following equation

$$-\frac{d[E]}{dt} = k_d r \tag{3.23}$$

where r is the volumetric rate of reaction and k_d is a deactivation constant. The model does give an adequate fit to the experimental values when fitting is performed on individual experiments (i.e. a parameter set is obtained from a single experiment rather than from experiments performed at different conditions). However, from a mechanistic point of view it is hard to believe that the rate of enzyme deactivation should only depend on the rate of reaction (i.e. the rate of base addition) and not on both the base addition rate as well as the enzyme concentration.

One interesting observation of this study is that the oxidase is protected from denaturation by the substrate at high local base concentrations. To the best of our knowledge this has not been reported for a carbohydrate oxidase before.

It can of course not be concluded in general that enzymes are affected in processes where strong base is used for neutralization. Whether or not the base used for titration affects process stability dependents on the pH stability of the enzyme. Thus, e.g. proteases used in the alkaline environment found in detergents are optimized to have good stability even at high pH values. Thompson (1987) examined the activity of a model enzyme, alkaline phosphatase present in a culture of *Saccharomyces cerevisiae* grown at a pH of 4.75. The enzyme activity of the phosphatase was inhibited at a pH of 4.75 and the maximum activity of the enzyme in the culture was 7.5 units at pH 10.5. 4 M NaOH was used for neutralization during the cultivation and the activity of the phosphatase could be correlated to the mixing intensity. At agitation rates above 400 RPM the enzyme remained inhibited, while the activity increased at lower agitation rates reaching a maximum of around 1.9 units at approximately 50 RPM.

The present study can serve as an example of how careful one should be during data analysis. Had we not performed experiments at different values of the initial lactose concentration and the enzyme dosage the first order deactivation model could easily have been accepted and totally wrong conclusions would have been drawn. Only by changing the conditions and thereby rendering the first order model more and more improbable we were led in the right direction.

As a final note - and on a rather different tack - the studies of Nienow and coworkers (Langheinrich and Nienow, 1999; Amanullah et al., 2001) of the influence of alkaline strength when titrating metabolic products from fermentations deserves to be mentioned. In Langheinrich and Nienow (1999)

titration with Na_2CO_3 of the slowly released CO_2 from a mammalian cell cultivation is studied as a function of operating parameters such as impeller speed and the location of the feed point (at the top or close to the impeller). A semi-quantitative model for the influence of the operational parameters on the size and duration of the pH overshoot is derived. In Amanullah et al. (2001) the effect of operating parameters on a model reaction (acetolactate conversion to either acetoin or to 2,3- butanediol as a function of the local pH) is studied. It is likely that the large data set collected in the present study of lactose oxidation and deactivation of the LOX enzyme can be used to derive a good mechanistic model for mixing in stirred tanks. This topic is, however, not pursued here. A clear message to be derived from the present study is that non-ideal mixing can cause a severe distortion of kinetic experiments even when they are carried out in what is euphemistically termed an ideal laboratory bioreactor.

Chapter 4

Enzymatic oxidation of lactose to lactobionic acid II: scale-up

In the last chapter the kinetics for the oxidation of lactose to lactobionic acid by *Microdochium nivale* carbohydrate oxidase was obtained. In this chapter the implications of the low affinity of the oxidase for oxygen (K_{mO} equal to 0.97 mM at 38°C) are analyzed and results of experiments performed in a 600 L pilot-scale reactor equipped with a rotary jet head for mass transfer are presented.

4.1 Effect of mass transfer and enzyme dosage on the reaction rate

When the lactose concentration is much higher than the saturation constant for lactose - which is the case during a batch reaction - the volumetric rate of lactobionic acid production can be written as[1]

$$r = k_{cat}[E]\frac{c_l}{c_l + K_{mO}} \tag{4.1}$$

provided that there is sufficient catalase and therefore no inhibition by hydrogen peroxide. At the same time the volumetric rate of mass transfer is given by

$$OTR = k_l a(c_l^* - c_l) \tag{4.2}$$

where c_l^* is the saturation concentration of oxygen.

During the reaction the volume will change somewhat due to dilution by base. This will lead to dilution of the enzyme and the volumetric rate of

[1] c_l which is normally used as the oxygen concentration in mass transfer equations will be used instead of $[O_2]$ in the following

production will decrease while the overall rate (mmol h^{-1}) remains constant provided that there is no enzyme deactivation and provided that the oxygen concentration is constant. This last assumption is not true since the $k_l a$-value will decrease if the same power input (W) and gas flow rate is used in the slightly larger volume. However, the overall effect of the dilution is very small unless dilute base is used. Consequently, since the reaction is essentially zero order in lactose, a steady state in dissolved oxygen concentration is reached during batch conversion of lactose. Half the rate of oxygen consumption by the reaction equals the rate of mass transfer - the remaining oxygen is supplied by the conversion of H_2O_2

$$\frac{k_{cat}[E]}{2}\frac{c_l}{c_l + K_{mO}} = k_l a(c_l^* - c_l) \tag{4.3}$$

4.1.1 Approximate solution

For moderate oxygen concentrations Eq.(4.3) can be approximated by first order kinetics

$$\frac{k_1[E]c_l}{2} = k_l a(c_l^* - c_l) \tag{4.4}$$

where k_1 can be obtained by fitting experimental values of the volumetric rate of reaction versus dissolved oxygen to a linear relationship. Solving for c_l gives

$$c_l = \frac{2k_l a c_l^*}{k_1[E] + 2k_l a} \tag{4.5}$$

which is inserted in Eq.(4.1) resulting in the following equation for the volumetric rate of lactobionic acid production

$$r = k_1[E]\frac{2k_l a c_l^*}{k_1[E] + 2k_l a} \tag{4.6}$$

This expression has two limiting cases

$$\text{fast reaction:} \quad k_1[E] >> 2k_l a: \quad r = 2k_l a c_l^* \tag{4.7}$$

$$\text{slow reaction:} \quad k_1[E] << 2k_l a: \quad r = k_1[E]c_l^* \tag{4.8}$$

In the first case the reaction is limited by mass transfer, while in the second case the enzyme concentration is the limiting factor.

Furthermore, the enzyme concentration needed to achieve a certain volumetric rate of reaction can be calculated

$$[E] = \frac{2k_l a r}{2k_1 k_l a c_l^* - k_1 r} \tag{4.9}$$

The approximate effect of using moderately enriched air on the required enzyme concentration to obtain a given volumetric rate of reaction can be

found from this equation. The equation shows that the enzyme concentration needed to achieve a certain volumetric rate of reaction is at least inversely proportional to the saturation concentration of oxygen.

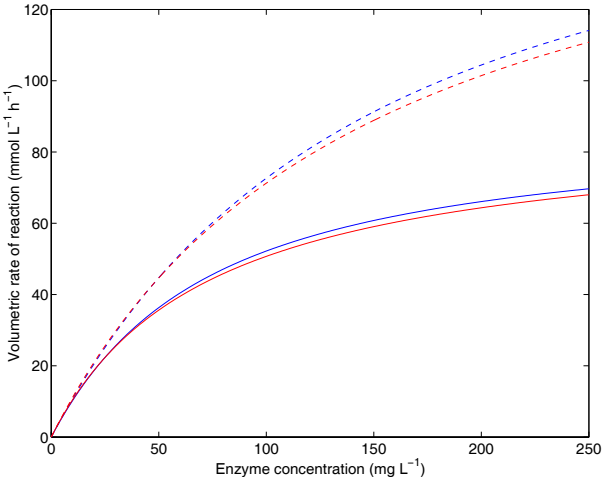

Figure 4.1. Volumetric productivity of lactobionic acid, r, as a function of the enzyme concentration for two different $k_l a$-values: full lines: $k_l a = 200$ h^{-1}, broken lines: $k_l a = 400$ h^{-1}. Red lines are first order approximations calculated from Eq.(4.6), while blue lines are based on Eq.(4.10) and Eq.(4.1). A saturation concentration, c_l^*, of 0.22 mmol L^{-1} was used.

4.1.2 Exact solution

When pure oxygen or enriched air with a large fraction of oxygen is used the reaction cannot be assumed to be first order in oxygen, and Eq.(4.3) has to be solved

$$c_l = \frac{-\left(\frac{k_{cat}[E]}{2} + k_l a(K_{mO} - c_l^*)\right) + \sqrt{\left(\frac{k_{cat}[E]}{2} + k_l a(K_{mO} - c_l^*)\right)^2 + 4k_l a^2 K_{mO} c_l^*}}{2k_l a} \tag{4.10}$$

which can be inserted in Eq.(4.1) to find the volumetric rate of production of lactobionic acid. The enzyme concentration needed to reach a certain volumetric rate of production can be found by solving this equation and Eq.(4.1) iteratively for $[E]$.

4.1.3 Simulations

The following values - taken from section 3.4.3 in the previous chapter - were used in the simulations: $k_{cat} = 6.18$ mmol (h mg protein)$^{-1}$, $K_{mO} =$

0.97 mmol O_2 L^{-1}. The constant k_1 used for the first order approximation Eq.(4.4) was found to be 5.44 mmol L (h mg protein mmol O_2)$^{-1}$ by fitting values of r calculated by Eq.(4.1) to a linear relationship in the interval $0 <$ [O_2] $<$ 0.22 mmol O_2 L^{-1} (0 to 100 % DOT relative to saturation with air at 38°C and 1 bar).

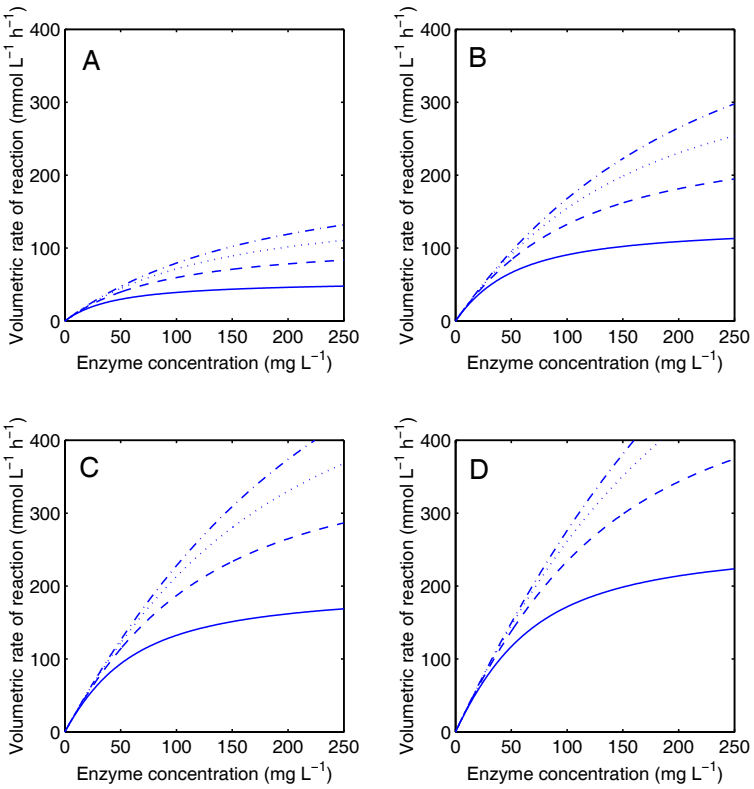

Figure 4.2. Volumetric productivity of lactobionic acid, r, as a function of the enzyme concentration for four different $k_l a$-values: 125 (full line), 250 (-), 375 (·) and 500 (· -) h^{-1}, and for four different values of c_l^*: A: 0.222 mmol L^{-1}, B: 0.424 mmol L^{-1}, C: 0.635 mmol L^{-1}, D: 0.847 mmol L^{-1} corresponding to saturation of water with air or air enriched to 40, 60, and 80% oxygen at 38°C and 1 bar.

Figure 4.1 shows the dependence of enzyme concentration on the volumetric rate of lactobionic acid production for two different values of $k_l a$ at a saturation concentration corresponding to saturation of water with air at 38°C and 1 bar. It is seen that there is only a small difference ($< 5\%$) between the exact solution and the first order approximation.

Figure 4.2 shows the dependence of enzyme concentration at different values of $k_l a$ and c_l^*. Running the catalyzed reaction in a pressurized tank or using enriched air leads to a dramatic increase in the volumetric rate of production as anticipated from the approximate Eq.(4.9) for a given $k_l a$-value. The value of increasing c_l^* is further illustrated in figure 4.3 which

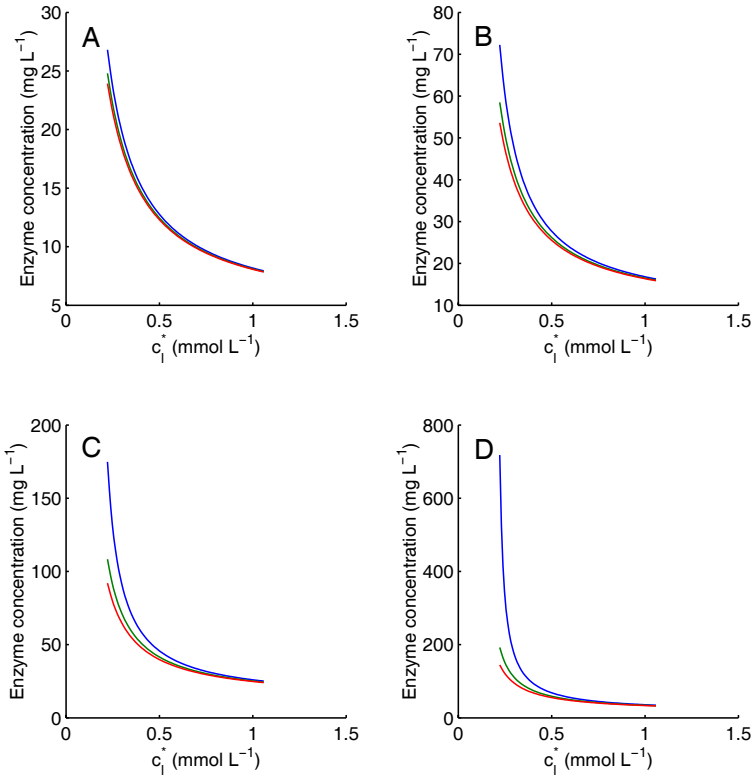

Figure 4.3. Enzyme concentration needed to reach the following volumetric lactobionic acid production rates as a function of c_l^*: A: 25 mmol L^{-1} h^{-1}, B: 50 mmol L^{-1} h^{-1}, C: 75 mmol L^{-1} h^{-1}, D: 100 mmol L^{-1} h^{-1}. The following $k_l a$-values were used: 250 (blue), 375 (green) and 500 (red) h^{-1}.

shows the enzyme concentration required to reach a certain volumetric rate of production as a function of c_l^*. It is seen that when c_l^* is increased the influence of $k_l a$ diminishes. Consequently by using enriched air the required $k_l a$-value decreases and/or the amount of enzyme needed to obtain a given volumetric productivity decreases.

In the simulations presented here different values of c_l^* were assumed. For an actual process c_l^* can be estimated from a gas phase balance if $k_l a$ is known and a gas phase mixing model is assumed. If e.g. sodium carbonate is used for neutralization it also needs to be considered in the gas phase balance that CO_2 will be released during the process.

4.2 Materials and methods

4.2.1 Enzymes and chemicals

The carbohydrate oxidase and catalase (Catazyme 25 L) used were identical to the enzymes described in the previous chapter. Lactose monohydrate (Pharmatose 350M, produced by DMV International) was a kind donation from Novozymes A/S, while whey permeate powder (produced by LNA/CLP) was donated by Chr. Hansen A/S. According to the certificate of analysis it contained 0.5% fat, 2.9% protein, 10% salts, and a minimum of 83.3% lactose by weight.

4.2.2 Experimental set-up and operating conditions

Figure 4.4 shows an outline of the experimental system used for the enzymatic oxidation of lactose in pilot-scale. The tank has an inner diameter of 0.96 m and the tubing is made of 2 inch pipe. The liquid volume during experiments was 600 L. Liquid is pumped from the bottom of the tank by a lobe pump and reinjected into the tank by a rotary jet head. The rotary jet head used was an IM15 mixer from ISO-MIX A/S (Ishøj, Denmark) equipped with 4 nozzles with a diameter of 7 mm. Air is added in the loop on the pressure side of the pump.

The pressure in the loop was measured just before the inlet to the tank by a pressure transmitter (Haenni, model ED510/324.241/A25). The air flow rate was controlled by a mass flow controller (Brooks Instrument, model 5853S), while the liquid flow rate was measured by a Promass 60M/63M mass flow meter from Endress & Hauser. The dissolved oxygen tension tension was monitored at two different positions in the tank and in the loop on the pressure side of the pump by polarographic oxygen sensors (Mettler Toledo). The sensors were calibrated to 100% relative to saturation with air at 38°C and 1 bar. This was done by running the system in pure water and injecting 100 NL min^{-1} air for 20 min after which the gas flow rate was turned off and the system was left running until a steady reading was recorded. pH was monitored during the reaction and controlled at 6.4 by a pH-regulator (Consort) controlling a base addition pump, that introduces base into the recirculation loop on the suction side of the pump. The base container was placed on a balance, and the balance readings were logged by a PC. The temperature in the tank was measured by a Pt100 temperature sensor. The temperature signal was used to control an on/off-controller that opens or closes a valve to feed cooling water into the tank jacket. Thereby the temperature was controlled at 38°C during reaction.

The medium was prepared by dissolving 30 kg of lactose in 600 L of water

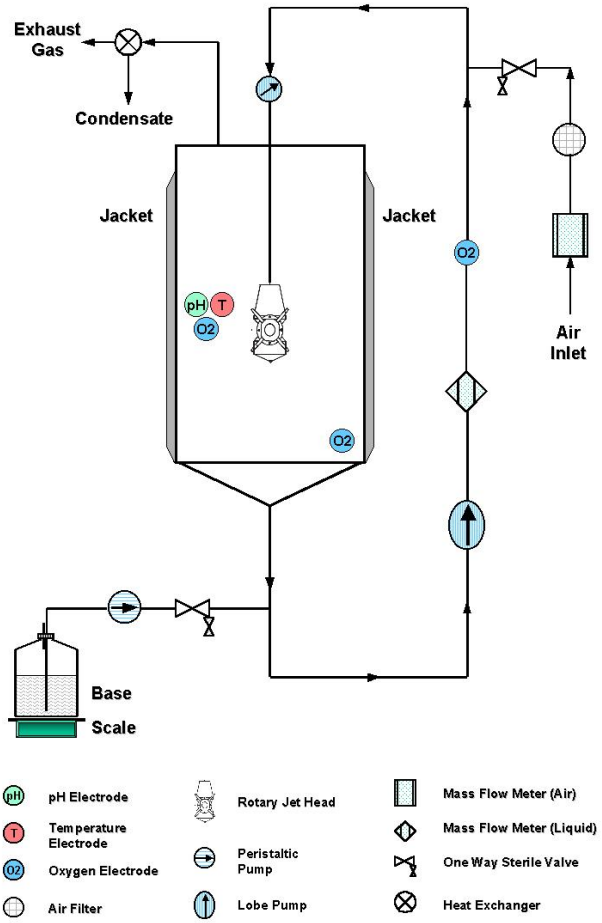

Figure 4.4. Experimental set-up of the rotary jet head reactor system.

- both when lactose or whey permeate was used as substrate. When lactose was used as substrate 3.6 mol of KH_2PO_4 was added as buffer, i.e. in a concentration of 6 mM. To avoid foaming 5-10 mL antifoam (Synperonic PE/L61 from Brenntag) was added to the solution when whey permeate was used as substrate. The reaction was started by adding 300 g LOX solution containing 59 mg enzyme protein g^{-1}, (i.e. 17700 mg enzyme protein) to give a concentration of 29.5 mg L^{-1} oxidase protein and 75 g Catazyme 25 L was added.

Unless stated otherwise 24wt% ammonia solution was used to keep pH constant at 6.4

4.3 Results

Conversion of lactose to lactobionic acid was done in 600 L scale in the rotary jet head system at a constant pH of 6.4 and at 38°. The base addition rate - which is proportional to the rate of reaction - was monitored and used to calculate the volumetric reaction rate. The system was aerated by injecting air into the recirculation loop at different flow rates (10-200 NL min^{-1}) and the dissolved oxygen tension was monitored by two oxygen sensors in the tank and one in the loop.

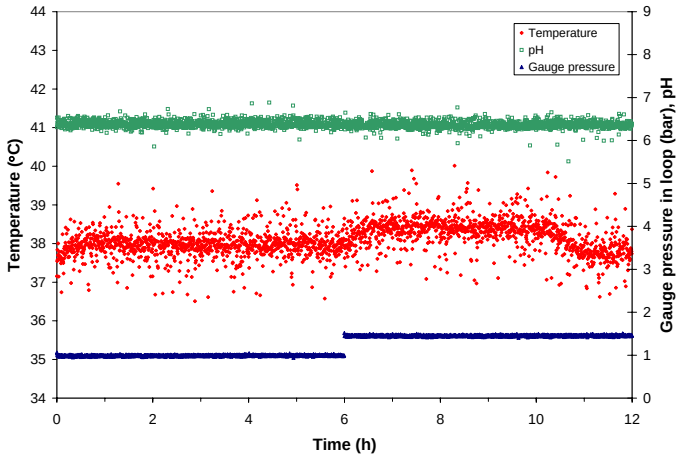

Figure 4.5. pH, temperature and gauge pressure in loop versus time.

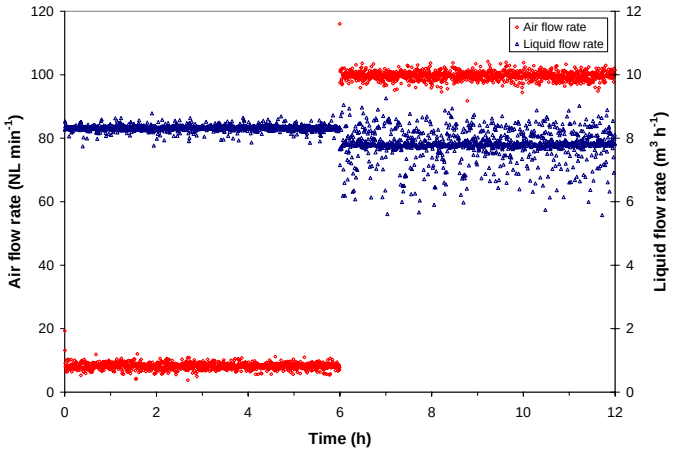

Figure 4.6. Air flow rate and liquid flow rate versus time.

Figures 4.5 to 4.8 present the results of a typical experiment. The initial air flow rate was set to 10 NL min^{-1}. After 6 hours of reaction the set-point

was changed to 100 NL min^{-1}. Figure 4.5 shows values of temperature, pH, pressure in the loop versus time, while liquid as well as gas flow rates are depicted in figure 4.6. Figure 4.7 presents the dissolved oxygen tension, and the total amount of base added is shown in figure 4.8, again with time on the abscissa.

From figure 4.5 it is observed that when the airflow was increased, the pressure in the loop increased from 0.99 to 1.45 bar gauge pressure, while the liquid flow rate dropped from 8.33 to 7.76 m^3 h^{-1}. The rather unstable reading of the liquid flow rate in the case of an air flow rate of 100 NL min^{-1} is caused by air bubbles entering the mass flow meter leading to unstable measurements. The actual liquid flow rate as such is not fluctuating much as might be inferred from figure 4.6, and it is possible to read the liquid flow rate from the figure. When the air flow rate was changed to 100 NL min^{-1} a small increase in temperature was observed because the higher rate of reaction leads to a higher rate of heat generation. The temperature was, however, still controlled within 38±1°C.

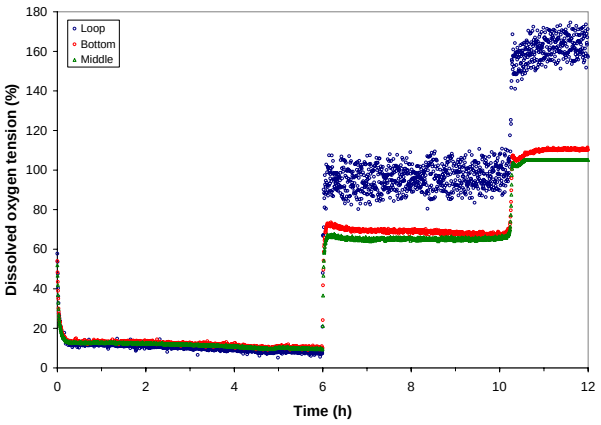

Figure 4.7. Dissolved oxygen tension relative to saturation of water with air at 38°C and 1 bar measured in the loop, the middle, and the bottom of the tank versus time.

Figure 4.7 shows that the DOT level decreased rapidly when the enzymes were added at time 0 until a steady state in the dissolved oxygen tension was reached. When the air flow rate was increased from 10 to 100 NL min^{-1}, the dissolved oxygen tension increased. With depletion of substrate the DOT level rapidly rose. It was found that when the air flow rate was 10 NL min^{-1}, the DOT measured at the three positions was almost the same. When the air flow rate was increased to 100 NL min^{-1}, the DOT in the loop was higher than in the tank. Notice that the DOT levels measured by the two sensors in the tank are almost identical. Thus liquid mixing is sufficiently good to avoid gradients in the DOT in the tank. The oxygen sensors are calibrated

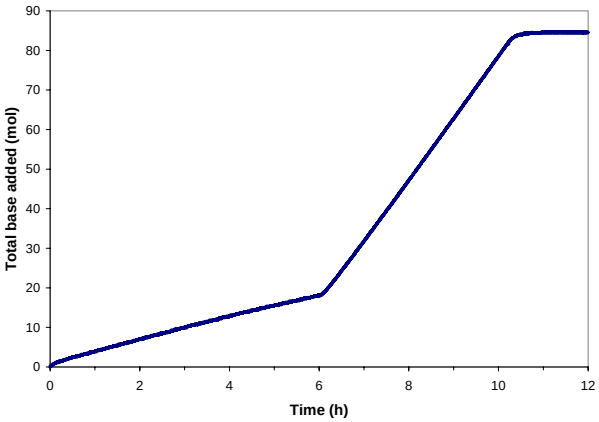

Figure 4.8. Total amount of base added versus time.

in such a way that 100% is relative to saturation of pure water with air at 1.00 bar and 38°C. Due to the hydrostatic pressure (liquid height of 0.83 m when no gas is present) the DOT measured when the rate of reaction is very low or zero will be above 100%. This is observed when the reaction terminates. The bottom sensor gives a slightly higher DOT level than the one placed in the middle. The reason for the higher DOT in the loop is to be found in the higher pressure in the loop. Consequently, the saturation concentration of oxygen increases, and since bubbles will be present in the loop also (although in a smaller number than in the tank) the DOT increases in the loop compared to the tank. The plot of total base added versus time shows that for a given air flow rate, the slope of the plot is constant, and consequently the rate of base addition and thus the rate of reaction was constant. Also, the rate increased almost proportionally to the dissolved oxygen tension in the tank, which should be the case when operating at an oxygen concentration far from the saturation constant K_{mO} of the oxidase for oxygen. The total molar amount of base added was always more than 98% of the molar amount of lactose present initially supporting the validity of the method. During the course of the reaction, no deactivation was observed as seen from the non-declining base addition rate.

Figure 4.9 shows a comparison between the specific rate of reaction obtained in the 1 L reactor with rates obtained in the 600 L pilot-scale reactor versus dissolved oxygen tension measured in the reactor. Good agreement between the experimental values is observed. For dissolved oxygen tensions above 55% DOT, the specific rate of reaction is, however, up to 17% higher in the pilot-scale rotary jet head reactor than in the 1 L stirred reactor. This can be partly explained by the higher dissolved oxygen tension in the loop. Furthermore, the dissolved oxygen tension in the sweeping jet is higher than in the bulk liquid. Due to the response time of the oxygen sensor this is not

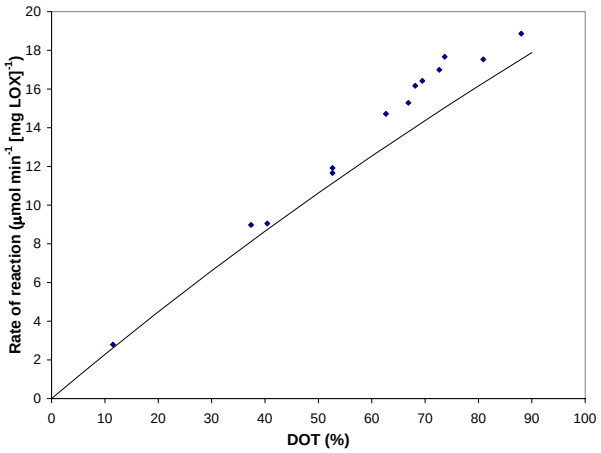

Figure 4.9. Specific rate of reaction versus dissolved oxygen tension (relative to saturation of water with air at 38°C and 1 bar). Points are for experiments in rotary jet head set-up, while the curve represents data obtained in 1 L scale.

adequately captured by the sensor when the jet sweeps by.

Experiments with whey permeate showed that the kinetics were the same with whey permeate as substrate as with lactose. The specific rate of reaction achieved was the same for a given dissolved oxygen tension, see figure 4.10. Thus the whey permeate contains no substances that inhibit or deactivate the oxidase.

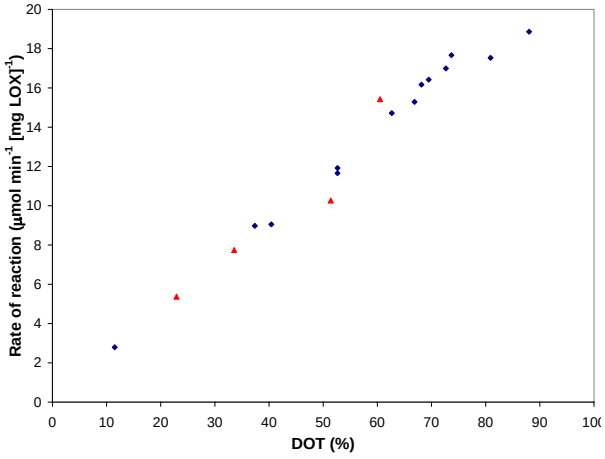

Figure 4.10. Specific rate of reaction versus dissolved oxygen tension (relative to saturation of water with air at 38°C and 1 bar) for experiments with whey (triangles) and lactose (diamonds).

Table 4.1 shows values of the volumetric rate of reaction and values of $k_l a$ at different operating conditions with lactose as substrate, while table 4.2 shows

the situation with whey permeate as substrate. Note that the volumetric rate of reaction is smaller with whey permeate as substrate than with lactose for similar operating conditions. This is caused by the addition of antifoam which leads to a decrease in $k_l a$ giving a decrease in the dissolved oxygen tension in the medium which in turn leads to a decrease in the volumetric rate of reaction. An important conclusion is that mass transfer is indeed a relevant process variable for lactobionic acid production.

Table 4.1. Volumetric rate of reaction and $k_l a$ at different operating conditions for experiments with lactose as substrate. $k_l a$-values are given both for a gas phase in plug flow and for the backmixed case. The saturation concentration of pure oxygen at 1 bar and 38°C was taken to be 1.05 mM and the mean pressure was set to 1.04 bar (corresponding to the middle of the liquid height).

Air flow NL min^{-1}	Pressure barg	Liquid flow m^3 h^{-1}	DOT %	Rate mmol L^{-1} h^{-1}	$k_l a$ (plug flow) h^{-1}	$k_l a$ (backmixed) h^{-1}
10	0.99	8.33	11.5	4.95	14	16
25	1.10	8.27	37.4	15.9	72	99
50	1.23	8.08	52.6	20.7	114	145
100	1.45	7.76	66.9	27.1	201	247
200	1.72	7.41	73.7	31.3	266	304

Table 4.2. Volumetric rate of reaction and $k_l a$ at different operating conditions for experiments with whey permeate as substrate. $k_l a$-values are given both for a gas phase in plug flow and for the backmixed case. The saturation concentration of pure oxygen at 1 bar and 38°C was taken to be 1.05 mM and the mean pressure was set to 1.04 bar (corresponding to the middle of the liquid height).

Air flow NL min^{-1}	Pressure barg	Liquid flow m^3 h^{-1}	DOT %	Rate mmol L^{-1} h^{-1}	$k_l a$ (plug flow) h^{-1}	$k_l a$ (backmixed) h^{-1}
15	1.01	8.24	22.9	9.5	33	42
25	1.09	8.31	33.6	13.7	53	69
50	1.23	8.09	51.4	18.2	94	115
150	1.55	7.67	60.5	27.4	158	176

4.3.1 Deactivation by strong base

To investigate the effect of using strong base for titration in the pilot-scale equipment, a single experiment was performed where 17.84 wt% NaOH was used for neutralization instead of NH_3. Lactose was used as substrate at an initial concentration of 50 g L^{-1} and the enzyme and buffer concentrations were as given previously. Likewise with pH and temperature. The air flow

rate was 100 NL min^{-1}. The actual values of pH, temperature, pressure, and liquid and gas flow rates are given in figures 4.11-4.12. Between 6 and 8 hours the air flow rate fluctuated considerably around the set-point value (see figure 4.12) which also gave rise to fluctuations in the pressure in the loop (see figure 4.11). Figure 4.13 shows the dissolved oxygen tension in the loop and in the bottom of the tank versus time (the sensor in the middle of the tank was out of order). Finally figure 4.14 shows the total amount of base added versus time. From this figure it is clearly seen that the oxidase deactivates during the experiment since the slope of the curve decreases with time. This is also observed from figure 4.13 showing that the dissolved oxygen tension increases with time. Since the operating parameters are constant this occurs because the rate of reaction decreases.

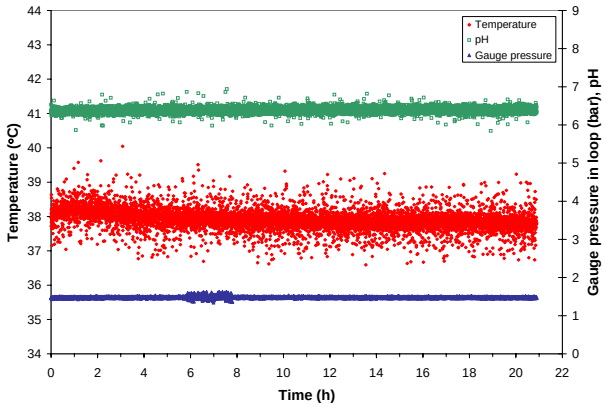

Figure 4.11. pH, temperature and gauge pressure in loop versus time during experiment where strong base (17.84 wt% NaOH) was used for titration.

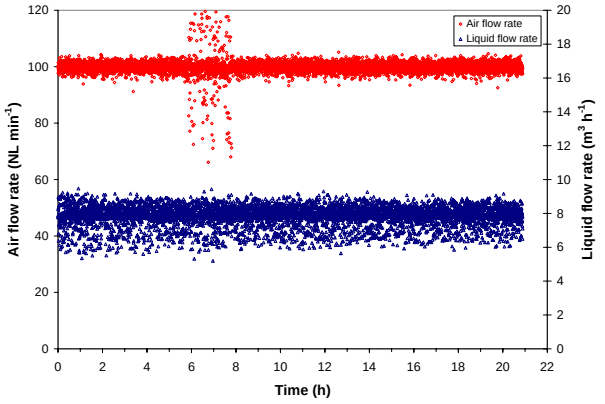

Figure 4.12. Air flow rate and liquid flow rate versus time during experiment where strong base (17.84 wt% NaOH) was used for titration.

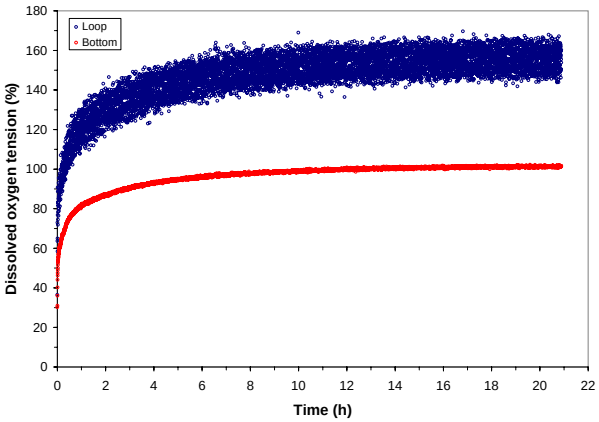

Figure 4.13. Dissolved oxygen tension relative to saturation of water with air at 38°C and 1 bar measured in the loop and the bottom of the tank versus time during experiment where strong base (17.84 wt% NaOH) was used for titration.

To model the deactivation Eq.(3.17) from the previous chapter was used

$$-\frac{d[E]}{dt} = k_d[E]r \tag{4.11}$$

The protective effect of substrate was not included since this is minor when the initial lactose concentration is 50 g L^{-1}. The equation was combined with Eq.(4.6)

$$-\frac{d[E]}{dt} = k_1 k_d [E]^2 c_l = k_1 k_d [E]^2 \frac{2k_l a c_l^*}{k_1[E] + 2k_l a} \tag{4.12}$$

This equation can be solved analytically to give $[E]$ implicitly as a function of time

$$\frac{\ln [E]_0 - \ln [E]}{2k_d k_l a c_l^*} + \frac{[E]^{-1} - [E]_0^{-1}}{k_d k_1 c_l^*} = t \tag{4.13}$$

Thus for a given set of parameters and at a given time, $[E]$ can be found from Eq.(4.13) by iteration using Newton's method, and the dissolved oxygen concentration c_l can then be calculated from

$$c_l = \frac{2k_l a c_l^*}{k_1[E] + 2k_l a} \tag{4.14}$$

When these two values are known, the volumetric rate of reaction can be calculated by the first order approximation

$$r = k_1[E]c_l \tag{4.15}$$

From a gas phase balance the molar fraction of oxygen in the outlet gas was computed, and c_l^* was assumed to be the mean value of the equilibrium value

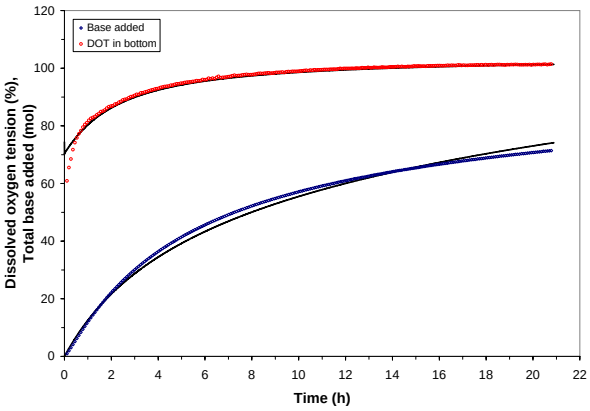

Figure 4.14. Total amount of base added as well as dissolved oxygen tension measured in bottom of tank versus time during experiment where strong base (17.84 wt% NaOH) was used for titration. Curves are simulations.

found with the inlet gas phase and the equilibrium value for the outlet gas (a reasonable approximation if the gas phase is assumed to travel in plug flow).

The parameter $k_l a$ was assumed to be equivalent to the value of 201 h^{-1} found in the experiment performed with ammonia for neutralization but at the same pressure and gas and liquid flow rates and with assumption of plug flow for the gas phase. k_1 was taken to be equivalent to 5.44 mmol L (h mg protein mmol O_2)$^{-1}$. k_d was now obtained by least squares analysis of both the dissolved tension and the total base added and found to be equivalent to 0.0229 L mmol^{-1}. Simulated curves are presented in figure 4.14 together with experimental results. There is good agreement between experimental results and simulated values. From the simulations a plot of the residual enzyme activity versus time was constructed, see figure 4.15

4.4 Discussion

In this chapter the importance of good mass transfer in the enzymatic oxidation of lactose to lactobionic acid has been demonstrated.

The results obtained in the 600 L pilot scale tank showed that the oxygen tension throughout the tank can be assumed constant, i.e. liquid mixing was sufficiently good to avoid gradients in the oxygen tension. The specific rate of reaction obtained in the 600 L system at a given oxygen tension the tank was in general somewhat higher than found in 1 L scale. This can be ascribed to the higher pressure in the recirculation loop. When ammonia was used for neutralization no deactivation was detected during the time course

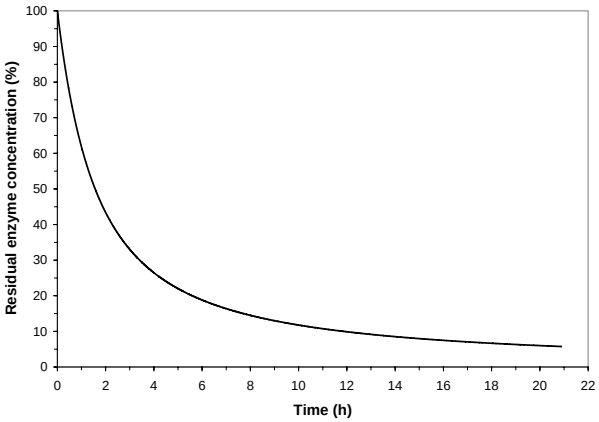

Figure 4.15. Residual enzyme concentration in % versus time obtained by simulation in experiment where strong base (17.84 wt% NaOH) was used for titration.

of a typical experiment and as in the small-scale experiments increasing the air flow rate did not lead to deactivation. This is an advantage compared to the study of the cellobiose dehydrogenase/laccase system studied by Ludwig et al. (2004) where the authors observed that an increase in the gas flow rate led to increased deactivation of both dehydrogenase and laccase.

It is of course relevant to try to make a comparison of the values of $k_l a$ obtained in the experiments presented here with values representative of stirred systems. Middleton and Smith (2004), who recently reviewed gas-liquid mixing, proposed to use the following correlation for $k_l a$ in the air-water system at 20°C

$$k_l a = 4320 \left(\frac{P}{\rho_l V} + u_g g \right)^{0.7} u_g^{0.6} \tag{4.16}$$

where $k_l a$ is in h^{-1}, P is the shaft power in W, V is in m^3, ρ_l is in kg m^{-3} and u_g is in m s^{-1} while $g = 9.81$ m s^{-2} . Note that this equation includes gas buoyancy power. Whitton and Nienow (1993) made a correction of $k_l a$-values for temperature and used that it has been proposed that $k_l a$ increases with temperature by 2.665% per °C. This would imply that $k_l a$ is 1.48 times higher at 38°C than at 20°C, and the factor 4320 is changed to 6392.

Comparison of results of this equation with results obtained in the 600 L rotary jet head system are presented in table 4.3. When evaluating Eq.(4.16) the total power input $P + u_g \rho_l g$ was set equal to the sum of the pumping work and the gas compression work (assuming isothermal compression) used in the rotary jet head system. The values obtained in this study are generally somewhat higher compared to the values calculated from Eq.(4.16) with correction for the temperature difference.

It may be speculated whether the medium composition has an impact on

Table 4.3. Comparison of $k_l a$-values obtained in the 600 L rotary jet head system with values obtained by the use of Eq.(4.16) with correction for temperature difference. The combined pumping work and gas compression work (assuming isothermal compression) was used in the comparison.

Air flow NL min^{-1}	Pressure barg	Liquid flow m^3 h^{-1}	$\frac{P}{V}$ W m^{-3}	$\frac{W_{iso}}{V}$ W m^{-3}	$k_l a$ (plug flow) h^{-1}	$k_l a$ (backmixed) h^{-1}	$k_l a$ from Eq(.4.16) h^{-1}
10	0.99	8.33	382	19	14	16	22
25	1.10	8.27	421	52	72	99	43
50	1.23	8.08	460	111	114	145	75
100	1.45	7.76	521	249	201	247	139
200	1.72	7.41	590	556	266	304	278

the coalescence properties. The phosphate buffer concentration gives rise to a ionic strength that is lower than the one leading to a decrease in the mean Sauter bubble diameter found in a bubble column (Keitel and Onken, 1982). Furthermore, the catalase concentration is lower than the one leading to an increase in $k_l a$ as found by Hickman (1988). The sugar does not give rise to coalescence, and if there was a contribution from the ammonium lactobionate in solution there should be an increase in the rate of mass transfer and consequently in the rate of reaction as ammonium lactobionate builds up. This was not the case. Thus, if there is an effect of the medium it should come from the carbohydrate oxidase solution, which is present at a concentration of 0.50 g L^{-1}. Alternatively the combined effect of the catalase, oxidase and phosphate buffer should be responsible for a change in coalescence properties.

The experiment with NaOH clearly showed that enzyme deactivation is also a problem in the rotary jet head system when strong base is used for titration and added in the loop. The constant k_d obtained in the deactivation experiment was a factor 4.55 higher than the constant k_d obtained from the 1 L scale experiments. Part of this is due to the fact that the model for deactivation in 1 L scale includes protection by substrate. However, if substrate protection had been included in the model used in this chapter it would only have resulted in a small decrease in the k_d value obtained. The larger value should primarily be found in the fact that the phosphate buffer concentration is only 6 mM and not 50 mM as used in 1 L scale, and that the NaOH is more concentrated. Furthermore, the difference in addition method also plays a role. However, on the basis of the data presented here it is not possible to assess whether addition of base in the loop of the rotary jet head system results in less or more deactivation than obtained when base is added to the surface of the 1 L stirred tank.

Chapter 5

Continuous yeast cultivation - preliminary results

5.1 Introduction

Cultivation of Baker's yeast *Saccharomyces cerevisiae* at aerobic conditions is relatively uncomplicated (although much easier in small scale than in pilot scale) and was used to test the efficiency of mass transfer of the rotary jet head system in a typical cultivation situation.

In ideally mixed glucose-limited continuous cultivation of *S. cerevisiae* two distinct patterns of carbon distribution are seen under aerobic conditions. At low dilution rate (i.e. at low specific growth rate), the growth is fully respiratory and biomass and carbon dioxide are produced as main products. When the dilution rate is increased above the dilution rate known as the critical dilution rate significant amounts of ethanol are produced and the growth situation is known as respirofermentative (Lei et al., 2003). The shift is normally referred to as the Crabtree effect and the production of ethanol is seen as an 'overflow mechanism'. It is well known that production of ethanol will occur below the critical dilution rate (or the critical specific growth rate in fed-batch systems) if glucose mixing is inadequate and significant glucose gradients occur (Hansford and Humphrey, 1966; Fowler and Dunlop, 1989; George et al., 1998). Likewise zones of oxygen depletion will lead to a decrease in biomass yield due to the overflow metabolism (Sweere et al., 1988b,a). In production of Baker's yeast or in the production of enzymes or pharmaceutical proteins where the volumetric rate of production is proportional to the volumetric rate of production of biomass a waste of glucose to ethanol is of course unwanted.

5.2 Materials and methods

5.2.1 Reactor set-up

The bioreactor set-up was essentially as the set-up reported in section 4.2.2 of the last chapter with the modification that only a single oxygen electrode was used. The tank reactor was an 800 L stainless steel tank with diameter 0.96 m. The circulation loop was made from 2 inch tubing. Medium was pumped through the loop by a lobe pump (Johnson Pump, model 3/0054) passing a tubular heat exchanger and a point for injection of air into the circulating fluid.

Glucose and salt solutions (see below), and demineralised water were added separately in the loop on the suction side of the pump to give the desired medium composition in the feed. Sterile filters were used on all liquid feeds, and both the gas inlet and the gas effluent were filtered through sterile filters. The rotary jet head, which was located in the middle of the liquid volume, was an IM15 with a nozzle diameter of 7 mm.

The pressure in the loop was measured just before the inlet to the tank by a pressure transmitter (Haenni model ED 510/324.241/A25). The liquid flow rate was measured by a Promass 60M/63M mass flow meter from Endress & Hauser. The gas flow rate was controlled by a mass flow controller (Brooks Instrument model 5853 S).

The oxygen tension in the tank was measured with a polarographic oxygen sensor (Mettler Toledo). The electrode was calibrated by saturating the medium with dry air and setting this value equal to 100%. When defined in this way, a dissolved oxygen tension of 100% corresponds to an oxygen concentration of $2.44 \cdot 10^{-4}$ mol L^{-1} (pure water, 30°C, 1 atm). The temperature was measured by a Pt100 temperature sensor and controlled at 30°C during cultivation. The pH in the reactor was measured (Mettler Toledo InPro 3030 pH electrode) and the signal was sent to a Consort R400 pH controller to regulate the rate of addition of 5 M KOH to give the desired cultivation pH of 5.0. The pH electrode, the oxygen electrode, and the temperature sensor were all located in the middle of the reactor, approximately 10 cm from the wall of the vessel.

During the cultivation, the total medium volume was 522 L of which approximately 20 L was residing in the loop.

5.2.2 Strain and cultivation conditions

The haploid, prototrophic *S. cerevisiae* strain CEN.PK113-7D was used in the cultivation.

Glucose (65 wt%) feed and a salt medium for yeast fermentation were kindly donated by Novo Nordisk A/S. To avoid problems with precipitation in the sugar feed tank the glucose medium was diluted to 50 wt% before use. The final medium, which was a modified version of the medium suggested by Verduyn et al. (1992), was obtained by scaling the addition rate of salt solution and demineralised water to the feed rate of glucose solution. Consequently, all components in the final medium were present in a fixed ratio to the glucose concentration, independent of the glucose concentration in the final feed. The concentrations measured per g glucose in the feed were: 0.39 g $(NH_4)_2SO_4$, 0.092 g KH_2PO_4, 0.13 g $MgSO_4{\cdot}7H_2O$, 0.092 mL trace metal solution, 0.092 mL vitamin solution. The trace metal solution consisted of: 15.0 g L^{-1} EDTA, 4.50 g L^{-1} $ZnSO_4{\cdot}7H_2O$, 0.84 g L^{-1} $MnCl_2{\cdot}2H_2O$, 0.30 g L^{-1} $CoCl_2{\cdot}6H_2O$, 0.30 g L^{-1} $CuSO_4{\cdot}5H_2O$, 0.40 g L^{-1} $Na_2MoO_4{\cdot}2H_2O$, 4.50 g L^{-1} $CaCl_2{\cdot}2H_2O$, 3.00 g L^{-1} $FeSO_4{\cdot}7H_2O$, 1.00 g L^{-1} H_3BO_3, 0.2 g L^{-1} KI. The vitamin solution contained: 0.05 g L^{-1} biotin, 1.00 g L^{-1} calcium pantothenate, 1.00 g L^{-1} nicotinic acid, 25.00 g L^{-1} *myo*-inositol, 1.00 g L^{-1} thiamin HCl, 1.00 g L^{-1} pyridoxine HCl, 0.20 g L^{-1} *p*-aminobenzoic acid.

Antifoam (Synperonic PE/L61 from Brenntag) was added during the cultivation to avoid excessive foaming.

5.2.3 Analytical methods

The biomass concentration was monitored spectrophotometrically by measuring the optical density at 600 nm and correlating the optical density with cell dry weight measurements. Cell dry weight measurements were performed by filtration of cultivation samples on nitrocellulose filters. The filters (pore size 0.45 μm) were weighed after drying in a microwave oven at 160 W for 10 min. The biomass from 5 mL culture was collected on a filter and washed with distilled water before being dried and weighed as stated above. For calculation of the amount of biomass in C-mol, the following biomass composition $CH_{1.60}O_{0.40}N_{0.216}S_{0.024}P_{0.017}$ with 6% ash was assumed (Nielsen et al., 2003).

To determine extracellular metabolite concentrations, samples were filtered through 0.45 μm filters. Glucose, ethanol, acetate, glycerol, succinate, and pyruvate were separated by high-pressure liquid chromatography using an Aminex HPX-87H column (Bio-Rad) at 65°C by using 5 mM H_2SO_4 at a flow rate of 0.6 mL min^{-1} as the mobile phase. Glucose, ethanol, glycerol, and succinate were measured refractometrically on an RI-71 detector from Shodex. Acetate and pyruvate were quantified on a UVD340S absorbance detector from Dionex set at 210 nm.

The concentration of CO_2 and O_2 in the off gas was analyzed by an acoustic gas analyzer from Brüel & Kjær (model 1308).

5.3 Results

The cultivation was started in batch mode using an inoculum of 3 mg biomass L^{-1}, and after a sharp decrease in CO_2 production rate at the end of the exponential growth phase the switch to continuous operation was made. The time-profile of the experiment is shown in figure 5.1. A number of different process conditions were applied as seen in table 5.1.

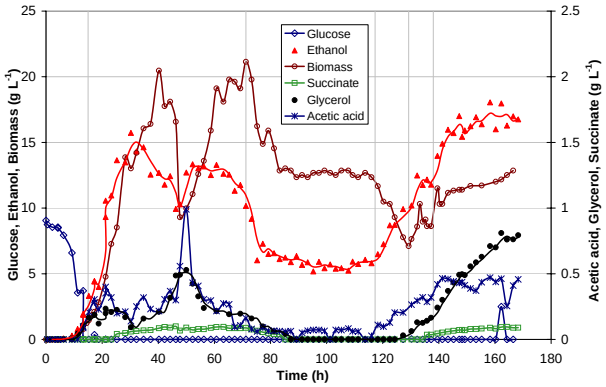

Figure 5.1. Time profile of yeast cultivation. Vertical lines indicate changes in process conditions.

Table 5.1. Operating conditions during aerobic yeast cultivation.

Time (h)	Dilution rate (h^{-1})	Glucose feed concentration (g L^{-1})	Air flow rate (NL min^{-1})	Comments
0	Batch	-	50	
15.00	0.096	70.0	50	Change to continuous operation
16.00			100	Change of air flow rate
22.25			200	Change of air flow rate
47.75				Upset of cultivation. Liquid volume decreased to 300 L (increase in dilution rate) in 10 min
62.25				Exit air filter blocked
71.75	0.192	35.0		Steady state approached
117.25	0.287	35.0		Change of dilution rate
129.25	0.239	42.5		Change of glucose feed concentration
138.00	0.144	70.0		Change of glucose feed concentration
159.25			300	Change of air flow rate
169.25				Cultivation closed down

The initial batch phase (initial biomass concentration: 3 mg cdw L^{-1}, initial glucose concentration 8.71 g L^{-1}) lasted 15 hours. At this time the biomass concentration was 1.46 g cdw L^{-1}, and the liquid phase composition (glucose, ethanol, glycerol, acetic acid) was (0.03 g L^{-1}, 3.31 g L^{-1}, 0.167 g L^{-1}, 0.209 g L^{-1}). 51.3 moles of CO_2 had been produced. The carbon balance for the batch phase closed within 0.07 C-mole per C-mole glucose. The specific

growth rate was determined to 0.36 h^{-1}, a value that fits well with the maximum specific growth rate found in many previous experiments with this yeast strain.

Continuous operation was performed with glucose feed concentrations and dilution rates varying during the experiment as seen in table 5.1. The upset of the process after 47.75 hours was caused by a fault in the liquid level controller that led to a decrease of medium volume to about 300 L, but after correction of the level control a steady state was obtained between 85 and 112 hours using a glucose feed concentration of 35 g L^{-1} and a dilution rate of D = 0.191 h^{-1}. The biomass concentration was 12.73 ± 0.04 g L^{-1} and the ethanol concentration 5.47 ± 0.20 g L^{-1} with minute amounts of glycerol and acetic acid. The glucose concentration was 18.5 mg L^{-1}. Consequently, the metabolism was not fully respiratory.

At this steady state, the circulation flow rate was 6.7 m^3 h^{-1} corresponding to a recirculation rate of 13.4 tank volumes per hour. The pressure in the loop was 1.8 bar gauge. The inlet air flow rate was 12.0 Nm^3 h^{-1} with 20.95 % O_2 content, and the exit gas contained 8.72 % CO_2 and 13.4 % O_2. From a gas phase balance on the inert nitrogen, the outlet gas flow rate is calculated to 12.2 Nm^3 h^{-1}. From this the oxygen consumption rate is calculated to 39.4 mol h^{-1}. The oxygen tension in the medium was 24 % of the value for saturation with air in the gas phase. The carbon balance closed to within 0.04 C-mole per C-mole glucose.

In the last 50 hours of the experiment various combinations of glucose feed concentration and dilution rate were applied without achieving a steady state. It is the steady state obtained between 85 and 112 hours that will be analyzed further.

Based on the measured oxygen uptake rate, the oxygen tension, and the gas phase O_2 content a value of $k_l a$ can be calculated by the direct method by

$$k_l a = \frac{OTR}{c_l^* - c_l} \tag{5.1}$$

In this process where the oxygen content in the gas outlet is considerably smaller than the content in the inlet, the value is very sensitive to the choice of model for gas phase mixing.

If the gas phase is assumed to be fully backmixed c_l^* is the saturation concentration of oxygen in the medium when it is assumed to be in equilibrium with the outlet gas phase. When the gas phase is assumed to travel in plug flow, the driving force should be a logarithmic mean. When a fully backmixed gas phase is assumed the $k_l a$-value is calculated to 774 h^{-1}, while the plug flow model gives a value of 552 h^{-1}.

5.4 Discussion

It has been shown that cultivation of yeast can be safely done for about 170 hours without any risk of infection by circulation of the medium through an exterior pump (a common worry in the fermentation industry).

The formation of ethanol in continuous aerobic culture in an ideal bioreactor with the strain used in this study sets in at a dilution rate of 0.31 h^{-1} (Lei et al., 2003), which is above the dilution rate of 0.191 h^{-1} investigated in this study. The formation of ethanol observed could in principle be caused by either local zones with oxygen depletion or by glucose gradients. The oxygen tension monitored inside the tank was 24 % of the saturation value. In the lactobionic acid experiments in the same set-up gradients in dissolved oxygen tension could not be detected in the tank, and the oxygen concentration in the loop - monitored before the air addition point - was higher than or equal to the concentration in the tank. Even though we cannot be certain that these observations hold in general, it is hard to believe that there should be zones with oxygen depletion. It is more likely that the formation of ethanol is triggered by high local concentrations of glucose in the recirculation loop. The glucose was fed as a 50 wt% solution on the suction side of the pump, and the residence time in the loop was around 10 s. This feeding method is probably what causes the respirofermentative metabolism observed. Feed should ideally by added by a separate pipe inserted directly into the mixer whereby it will enter the zone of maximum turbulent kinetic energy dissipation in less than 1 s.

The value of $k_l a$ obtained during the steady state of the cultivation was between 552 h^{-1} and 774 h^{-1} depending on the model for gas phase mixing. This is between 5.52 and 7.74 times higher than the value of $k_l a = 100$ h^{-1} determined by the hydrogen peroxide method in the same equipment (data not shown) at the same values of the gas flow rate and the liquid flow rate but with water instead of cultivation medium and at 25°C. The cultivation medium does of course contain salts which will decrease the coalescence. Furthermore, ethanol is known to enhance mass transfer even at low concentrations. Zlokarnik (1978) found an increase in $k_l a$ of a factor of 4 compared to in water at an ethanol concentration of 3 g L^{-1}, while the factor was 6.5 at 32 g L^{-1}. On the contrary addition of antifoam is known to lead to a decrease in $k_l a$. Considering these effects the enhancement in $k_l a$ is still surprisingly strong compared to what was obtained with the hydrogen peroxide method in water.

Chapter 6

Summary

The primary topic of this Ph.D. study has been mixing and mass transfer in a new tank reactor system based on rotating liquid jets for mixing and mass transfer. In this system liquid is drawn from the bottom of a tank, circulated by a pump, and reinjected into the bulk liquid through the nozzles of a rotary jet head located below the liquid surface. Liquid feed can be added either to the liquid surface or in the recirculation loop. Gas is added in the loop on the pressure side of the pump. Heat exchange can be performed by a heat exchanger located in the loop, and thus plate-type exchanger with high overall heat transfer coefficient can be used. Baffles and other internals such as heating coils are not present in the tank which just becomes a shell for containment of the liquid.

Experiments in a tank with liquid volume 3.4 m^3 and a diameter of 1.256 m showed that the mixing capability of the system is very dependent on the feed injection point. Thus a much lower mixing time was obtained when tracer was added in the loop compared to when tracer was added to the liquid surface. The mixing time functionality was different from what is observed for stationary jets, at least when tracer was added to the liquid surface. Thus the mixing time was only a function of the volumetric liquid flow rate for the nozzle diameters investigated.

Volumetric mass transfer coefficients were obtained in the air/water system by the hydrogen peroxide steady state technique in the 3.4 m^3 tank reactor using one or two rotary jet heads. Surprisingly, the volumetric mass transfer coefficient could be correlated in terms of the superficial gas velocity and the volumetric liquid flow rate rather than by the superficial gas velocity and the power input. The values obtained were lower than what is obtained in mechanically stirred systems.

Enzymatic oxidation of lactose to lactobionic acid by a carbohydrate oxidase from *Microdochium nivale* performed at a constant pH of 6.4 was investigated

both in laboratory-scale and in pilot-scale equipment.

Experiments in a 1 L stirred bioreactor showed that the operational stability of the enzyme was very dependent on the pH of the base used for neutralization and of the buffer strength of the medium. Thus when 2 M NaOH was used for neutralization in a medium containing 50 mM phosphate buffer significant deactivation was obtained, while deactivation could be avoided by using NH_3 or CO_3^{2-} for neutralization at the same buffer strength. Furthermore, it was found that the deactivation rate was dependent on the lactose concentration when 2 M NaOH was used for neutralization. The deactivation rate was lower at high lactose concentration. To the best of the author's knowledge this has not been reported before for an oxidase. A simple kinetic model was set up to explain the results obtained.

In pilot-scale (rotary jet head system with 600 L liquid volume) deactivation of the enzyme was also avoided when NH_3 was used for titration of the lactobionic acid formed (with 6 mM phosphate buffer). Experiments were performed both with pure lactose and with whey permeate as substrate. Relatively high volumetric mass transfer coefficients were obtained at low superficial gas velocity and specific power input when pure lactose solution was used as medium. With whey permeate foaming occurred and the volumetric mass transfer coefficient was lower due to the addition of antifoam.

Continuous aerobic cultivation of *S. cerevisiae* in 500 L scale was investigated in the rotary jet head system. Even though the dilution rate was below the critical dilution rate of the organism and the oxygen tension was 24% of the saturation value, a significant amount of ethanol was produced. It is speculated that this was caused by high local concentrations of glucose in the recirculation loop where the feed was added. Moving the feed point close to the rotary jet head would probably reduce the problem significantly.

Chapter 7

Suggestions for future work

7.1 Mixing and mass transfer characterization of the rotary jet head system

Due to the differences in functionality of mixing time results obtained with the rotary jet head system compared to stationary jets it is desirable to measure mixing times in tanks of different scales in an improved set-up

1. With several probes placed at different positions in the tank.
2. Using an analysis approach similar to that suggested by e.g. Brown et al. (2004), see section 1.1.1.
3. With tracer addition to the loop as close to the rotary jet head as possible and in as short a time period as possible. Furthermore tracer addition to the liquid surface should still be investigated.

To meet this end two tanks (the tank investigated so far and a tank of inner diameter 2.86 m and with aspect ratio 1) have been modified to allow measurements at three different locations in the tank. Furthermore, high capacity positive displacement pumps have been installed, allowing a tracer pulse to be dispensed in around 1 s. Unfortunately, the results obtained with this new set-up in the last phases of this project turned out to be flawed due to a problem in the data logging system giving rise to signals that interfered with one another. The problem has now been resolved and results will be obtained as soon as possible. Experiments will be performed in both tanks with adjustment of the liquid height to give an aspect ratio of 1 in both tanks. Furthermore, experiments will be performed in the small tank with a liquid volume of 3.4 m^3 as investigated in this study.

Also, it would be interesting to perform a systematic study with both pH probes and conductivity electrodes to investigate whether there is a difference in the results obtained due to e.g. the response time of the pH electrode.

The values of $k_l a$ obtained with the hydrogen peroxide method were low compared to the values obtained in the two applications (Enzymatic oxidation of lactose to lactobionic acid and aerobic continuous cultivation of *Saccharomyces cerevisiae*) even when the difference in medium composition is considered. The reason *could* be the following.

In the enzymatic oxidation experiments performed in 600 L scale it was found that the dissolved oxygen tension was the same at two different positions in the tank. Furthermore, it was found that the specific rate of reaction for a given dissolved oxygen tension measured in the tank was higher in the rotary jet head system than in a 1 L stirred tank reactor which was explained by the higher pressure in the loop. The increase was in most cases less than 10% and it should therefore be possible to estimate a $k_l a$ value for the system from the overall volumetric oxygen transfer rate of the system and the driving force using the dissolved oxygen tension measured in the tank, also with the hydrogen peroxide method. There is, however, one big difference between the hydrogen peroxide method and the applications investigated. In both the enzymatic oxidation experiments and in the cultivation experiment the transfer of oxygen occurs from the gas phase to the liquid both in the tank and in the loop. With the hydrogen peroxide method the net transfer occurs from liquid phase to gas phase in the tank at atmospheric pressure. However, in the loop the net transfer may very well be in the opposite direction due to the higher pressure in the loop. Thus when the jets emerge from the nozzles, oxygen that was just transferred from the gas phase to the liquid will now be transferred from liquid to gas. If this effect is significant it may lead to a considerable underestimation of $k_l a$ when the hydrogen peroxide method is used as recommended in the literature, i.e. with air.

Mass transfer experiments should be performed with the hydrogen peroxide method with both air and with pure nitrogen. If the use of nitrogen gives rise to a higher $k_l a$ value than with air it can safely be concluded that the hydrogen peroxide method underestimates $k_l a$ in the rotary jet head system when air is used.

7.2 Kinetics of enzymatic oxidation of lactose to lactobionic acid

In relation to the kinetics of the *Microdochium nivale* carbohydrate oxidase, it would be tempting to investigate the effect of hydrogen peroxide on the enzyme in further details. It is of course desirable to separate the effect

of inhibition from that of deactivation. Experiments should be done where different amounts of hydrogen peroxide are added to a mixture of lactose and oxidase, which is kept at a constant oxygen concentration. Thus from the decrease in the rate it should be possible to obtain the kinetic constant which characterizes the inhibition (which is known to be competitive in the case of glucose oxidase). The effect of hydrogen peroxide on deactivation can be studied by incubating the enzyme with different concentrations of hydrogen peroxide before measuring the residual activity after removal of hydrogen peroxide. Since the reduced form of glucose oxidase is known to be much more sensitive towards hydrogen peroxide than the oxidized form (Kleppe, 1966), it is advised to investigate deactivation of both forms.

To completely optimize the enzymatic oxidation process it would be desirable to obtain the deactivation kinetics for the catalase used. Catalase is known to be deactivated by its substrate H_2O_2, and the catalase activity will diminish during the oxidation process. If the kinetic parameters for inhibition and deactivation of the oxidase are known together with the deactivation kinetics for catalase, it should in principle be possible to model the time course of any reaction with oxidase and catalase, and the model can be used to minimize the amount of catalase used.

Furthermore, to optimize pH and temperature an experimental design could be performed which determines the effect of temperature and pH on the kinetic parameters for the oxidase. I suggest that the reaction rate of the oxidase is followed over, say 24 h in each experiment. Experiments of this kind would give results concerning the stability of the enzyme at operating conditions, and they would be much more useful than traditional incubation experiments.

Finally it would be interesting to investigate the effect of mixing when using NaOH for neutralization in further detail. Is there e.g. an effect of adding the base close to the impellers instead of dispensing it to the liquid surface (as pointed out by Langheinrich and Nienow (1999) for pH adjustment of animal cell culture in a tank reactor stirred at low impeller speed) and can gradients in pH be visualized by adding a suitable pH indicator to the bioreactor?

7.3 Scale-up of enzymatic oxidation process

It is known that high local turbulent kinetic energy rates are found in jets. Baldyga et al. (1994) studied a jet nozzle with diameter 8 mm in a 0.03 m^3 tank. Silicone oil was injected in a flow of water and allowed to circulate for 1 h. The maximum droplet size should reflect the maximum turbulent kinetic energy dissipation rate experienced in the flowing dispersion. At a linear jet velocity of 10 m s^{-1} the maximum kinetic energy dissipation rate

was estimated to 13.5 kW kg^{-1} while it was 42 kW kg^{-1} at a velocity of 16 m s^{-1}. These local turbulent kinetic energy dissipation rates are much higher than what is obtained in e.g. a tank stirred by a Rushton turbine (Baldyga et al., 1994).

If base could be fed close to the nozzles in the rotary jet head system and thereby rapidly enter the zone of maximum kinetic turbulent energy dissipation it may be that deactivation of the enzyme could be avoided even when strong base is used for titration.

7.4 Microbial cultivations

Likewise it would be interesting to investigate whether the respirofermentative metabolism observed in the cultivation of *Saccharomyces cerevisiae* can be avoided by adding substrate close to the nozzles of the rotary jet head.

The impact of fluid mechanical stress on the cells would be an interesting topic to investigate given that the local turbulent kinetic energy dissipation rate is known to be high in a jet. In a yeast cultivation in batch mode performed in the rotary jet head system at DTU cell samples were taken and stained with methylene blue to assess cell viability (data not shown). The percentage of dead cells found with this method during the exponential phase on glucose was measured to be less than 1%. It would, however, be interesting to investigate the effect by flow cytometry as has been done by Boswell et al. (2003) for a stirred laboratory reactor.

The large local dissipation of turbulent kinetic energy experienced in a jet also opens up two other fields which could be interesting from both a scientific and an industrial point of view: one is the production of e.g. oil in water emulsions, and the other is whether the rotary jet head system can be used with advantage in reaction systems where micromixing is of importance.

Chapter 8

Dansk resume

I det foreliggende ph.d.-projekt er blanding og ilttransport i et nyudviklet tankreaktorsystem, der baserer sig på roterende væskejets, blevet undersøgt. I systemet cirkuleres væske fra en tank og genindsprøjtes i tanken gennem dyserne på et roterende jethoved (RJH), der er placeret under væskeoverfladen. Væskeføde kan tilsættes til væskeoverfladen eller direkte i cirkulationssløjfen, mens gas tilsættes i sløjfen på tryksiden af pumpen. Varmeoverførsel kan med fordel ske i cirkulationssløjfen, og pladevarmevekslere med højt varmegennemgangstal kan benyttes.

Blandingstider blev bestemt vha en pulsreponsteknik i en tank med 3,4 m^3 væskevolumen og en indre diameter på 1,256 m, mens volumetriske stofovergangstal i samme system blev fundet vha hydrogenperoksidmetoden.

En række anvendelser af systemet er blevet undersøgt. Enzymatisk oksidation af laktose til laktobionsyre vha en kulhydratoksidase fra *Microdochium nivale* blev undersøgt i såvel laboratorieskala i en mekanisk omrørt reaktor samt i en RJH-reaktor med 600 L væskevolumen. Endelig er kontinuert aerob gæring med *Saccharomyces cerevisiae* blevet undersøgt i RJH-systemet i 500 L skala.

Part I

Appendix

Appendix A

Outline of some industrial applications of rotary jet heads

This appendix is included in the thesis to give the interested reader an idea about some of the applications where the rotary jet head system has already found use.

Most of the rotary jet heads installed so far are used in installations for blending of miscible liquids. The largest customer segment for ISO-MIX A/S until now is undoubtedly the beer and beverage industry and other food industries producing liquid food products. A typical installation will be one in which the customer wants to mix liquid ingredients such as an aroma solution or concentrated sugar syrup into a bulk liquid.

In this appendix two other applications that I developed during my Ph.D. study will be highlighted: deoxygenation of liquid products and dispersion and dissolution of solid material.

The data presented have been obtained in industrial equipment at the customer's site and some of the variables that would undoubtedly have been measured in scientific work have not been measured in these applications. Thus the appendix is only included to convey a general picture to the reader.

A.1 Deoxygenation of water

In 'high-gravity brewing', a high alcohol containing beer is produced by fermentation. This brew is diluted by addition of water to the final strength. The water must be virtually oxygen free to preserve the quality of the beer ($<$ about 100 ppb O_2). The water also has to be carbonated to give a final CO_2 pressure of around 1.8 bar absolute pressure in the bottled beer.

The rotary jet head system has been tested for deoxygenation of water at the Tuborg brewery in Fredericia, Denmark. Using the rotary jet head system the water is treated with CO_2 that is injected into the circulation loop. In this way stripping of O_2 is facilitated, and deoxygenation is combined with carbonation into one process.

A.1.1 Materials and methods

From the bottom of a pressureless tank, diameter 3.23 m and containing 20 m^3 water at 12°C, 22 m^3 h^{-1} water was withdrawn and circulated through a loop at 4.5 bar gauge pressure to an IM20 rotary jet head (nozzle diameter = 10 mm). CO_2 (99.97 % pure supplied from cylinders) was injected into the circulating water on the pressure side of the pump. The CO_2 and the O_2 content in the water was monitored with instruments from Orbisphere during the experiment, and the mass of CO_2 injected into the reactor was monitored by weighing the cylinders.

A.1.2 Results

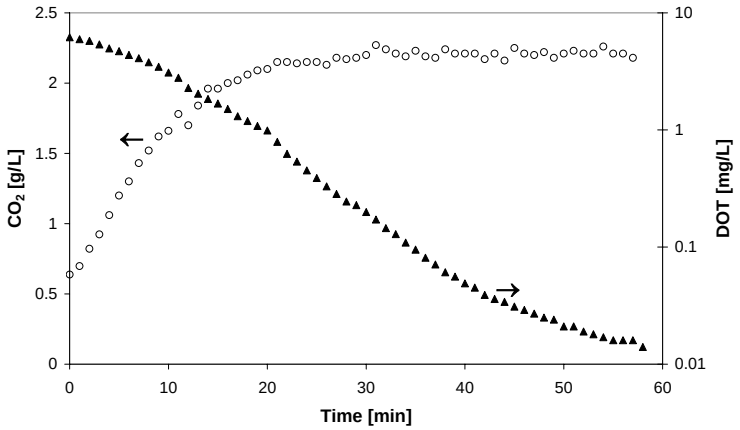

Figure A.1. Concentration of CO_2 and O_2 during deoxygenation experiment.

Figure A.1 shows the concentrations in the water of CO_2 and of O_2 during an experiment of duration about 60 minutes.

During the first 21 minutes 48 kg CO_2 was injected into the tank, and the CO_2 concentration increased from 0.57 to 2.2 g L^{-1} (corresponding to the equilibrium concentration). This means that 68 % of the CO_2 fed in this period was used to carbonate the water. The O_2 tension was reduced from 6.2 to 0.8 mg L^{-1}.

During the remainder of the experiment the CO_2 concentration in the water stayed at 2.2 g L^{-1}, and 80 kg CO_2 was used to strip the water of O_2 from about 0.8 mg L^{-1}, first in an exponential process to about 0.05 mg L^{-1} at 40 min, and finally with a decreasing rate constant to 0.014 mg L^{-1} (14 ppb) at 59 min. From the slope of the exponentially decreasing part of the time profile (21 to 40 min) one determines a volumetric mass transfer coefficient $k_l a = 9$ h^{-1}.

A.1.3 Discussion

The most obvious flaw of the procedure described above is that all the CO_2 that is fed to the tank after the carbonation has finished is unnecessarily wasted. This could be avoided if an ejector located in the recirculation loop is used to draw part of the off gas content back into the recirculation loop. This option does, however, complicate the system.

The investment cost of the rotary jet head system is small, especially if the tanks are already installed. For a small brewery, which is considering high-gravity brewing, installation of a rotary jet head system for production of deoxygenated water may be the optimal choice, even with the simple system. This kind of system has already been installed at a small Belgium brewery producing trappist ale. The ale served for the monks is a diluted version of the ale otherwise produced. The brewery has installed a rotary jet head in an existing tank and are now able to produce the ale with increased shelf life. The rotary jet head configuration can also be used to deoxygenate a batch of beer containing too high an oxygen concentration. This cannot be done with counter-current absorption or with flashing of oxygen under vacuum, the two methods most often used in the big breweries for deoxygenation of water.

The deoxygenation technology has also been applied to deoxygenate different oil products with nitrogen (data not shown): cold pressed olive oil, linseed oil, rape seed oil and fish oil. Oxygen is unwanted in these products since the presence of oxygen will result in production of oxidation products and rancidity. By manufacturing a product containing a low oxygen content the oxidation process is delayed and the amount of antioxidant used in some of these products can be minimized. The oxidation process is especially a problem in oils high in omega-3 fatty acids such as fish oil or linseed oil.

A.2 Dissolution of salt in syrup

The sugar-producing company Danisco A/S was interested in investigating whether the rotary jet head system can be used to dissolve NaCl in a sugar

syrup. Currently this is performed by a small down-pumping impeller in an unbaffled tank, see figure A.2, and the process of dissolving 25 kg NaCl in 10 tons of syrup takes several hours and even then all the salt has not been dissolved (the operator terminates the process when the desired salt concentration in the syrup has been reached).

Figure A.2. The inside of the tank used for dissolving NaCl in sugar syrup. Both the impeller and the IM20 rotary jet head are seen.

A.2.1 Materials and methods

Two different tanks were studied.

In the first experiment performed a cylindrical tank with conical bottom was used. The tank has an inner diameter of 3.00 m, and the rotary jet head (IM20 with 10.0 mm nozzles) was placed 30 cm above the tank outlet, see figure A.2.

10 tons of syrup was added to the tank. The syrup contained 77.4 wt% partly inverted sucrose. The temperature of the syrup was approximately 60°C. 25 kg of NaCl was added from the top of the tank. The liquid flow rate was 19.6 m^3 h^{-1}.

The second experiment was performed in a pallet tank containing 1.0 tons of syrup with a sugar content of approximately 73%, see figure A.3. The temperature was approximately 60°C. An IM10 rotary jet head with 5.5 mm nozzles was used. The flow rate of liquid was not measured.

A funnel was installed in the recirculation loop on the suction side of the pump. A butterfly valve was inserted in the loop before the funnel, and another butterfly valve was installed between the funnel and the recirculation loop. By adequate manipulation of these valves a small vacuum could be established in the recirculation line on the suction side of the pump allowing salt to be sucked into the loop. 2.5 kg of NaCl was added this way.

Samples were taken during both processes, and the conductivity was measured after appropriate dilution.

Figure A.3. Pallet tank used for dissolution of salt in syrup in the second experiment. The funnel is installed on the suction side of the pump and used to draw salt into the circulating syrup.

A.2.2 Results

The first experiment was conducted in a tank with 10 tons of syrup, and 25 kg of NaCl was added from the top of the tank. The conductivity of the syrup kept increasing even after 2 hours of syrup circulation. The tank was emptied, and it was observed that a substantial amount of salt was sticking to the bottom of the tank from which it was only slowly being dissolved, see figure A.4.

Figure A.4. Salt sticking to tank bottom. Left hand picture was shot from the top of the tank, while the right hand picture was taken through a man hole.

We hypothesized that the addition method could probably be improved. It would be desirable to add the salt in the recirculation line. To test this hypothesis experiments were performed in a pallet tank containing 1 tons of syrup, and 2.5 kg NaCl was sucked into the recirculation loop on the suction side of the pump. The first sample was taken 1 minute after all salt had been added. Conductivity measurements showed that all salt had been dissolved at this time point.

A.2.3 Discussion

Even though the two experiments were performed in different scales and with slightly different syrups, it is probably safe to state that the addition method where salt is added in the recirculation line is superior to the method where salt is added to the top of a tank.

The method where a funnel is used for addition of solid materials to the loop has also been used with succes for some polymers typically used in the food industry, e.g. CMC (data not shown).

Bibliography

Agusti, R., París, G., Ratier, L., Frasch, A. C. C. and de Lederkremer, R. M. (2004). Lactose derivatives are inhibitors of *Trypanosoma cruzi* trans-sialidase activity toward conventional substrates *in vitro* and *in vivo*, *Glycobiology* **14**: 659–670.

Ahmad, S. K., Brinch, D. S., Friis, E. P. and Pedersen, P. B. (2004). Toxicological studies on lactose oxidase from *Microdochium nivale* expressed in *Fusarium venenatum*, *Regul. Toxicol. Pharm.* **39**: 256–270.

Aiba, S. and Huang, S. Y. (1969). Oxygen permeability and diffusivity in polymer membranes immersed in liquids, *Chem. Eng. Sci.* **24**: 1149–1159.

Amanullah, A., McFarlane, C. M., Emery, A. N. and Nienow, A. W. (2001). Scale-down model to simulate spatial pH variations in large-scale bioreactors, *Biotechnol. Bioeng.* **73**: 390–399.

Arjunwadkar, S. J., Sarvanan, K., Kulkarni, P. R. and Pandit, A. B. (1998). Gas-liquid mass transfer in dual impeller bioreactor, *Biochem. Eng. J.* **1**: 99–106.

Baldyga, J., Bourne, J. R. and Zimmermann, B. (1994). Investigation of mixing in jet reactors using fast, competitive-consecutive reactions, *Chem. Eng. Sci.* **49**: 1937–1946.

Baminger, U., Ludwig, R., Galhaup, C., Leitner, C., Kulbe, K. D. and Haltrich, D. (2001). Continuous enzymatic regeneration of redox mediators used in biotransformation reactions employing flavoproteins, *J. Mol. Catal. B* **11**: 541–550.

Bandyopadhyay, B. and Humphrey, A. E. (1967). Dynamic measurement of the volumteric oxygen transfer coefficient in fermentation systems, *Biotechnol. Bioeng.* **9**: 533–544.

Bao, J., Furumoto, K., Yoshimoto, M., Fukunaga, K. and Nakao, K. (2003). Competitive inhibition by hydrogen peroxide produced in glucose oxidation catalyzed by glucose oxidase, *Biochem. Eng. J.* **13**: 69–72.

Bean, R. C. and Hassid, W. Z. (1956). Carbohydrate oxidase from a red alga, *Iridophycus flaccidum*, *J. Biol. Chem* **218**: 425–436.

Bentley, R. and Slechta, L. (1960). Oxidation of mono- and disaccharides to aldonic acids by *Pseudomonas* species, *J. Bacteriol.* **79**: 346–355.

Booij, C. J. (1985). Use of lactose in the pharmaceutical and chemical industry, *J. Soc. Dairy Technol.* **38**: 105–109.

Boswell, C. D., Nienow, A. W., Gill, N. K., Kocharunchitt, S. and Hewitt, C. J. (2003). The impact of fluid mechanical stress on *Saccharomyces cerevisiae* cells during continuous cultivation in an agitated, aerated bioreactor; its implication for mixing in the brewing process and aerobic fermentations, *Food Bioprod. Process.* **81**: 23–32.

Brown, D. A. R., Jones, P. N. and Middleton, J. C. (2004). Experimental methods, Part A: Measuring tools and techniques for mixing and flow visualization studies, *in* E. L. Paul, V. A. Atiemo-Obeng and S. M. Kresta (eds), *Handbook of Industrial Mixing*, Wiley-Interscience, pp. 145–202.

Bylund, F., Collet, E., Enfors, S.-O. and Larsson, G. (1998). Substrate gradient formation in the large-scale bioreactor lowers cell yield and increases by-product formation, *Bioproc. Eng.* **18**: 171–180.

Bylund, F., Guillard, F., Enfors, S.-O., Trägårdh, C. and Larsson, G. (1999). Scale down of recombinant protein production: a comparative study of scaling performance, *Bioproc. Eng.* **20**: 377–389.

Charloux, C., Paul, M., Loisance, D. and Astier, A. (1995). Inhibition of hydroxyl radical production by lactobionate, adenine and tempol, *Free Radical Bio. Med.* **19**: 699–704.

Code of federal regulations (2004). Title 21 - Food and drugs. Volume 3. Chapter I - Food and drug administration, Department of health and human services. Subchapter B - Food for human consumption. §172.720 Calcium lactobionate.

Cooke, M., Dawson, M. K., Nienow, A. W., Moody, G. W. and Whitton, M. J. (1991). Mass transfer in aerated agitated vessels: Assessment of the NEL/Hickman steady state method, *Proc. 7th Eur. Conf. Mixing*, pp. 409–418.

Cooke, M., Heggs, P. J., Eaglesham, A. and Housley, D. (2004). Spinning cones as pumps, degassers and level controllers in mechanically stirred tanks, *Chem. Eng. Res. Des.* **82**: 719–729.

Cooke, M., Middleton, J. C. and Bush, J. R. (1988). Mixing and mass transfer in filamentous fermentations, *Proc. 2nd Int. Conf. on Bioreactor Fluid Dynamics*, pp. 37–64.

Cort, W. M., Connors, W. M., Roberts, H. R. and Bucek, W. (1956). Evidence for the formation and utilization of lactobionic acid by *Penicillium chrysogenum*, *Arch. Biochem. Biophys.* **63**: 477–478.

Cronin, D. G., Nienow, A. W. and Moody, G. W. (1994). An experimental study of mixing in a proto-fermenter agitated by dual Rushton turbines, *Food Bioprod. Process.* **72**: 35–40.

Dang, N. D. P., Karrer, D. A. and Dunn, I. J. (1977). Oxygen transfer coefficients by dynamic model moment analysis, *Biotechnol. Bioeng.* **19**: 853–865.

de Wit, G., de Vlieger, J. J., van Dalen, A. C. K., Heus, R., Laroy, R., van Hengstum, A. J., Kieboom, A. P. G. and van Bekkum, H. (1981). Catalytic dehydrogenation of reducing sugars in alkaline solution, *Carbohydr. Res.* **91**: 125–138.

Delaplace, G., Bouvier, L., Moreau, A., Guérin, R. and Leuliet, J.-C. (2004). Determination of mixing time by colourimetric diagnosis - application to a new mixing system, *Exp. Fluids* **36**: 437–443.

Denis, A., Thibault, J. and Leduy, A. (1990). On the methods for the determination of the oxygen-transfer coefficient in mechanically agitated vessels, *Chem. Eng Commun.* **94**: 35–51.

Dominguez, J., Abreu, A. M., McCalla, R., Borroto, J., Ortueta, M. and Perez, E. (1999). Mixing characterization in batch reactors using the radiotracer technique, *J. Radional. Nucl. Ch.* **241**: 337–340.

Druliolle, H., Kokoh, K. B. and Beden, B. (1995). Selective oxidation of lactose to lactobionic acid on lead-adatoms modified platinum electrodes in Na_2CO_3 + $NaHCO_3$ buffered medium, *J. Electroanal. Chem.* **385**: 77–83.

Dunn, I. J. and Einsele, A. (1975). Oxygen-transfer coefficients by dynamic method, *J. Appl. Chem. Biotechnol.* **25**: 707–720.

Dutta, S. K. and Basu, S. K. (1979). Erythromycin aldobionates, US Patent 4,137,397.

Eddy, B. P. (1958). Bacterial oxidation of lactose and melibiose, *Nature* **181**: 904–905.

Edison, B. L., Green, B. A., Wildnauer, R. H. and Sigler, M. L. (2004). A polyhydroxy acid skin care regimen provides antiaging effects comparable to an α-hydroxyacid regimen, *Cutis* **73**: 14–17 Suppl. S.

Einsele, A., Ristroph, D. L. and Humphrey, A. E. (1978). Mixing times and glucose uptake measured with a fluorometer, *Biotechnol. Bioeng.* **20**: 1487–1492.

Enfors, S.-O., Jahic, M., Rozkov, A., Xu, B., Hecker, M., Jürgen, B., Krüger, E., Schweder, T., Hamer, G., O'Beirne, D., Noisommit-Rizzi, N., Reuss, M., Boone, L., Hewitt, C., McFarlane, C., Nienow, A., Kovacs, T., Trägårdh, C., Fuchs, L., Revstedt, J., Friberg, P. C., Hjertager, B., Blomsten, G., Skogman, H., Hjort, S., Hoeks, F., Lin, H.-Y., Neubauer, P., van der Lans, R., Luyben, K., Vrabel, P. and Manelius, Å. (2001). Physiological responses to mixing in large scale bioreactors, *J. Biotechnol.* **85**: 175–185.

Fischer, E. and Meyer, J. (1889). Oxydation des Milchzuckers, *Ber. Deut. Chem. Ges.* **23**: 361–364.

Fossett, H. (1951). The action of free jets in the mixing of fluids, *Trans. Inst. Chem. Eng.* **29**: 322–332.

Fossett, H. and Prosser, L. E. (1949). The application of free jets to the mixing of fluids in bulk, *Proc. Inst. Mech. Eng.* **160**: 224–232.

Fowler, J. D. and Dunlop, E. H. (1989). Effects of reactant heterogeneity and mixing on catabolite repression in cultures of *Saccharomyces cerevisiae*, *Biotechnol. Bioeng.* **33**: 1039–1046.

Fox, E. A. and Gex, V. E. (1956). Single-phase blending of liquids, *AIChE J.* **2**: 539–544.

Fuertes, P. M. and Fleche, G. M. (1991). Process for the oxidation of di-, tri-, oligo-, and polysaccharides into polyhydroxycarboxylic acids, catalyst used and products thus obtained, US Patent 4,985,553.

George, S., Larsson, G., Olsson, K. and Enfors, S.-O. (1998). Comparison of the Baker's yeast process performance in laboratory and production scale, *Bioproc. Eng.* **18**: 135–142.

Gerling, K.-G. (1998). Large-scale production of lactobionic acid - use and new applications, *Int. Dairy Fed.* **9804**: 251–261.

Gerling, K.-G., Joisten, S., Wendler, K. and Schreer, C. (1996). Lactobionic acid amide compositions and their use, US Patent 5,525,333.

Gerling, K.-G., Rau, H., Wendler, K., Schwarz, P. and Uhlig, K. (1998a). Corrosion preventing composition comprising lactobionic acid amides, US Patent 5,756,003.

Gerling, K.-G., Rau, H., Wendler, K. and Uhlig, K. (1998b). Process for treating metals using anti-corrosion agents and corrosion inhibitors containing lactobionic acid amides, US Patent 5,795,851.

Gerling, K.-G. and Wilke, D. (1991). Washing or detergent composition containing lactobionic acid or lactobionic acid salts, US Patent 5,069,808.

Ghadermarzi, M. and Moosavi-Movahedi, A. A. (1996). Determination of the kinetic parameters for the 'suicide substrate' inactivation of bovine liver catalase by hydrogen peroxide, *J. Enz. Inhib.* **10**: 167–175.

Gogate, P. R., Beenackers, A. A. C. M. and Pandit, A. B. (2000). Multiple-impeller systems with a special emphasis on bioreactors: a critical review, *Biochem. Eng. J.* **6**: 109–144.

Gogate, P. R. and Pandit, A. B. (1999). Survey of measurement techniques for gas-liquid mass transfer coefficient in bioreactors, *Biochem. Eng. J.* **4**: 7–15.

Goldstein, J. D. and Thatcher, D. R. (1990). Stabilized formulations of gamma interferons, US Patent 4,895,716.

Green, B. A., Wildnauer, R. H. and Edison, B. L. (2001). Lactobionic acid - a novel polyhydroxy bionic acid for skincare, http://www.neostrata.com/a_cse/cse_cs_04.asp.

Grenville, R. K. and Nienow, A. W. (2004). Blending of miscible liquids, *in* E. L. Paul, V. A. Atiemo-Obeng and S. M. Kresta (eds), *Handbook of Industrial Mixing*, Wiley-Interscience, pp. 507–542.

Grenville, R. K. and Tilton, J. N. (1996). A new theory improves the correlation of blend time data from turbulent jet mixed vessels, *Chem. Eng. Res. Des.* **74**: 390–396.

Groen, B. W., de Wries, S. and Duine, J. A. (1997). Characterization of the hexose oxidase from the red seaweed *Chondrus crispus*, *Eur. J. Biochem.* **244**: 858–861.

Hansford, G. S. and Humphrey, A. E. (1966). The effect of equipment scale and degree of mixing on continuous fermentation yield at low dilution rates, *Biotechnol. Bioeng.* **8**: 85–96.

Hari-Prajitno, D., Mishra, V. P., Takenaka, K., Bujalski, W., Nienow, A. W. and McKemmie, J. (1998). Gas-liquid mixing studies with multiple up- or down-pumping hydrofoil impellers: power characteristics and mixing time, *Can. J. Chem. Eng.* **76**: 1056–1068.

Harju, M. (1991). *Lactose, its derivatives and their hydrolysis*, PhD thesis, Helsinki University of Technology.

Haß, V. C. and Nienow, A. W. (1989). Ein neuer, axial fördernder Rührer zum Dispergieren von Gas in Flüssigkeiten, *Chem. Ing. Tech.* **61**: 152–154.

Hegenauer, J., Saltman, P., Ludwig, D., Ripley, L. and Bajo, P. (1979a). Effects of supplemental iron and copper on lipid oxidation in milk. 1. Comparison of metal complexes in emulsified and homogenized milk, *J. Agric. Food Chem.* **27**: 860–867.

Hegenauer, J., Saltman, P., Ludwig, D., Ripley, L. and Ley, A. (1979b). Iron-supplemented cow milk. Identification and spectral properties of iron bound to casein micelles, *J. Agric. Food Chem.* **27**: 1294–1301.

Heineken, F. G. (1970). On the use of fast-response dissolved oxygen probes for oxygen transfer studies, *Biotechnol. Bioeng.* **12**: 145–154.

Heineken, F. G. (1971). Oxygen mass transfer and oxygen respiration rate measurements utilizing fast response oxygen electrodes, *Biotechnol. Bioeng.* **13**: 599–618.

Hickman, A. D. (1988). Gas-liquid oxygen transfer and scale-up. A novel experimental technique with results for mass transfer in aerated agitated vessels, *Proc. 6th Eur. Conf. Mixing*, pp. 369–374.

Hoffhine, C. E. (1956). Aqueous soluble salts of erythromycin, US Patent 2,761,859.

Hoogendoorn, C. J. and den Hartog, A. P. (1967). Model studies on mixers in the viscous flow region, *Chem. Eng. Sci.* **22**: 1689–1699.

Hudcova, V., Machon, V. and Nienow, A. W. (1989). Gas-liquid dispersion with dual Rushton turbine impellers, *Biotechnol. Bioeng.* **34**: 617–628.

Hudson, C. S. and Isbell, H. S. (1929). Relations between rotary power and structure in the sugar group. XIX. Improvements in the preparation of aldonic acids, *J. Am. Chem. Soc.* **51**: 2225–2229.

Hummer, J. S. (2004). A method and a process plant for treating a batch of liquids, Eur. Patent 1,324,818.

Imai, Y., Takei, H. and Matsumura, M. (1987). A simple Na_2SO_3 feeding method for K_La measurement in large-scale fermentors, *Biotechnol. Bioeng.* **29**: 982–993.

Isbell, H. S. and Frush, H. L. (1931). The oxidation of sugars. I. The electrolytic oxidation of aldose sugars in the presence of a bromide and calcium carbonate, *J. Res. Nat. Bur. Stand.* **6**: 1145–1152.

ISO-MIX A/S (2004). *ISO-MIX machine type IM 20 operators manual, no. 91I350-01, version 04.01*, Ishøj, Denmark.

Jayanti, S. (2001). Hydrodynamics of jet mixing in vessels, *Chem. Eng. Sci.* **56**: 193–210.

Joseph, J. P. and Bernstein, S. (1981). Lactobionic acid poly(H-sulfate) and salts thereof useful as complement inhibitors, US Patent 4,258,034.

Keitel, G. and Onken, U. (1982). The effect of solutes on bubble size in air-water dispersions, *Chem. Eng. Commun.* **17**: 85–98.

Khang, S. J. and Fitzgerald, T. J. (1975). A new probe and circuit for measuring electrolyte conductivity, *Ind. Eng. Chem. Fundam.* **14**: 208–213.

Kleppe, K. (1966). The effect of hydrogen peroxide on glucose oxidase from *Aspergillus niger*, *Biochem.* **5**: 139–143.

Kluyver, A. J., de Ley, J. and Rijven, A. (1951). The formation and consumption of lactobionic and maltobionic acids by *Pseudomonas* species, *Anton. van Lee. J. M. S.* **17**: 1–14.

Lane, A. G. C. and Rice, P. (1981). An experimental investigation of liquid jet mixing employing a vertical submerged jet, *IChemE Symp. Ser. 64*, pp. K1–K14.

Langheinrich, C. and Nienow, A. W. (1999). Control of pH in large-scale, free suspension animal cell bioreactors: Alkali addition and pH excursions, *Biotechnol. Bioeng.* **66**: 171–179.

Lei, F., Olsson, L. and Jørgensen, S. B. (2003). Experimental investigations of multiple steady states in aerobic continuous cultivations of *Saccharomyces cerevisiae*, *Biotechnol. Bioeng.* **82**: 766–777.

Leib, T. M., Pereira, C. J. and Villadsen, J. (2001). Bioreactors: a chemical engineering perspective, *Chem. Eng. Sci.* **56**: 5485–5497.

Leitner, C., Neuhauser, W., Volc, J., Kulbe, K. D., Nidetzky, B. and Haltrich, D. (1998). The Cetus process revisited: a novel enzymatic alternative for the production of aldose-free D-fructose, *Biocat. Biotrans.* **16**: 365–382.

Levenspiel, O. (1999). *Chemical Reaction Engineering*, 3rd edn, John Wiley & Sons.

Li, J.-K., Gomez, P. and Humphrey, A. E. (1990). The use of fluorometry for on-line measurement of mixing time and hold-up in fermentations, *Biotechnol. Tech.* **4**: 293–298.

Lidén, G. (2002). Understanding the bioreactor, *Bioproc. Biosyst. Eng.* **24**: 273–279.

Lin, S.-F., Hu, H.-M., Inukai, T. and Tsai, Y.-C. (1993). Production of novel oligosaccharide oxidase by wheat bran solid-state fermentation, *Biotechnol. Adv.* **11**: 417–427.

Lin, S.-F., Yang, T.-Y., Inukai, T., Yamasaki, M. and Tsai, Y.-C. (1991). Purification and characterization of a novel glucooligosaccharide oxidase from *Acremonium strictum* T1, *Biochim. Biophys. Acta - Protein Struct. M.* **1118**: 41–47.

Linek, V. (1972). Determination of aeration capacity of mechanically agitated vessels by a fast response oxygen probe, *Biotechnol. Bioeng.* **14**: 285–289.

Linek, V., Beneš, P. and Hovorka, F. (1981). The role of interphase nitrogen transport in the dynamic measurement of the overall volumetric mass transfer coefficient in air-sparged systems, *Biotechnol. Bioeng.* **23**: 301–319.

Linek, V., Beneš, P. and Sinkule, J. (1990). Critical assessment of the steady-state Na_2SO_3 feeding method for k_la measurement in fermentors, *Biotechnol. Bioeng.* **35**: 766–770.

Linek, V., Beneš, P., Sinkule, J. and Moucha, T. (1993). Non-ideal pressure step method for k_la measurement, *Chem. Eng. Sci.* **48**: 1593–1599.

Linek, V., Beneš, P. and Vacek, V. (1989a). Dynamic pressure method for k_la measurement in large-scale bioreactors, *Biotechnol. Bioeng.* **33**: 1406–1412.

Linek, V., Beneš, P. and Vacek, V. (1989b). Measurement of aeration capacity of fermenters, *Chem. Eng. Technol.* **12**: 213–217.

Linek, V., Havelka, P. and Sinkule, J. (1996a). Supersaturation effect in steady-state and dynamic methods for measuring k_La in gas-liquid dispersions, *Chem. Eng. Sci.* **51**: 5223–5226.

Linek, V., Moucha, T., Doušová, M. and Sinkule, J. (1994). Measurement of k_La by dynamic pressure method in pilot-plant fermentor, *Biotechnol. Bioeng.* **43**: 477–482.

Linek, V., Moucha, T. and Sinkule, J. (1996b). Gas-liquid mass transfer in vessels stirred with multiple impellers-I. Gas-liquid mass transfer characteristics in individual stages, *Chem. Eng. Sci.* **51**: 3203–3212.

Linek, V., Sinkule, J. and Beneš, P. (1991). Critical assessment of gassing-in methods for measuring k_la in fermentors, *Biotechnol. Bioeng.* **38**: 323–330.

Linek, V. and Vacek, V. (1981). Chemical engineering use of catalyzed sulfite oxidation kinetics for the determination of mass transfer characteristics of gas-liquid contactors, *Chem. Eng. Sci.* **36**: 1747–1768.

Ludwig, R., Ozga, M., Zámocky, M., Peterbauer, C., Kulbe, K. D. and Haltrich, D. (2004). Continuous enzymatic regeneration of electron acceptors used by flavoenzymes: cellobiose dehydrogenase-catalyzed production of lactobionic acid as an example, *Biocat. Biotrans.* **22**: 97–104.

Maa, Y.-F. and Hsu, C. C. (1997). Protein denaturation by combined effect of shear and air-liquid interface, *Biotechnol. Bioeng.* **54**: 503–512.

Marten, M. R., Wenger, K. S. and Khan, S. A. (1997). Rheology, mixing time, and regime analysis for a production-scale *Aspergillus oryzae* fermentation, *Proc. 4th Int. Conf. Bioreactor Bioprocess Fluid Dynamics*, pp. 295–313.

Martin, T., McFarlane, C. M. and Nienow, A. W. (1994). The influence of liquid properties and impeller type on bubble coalescence behaviour and mass transfer in sparged, agitated reactors, *Proc. 8th Eur. Conf. Mixing*, pp. 57–64.

Masiuk, S. (2000). Mixing time for a reciprocating plate agitator with flapping blades, *Chem. Eng. J.* **79**: 23–30.

McFarlane, C. M. and Nienow, A. W. (1996). Studies of high solidity ratio hydrofoil impellers for aerated bioreactors. 4. Comparison of impeller types, *Biotechnol. Prog.* **12**: 9–15.

Melton, L. A., Lipp, C. W., Spradling, R. W. and Paulson, K. A. (2002). DISMT - determination of mixing time through color changes, *Chem. Eng. Commun.* **189**: 322–338.

Metzner, A. B. and Otto, R. E. (1957). Agitation of non-Newtonian fluids, *AIChE J.* **3**: 3–10.

Middleton, J. C. and Smith, J. M. (2004). Gas-liquid mixing in turbulent systems, *in* E. L. Paul, V. A. Atiemo-Obeng and S. M. Kresta (eds), *Handbook of Industrial Mixing*, Wiley-Interscience, pp. 585–638.

Miyamoto, Y., Ooi, T. and Kinoshita, S. (2000). Production of lactobionic acid from whey by *Pseudomonas* sp. LS13-1, *Biotechnol. Lett.* **22**: 427–430.

Moucha, T., Linek, V. and Sinkule, J. (1995). Measurement of k_La in multiple-impeller vessels with significant axial dispersion in both phases, *Chem. Eng. Res. Des.* **73**: 286–290.

Murakami, H., Kawano, J., Yoshizumi, H., Nakano, H. and Kitahata, S. (2002). Screening of lactobionic acid producing microorganisms, *J. Appl. Glycosci.* **49**: 469–477.

Nidetzky, B., Fürlinger, M., Gollhofer, D., Scopes, R. K., Haltrich, D. and Kulbe, K. D. (1997). Improved operational stability of cell-free glucose-fructose oxidoreductase from *Zymomonas mobilis* for the efficient synthesis of sorbitol and gluconic acid in a continuous ultrafiltration membrane reactor, *Biotechnol. Bioeng* **53**: 623–629.

Niefenthaler, M. (2000). Mixing process design: Testing, *in* P. Hentrich (ed.), *EKATO Handbook of mixing technology*, 2nd edn, EKATO Rühr und Mischtechnic GmbH, pp. 51–63.

Nielsen, J., Villadsen, J. and Lidén, G. (2003). *Bioreaction Engineering Principles*, 2nd edn, Academic/Plenum Publishers.

Nienow, A. W. (1996). Gas-liquid mixing studies: a comparison of Rushton turbines with some modern impellers, *Chem. Eng. Res. Des.* **74**: 417–423.

Nienow, A. W. (1997). On impeller circulation and mixing effectiveness in the turbulent flow regime, *Chem. Eng. Sci.* **52**: 2557–2565.

Nienow, A. W. (1998). Hydrodynamics of stirred bioreactors, *Appl. Mech. Rev.* **51**: 3–32.

Nienow, A. W. (2000). Mixing: Studies at the University of Birmingham on this traditional technology critical in the manufacture of new biological products, *Food Bioprod. Process.* **78**: 145–151.

Nienow, A. W. and Bujalski, W. (2004). The versatility of up-pumping hydrofoil agitators, *Chem. Eng. Res. Des.* **82**: 1073–1081.

Nienow, A. W. and Elson, T. P. (1988). Aspects of mixing in rheologically complex fluids, *Chem. Eng. Res. Des.* **66**: 5–15.

Nienow, A. W., Warmoeskerken, M. M. C. G., Smith, J. M. and Konno, M. (1985). On the flooding/loading transition and the complete dispersal condition in aerated vessels agitated by a Rushton-turbine, *Proc. 5th Eur. Conf. Mixing*, pp. 143–154.

Nishizuka, Y. and Hayaishi, O. (1962). Enzymic formation of lactobionic acid from lactose, *J. Biol. Chem.* **237**: 2721–2728.

Nocentini, M. (1990). Mass transfer in gas-liquid, multiple-impeller stirred vessels: A discussion about experimental techniques for K_La measurement and model comparison, *Chem. Eng. Res. Des.* **68**: 287–294.

Nocentini, M., Fajner, D., Pasquali, G. and Magelli, F. (1993). Gas-liquid mass transfer and holdup in vessels stirred with multiple Rushton turbines: water and water-glycerol solutions, *Ind. Eng. Chem. Res.* **32**: 19–26.

Nordkvist, M., Grotkjær, T., Hummer, J. S. and Villadsen, J. (2003). Applying rotary jet heads for mixing and mass transfer in a forced recirculation tank reactor system, *Chem. Eng. Sci.* **58**: 3877–3890.

Okita, N. and Oyama, Y. (1963). Mixing characteristics of jet mixing, *Kagaku Kogaku* **27**: 252–259.

Otomo, N., Bujalski, W. and Nienow, A. W. (1995). The application of a compartment model to a vessel stirred with either dual radial or dual axial flow impellers, *The 1995 IChemE Research Event*, pp. 829–831.

Otomo, N., Bujalski, W., Nienow, A. W. and Takahashi, K. (2003a). Gas dispersion characteristics of newly developed impellers in a stirred vessel, *J. Chem. Eng. Japan* **36**: 166–171.

Otomo, N., Bujalski, W., Nienow, A. W. and Takahashi, K. (2003b). A novel measurement technique for mixing time in an aerated stirred vessel, *J. Chem. Eng. Japan* **36**: 66–74.

Paglianti, A., Pintus, S. and Giona, M. (2000). Time-series analysis approach for the identification of flooding/loading transition in gas-liquid stirred tank reactors, *Chem. Eng. Sci.* **55**: 5793–5802.

Parente, E. and Ricciardi, A. (1999). Production, recovery and purification of bacteriocins from lactic acid bacteria, *Appl. Microbiol. Biotechnol.* **52**: 628–638.

Patwardhan, A. W. (2002). CFD modeling of jet mixed tanks, *Chem. Eng. Sci.* **57**: 1307–1318.

Pedersen, A. G. (1992). *Characterization and modelling of bioreactors*, PhD thesis, Department of Biotechnology, Technical University of Denmark.

Pedersen, A. G. (1997). $k_l a$ characterization of industrial fermentors, *Proc. 4th Int. Conf. Bioreactor Bioprocess Fluid Dynamics*, pp. 263–267.

Pedersen, A. G., Bundgaard-Nielsen, M., Nielsen, J. and Villadsen, J. (1994). Characterization of mixing in stirred tank bioreactors equipped with Rushton turbines, *Biotechnol. Bioeng.* **44**: 1013–1017.

Pedersen, A. G., Bundgaard-Nielsen, M., Nielsen, J., Villadsen, J. and Hassager, O. (1993). Rheological characterization of media containing *Penicillium chrysogenum*, *Biotechnol. Bioeng.* **41**: 162–164.

Pinelli, D., Bujalski, W., Nienow, A. W. and Magelli, F. (2001). Comparison of experimental techniques for the measurement of mixing time in gas-liquid systems, *Chem. Eng. Technol.* **24**: 919–923.

Rand, A. G. (1972). Direct enzymatic conversion of lactose to acid: Glucose oxidase and hexose oxidase, *J. Food Sci.* **37**: 698–701.

Rand, A. G. and Hourigan, J. A. (1975). Direct enzymatic conversion of lactose in milk to acid, *J. Dairy Sci.* **58**: 1144–1150.

Revill, B. K. (1992). Jet mixing, *in* N. Harnby, M. F. Edwards and A. W. Nienow (eds), *Mixing in the process industries*, Butterworth Heinemann, pp. 159–183.

Ruszkowski, S. (1994). A rational method for measuring blending performance, and comparison of different impeller types, *Proc. 8th Eur. Conf. Mixing*, pp. 283–291.

Saito, F., Nienow, A. W., Chatwin, S. and Moore, I. P. T. (1992). Power, gas dispersion and homogenisation characteristics of Scaba SRGT and Rushton turbine impellers, *J. Chem. Eng. Japan* **25**: 281–287.

Satory, M., Fürlinger, M., Haltrich, D., Kulbe, K. D., Pittner, F. and Nidetzky, B. (1997). Continuous enzymatic production of lactobionic acid using glucose-fructose oxidoreductase in an ultrafiltration membrane reactor, *Biotechnol. Lett.* **19**: 1205–1208.

Savary, B. J., Hicks, K. B. and O'Connor, J. V. (2001). Hexose oxidase from *Chondrus crispus*: improved purification using perfusion chromatography, *Enz. Microb. Technol.* **29**: 42–51.

Schilling, B. M., Pfefferle, W., Bachmann, B., Leuchtenberger, W. and Deckwer, W.-D. (1999). A special reactor design for investigations of mixing time effects in a scaled-down industrial L-lysine fed-batch fermentation process, *Biotechnol. Bioeng.* **64**: 599–606.

Schmitt, G. and Saleh, A. O. (2000). Evaluation of environmentally friendly corrosion inhibitors for sour service, *Mater. Performance* **39(8)**: 62–65.

Schweder, T., Krüger, E., Xu, B., Jürgen, B., Blomsten, G., Enfors, S.-O. and Hecker, M. (1999). Monitoring of genes that respond to process-related stress in large-scale bioprocesses, *Biotechnol. Bioeng* **65**: 151–159.

Sen Gupta, M. L., Bhattacharya, N. and Basu, U. P. (1967). Preparation of calcium lactobionate by electrolytic oxidation of lactose: Part I -Oxidation in electrolytic cell using stationary electrodes, *Indian J. Technol.* **5**: 152–154.

Sen Gupta, M. L., Bhattacharya, N. and Basu, U. P. (1968). Preparation of calcium lactobionate by electrolytic oxidation of lactose: Part II - Oxidation in electrolytic cell using rotating anode, *Indian J. Technol.* **6**: 146–149.

Shepherd, R. E., Isaacson, Y., Chensny, L., Zhang, S., Kortes, R. and John, K. (1993). Lactobionic and gluconic acid complexes of Fe^{II} and Fe^{III}; Control of oxidation pathways by an organ transplantation preservant, *J. Inorg. Biochem.* **49**: 23–48.

Shi, L., Wang, X. and Pan, J. (1989). Stability of erythromycin lactobionate in five intravenous infusions, *Zhongguo Yaoxue Zazhi* **24**: 217–218.

Shioya, S. and Dunn, I. J. (1979). Model comparisons for dynamic k_La measurements with incompletely mixed phases, *Chem. Eng. Commun.* **3**: 41–52.

Simon, M. and Fonade, C. (1993). Experimental study of mixing performances using steady and unsteady jets, *Can. J. Chem. Eng.* **71**: 507–513.

Singh, V., Hensler, W., Fuchs, R. and Constantinides, A. (1986). On-line determination of mixing parameters in fermentors using pH transients, *Proc. Int. Conf. Bioreactor Fluid Dynamics*, pp. 231–256.

Southard, J. H. (2004). The right solution for organ preservation, *Business briefing: North American pharmacotherapy II*, Business Briefings. http://www.bbriefings.com/pdf/174/Southard_supp.pdf.

Southard, J. H. and Belzer, F. O. (1995). Organ preservation, *Annu. Rev. Med.* **46**: 235–247.

Stocks, S. M., Cooke, M. and Heggs, P. J. (2005). Inverted hollow spinning cone as a device for controlling foam and hold-up in pilot scale gassed agitated fermentation vessels, *Chem. Eng. Sci.* **60**: 2231–2238.

Stodola, F. H. and Lockwood, L. B. (1947). The oxidation of lactose and maltose to bionic acids by *Pseudomonas*, *J. Biol. Chem.* **171**: 213–221.

Sullivan, J. D. and Ikawa, M. (1973). Purification and characterization of hexose oxidase from the red alga *Chondrus crispus*, *Biochim. Biophys. Acta* **309**: 11–22.

Sweere, A. P. J., Janse, L., Luyben, K. C. A. M. and Kossen, N. W. F. (1988a). Experimental simulation of oxygen profiles and their influence on Baker's yeast production: II. Two-fermentor system, *Biotechnol. Bioeng.* **31**: 579–586.

Sweere, A. P. J., Mesters, J. R., Janse, L., Luyben, K. C. A. M. and Kossen, N. W. F. (1988b). Experimental simulation of oxygen profiles and their influence on Baker's yeast production: I. One-fermentor system, *Biotechnol. Bioeng.* **31**: 567–578.

Thýn, J., Novák, V. and Pock, P. (1976). Effect of the measured volume size on the homogenization time, *Chem. Eng. J.* **12**: 211–217.

Thompson, B. G. (1987). Effect of temporary localized operating conditions on fermentations of *Saccharomyces cerevisiae*, *Biotechnol. Bioeng.* **29**: 786–788.

Tomlinson, G. A., Strohm, M. P. and Hochstein, L. I. (1978). The metabolism of carbohydrates by extremely halophilic bacteria: the identification of lactobionic acid as a product of lactose metabolism by *Halobacterium saccharovorum*, *Can. J. Microbiol.* **24**: 898–903.

Toshiaki, S., Shuichi, Y., Seiichiro, A. and Sakanori, S. (1995a). Mineral absorption promoters containing lactobionic acid, Japanese Patent 07277991.

Toshiaki, S., Shuichi, Y., Tomoko, K. and Sakanori, S. (1995b). Bifidus factors containing lactobionic acid, Japanese Patent 07277990.

van Niel, E. W. J., Hofvendahl, K. and Hahn-Hagerdal, B. (2002). Formation and conversion of oxygen metabolites by *Lactococcus lactis* subsp. *lactis* ATCC 19435 under different growth conditions, *Appl. Environ. Microbiol.* **68**: 4350–4356.

van't Riet, K. (1979). Review of measuring methods and results in nonviscous gas-liquid mass transfer in stirred vessels, *Ind. Eng. Chem. Proc. Des. Dev.* **18**: 357–364.

Vasconcelos, J. M. T., Nienow, A. W., Martin, T., Alves, S. S. and McFarlane, C. M. (1997). Alternative ways of applying the hydrogen peroxide steady state method of K_La measurement, *Chem. Eng. Res. Des.* **75**: 467–472.

Vasconcelos, J. M. T., Orvalho, S. C. P., Rodrigues, A. M. A. F. and Alves, S. S. (2000). Effect of blade shape on the performance of six-bladed disk turbine impellers, *Ind. Eng. Chem. Res.* **39**: 203–213.

Venugopal, R. and Bradley, S. A. (1993). Effect of oxygen upon the kinetics of glucose oxidase inactivation, *Can. J. Chem. Eng* **71**: 917–924.

Verduyn, C., Postma, E., Scheffers, W. A. and van Dijken, J. P. (1992). Effect of benzoic acid on metabolic fluxes in yeasts: a continuous-culture study on the regulation of respiration and alcoholic fermentation, *Yeast* **8**: 501–517.

Vrábel, P., van der Lans, R. G. J. M., Luyben, K. C. A. M., Boon, L. and Nienow, A. W. (2000). Mixing in large-scale vessels stirred with multiple radial or radial and axial up-pumping impellers: modelling and measurements, *Chem. Eng. Sci.* **55**: 5881–5896.

Whitman, W. G. (1923). A preliminary experimental confirmation of the two-film theory of gas absorption, *Chem. Metall. Eng.* **29**: 146–148.

Whitton, M. J. and Nienow, A. W. (1993). Scale up correlations for gas holdup and mass transfer coefficients in stirred tank reactors, *Proc. 3rd Int. Conf. Bioreactor Bioprocess Fluid Dynamics*, pp. 135–149.

Wright, D. G. and Rand, A. G. (1973). Direct enzymatic conversion of lactose to acid: Lactose dehydrogenase, *J. Food Sci.* **38**: 1132–1135.

Xu, F., Golightly, E. J., Fuglsang, C. C., Schneider, P., Duke, K. R., Lam, L., Christensen, S., Brown, K. M., Jørgensen, C. T. and Brown, S. H. (2001). A novel carbohydrate:acceptor oxidoreductase from *Microdochium nivale*, *Eur. J. Biochem.* **268**: 1136–1142.

Yianneskis, M. (1991). The effect of flow rate and tracer insertion time on mixing times in jet-agitated vessels, *Proc. 7th Eur. Conf. Mixing*, pp. 121–129.

Zhu, Y., Bandopadhayay, P. C. and Wu, J. (2001). Measurement of gas-liquid mass transfer in an agitated vessel - a comparison between different impellers, *J. Chem. Eng. Japan* **34**: 579–584.

Zlokarnik, M. (1978). Sorption characteristics for gas-liquid contacting in mixing vessels, *Adv. Biochem. Eng.* **8**: 135–150.